Program and Abstract Volume

LUNAR AND PLANETARY INSTITUTE

LPI Contribution No. 1616

CONFERENCE ON MICRO-RAMAN AND LUMINESCENCE STUDIES IN THE EARTH AND PLANETARY SCIENCES (CORALS II)

May 18–20, 2011 • Madrid, Spain

Sponsors

Spanish National Research Council
Lunar and Planetary Institute

Scientific Organizing Committee

Javier Garcia-Guinea (Chair),
Museo Nacional de Ciencias Naturales (MMCN)
Virgilio Correcher (Co-Chair), *CIEMAT*
Sergio Sanchez-Moral, *MNCN, CSIC*
Soledad Cuezva, *MNCN, CSIC*
Angel Fernandez-Cortes, *MNCN, CSIC*
Elena Garcia Anton, *MNCN, CSIC*
Laura Tormo, *MNCN, CSIC*
Marta Furio, *MNCN, CSIC*
Alberto Jorge, *MNCN, CSIC*
Sagrario Martinez-Ramirez, *IEM, CSIC*
Santiago Sanchez Cortes, *IEM, CSIC*
Ana Cremades, *Univ. Complutense*
Javier Ruiz, *Univ. Complutense*
Elena Crespo-Feo, *Univ. Complutense*
Susana Jorge-Villar, *Univ. Burgos*
Miguel De la Guardia, *Univ. Valencia*

Lunar and Planetary Institute 3600 Bay Area Boulevard Houston TX 77058-1113

LPI Contribution No. 1616

Compiled in 2011 by

Meeting and Publication Services
Lunar and Planetary Institute
USRA–Houston
3600 Bay Area Boulevard, Houston TX 77058-1113

The Lunar and Planetary Institute is operated by the Universities Space Research Association under a cooperative agreement with the Science Mission Directorate of the National Aeronautics and Space Administration.

Abstracts in this volume may be cited as

Author A. B. (2011) Title of abstract. In *Conference on Micro-Raman and Luminescence Studies in the Earth and Planetary Sciences (CORALS II),* p. XX. LPI Contribution No. 1616, Lunar and Planetary Institute, Houston.

ISSN No. 0161-5297

Preface

This volume contains abstracts that have been accepted for presentation at the Conference on Micro-Raman and Luminescence Studies in the Earth and Planetary Sciences, May 18–20, 2011, Madrid, Spain.

Administration and publications support for this meeting were provided by the staff of the Meeting and Publication Services Department at USRA's Lunar and Planetary Institute.

Contents

Program

Wednesday, May 18, 2011
WELCOME AND OPENING CEREMONIES
9:30 a.m. Rocasolano Hall

9:30 a.m. Dr. Jose Vicente Garcia Ramos (Vice-President CSIC, Spain) and Javier Garcia Guinea (CORALS II Chair)
Welcome

LUMINESCENCE AND MICRO-RAMAN OF METEORITES AND SHOCK METAMORPHISM
9:45 a.m. Rocasolano Hall

Chairs: Javier Garcia-Guinea
Arnold Gucsik

9:45 a.m. Gucsik A. * Okumura T. Kayama M. Nishido H. Ninagawa K. [INVITED OVERVIEW TALK]
A Combined Cathodoluminescence and Micro-Raman Study of Planar Deformation Features in Quartz **[#4003]**

10:15 a.m. Boonsue S. * Spray J.
Shock-Induced Phase Transformations in Melt Pockets Within Martian Meteorite NWA 4468 **[#4007]**

10:30 a.m. Kayama M. * Nishido H. Sekine T. Nakazato T. Gucsik A. Ninagawa K.
Clarification of Shock-Induced Effect on Cathodoluminescence of Alkali Feldspar **[#4021]**

10:45 a.m. COFFEE BREAK

11:30 a.m. 11:00 a.m. Katsaros Th. * Ganetsos Th.
In Situ Study of a Collection of 20 Meteorites Using Raman Spectroscopy **[#4057]**

11:45 p.m. Kaliwoda M. * Hochleitner R. Hoffmann V. H. Mikouchi T. Gigler A. M. Schmahl W. W.
New Raman Spectroscopic Data of Almahata Sitta Meteorite **[#4037]**

12:00 p.m. Rubio-Ordóñez A. * Cárdenes V. Rodríguez-Terente L. Tormo L. García-Guinea J.
BSE, CL and Raman Spectroscopy Study of Phospates and Maskelenyte in the H6 Cangas de Onis Regolith Breccia **[#4024]**

12:15 p.m. Dutta P. * Duorah K.
Thermoluminescence Studies of Dergaon Meteorite **[#4011]**

12:30 p.m. Shiryaev A. A. * Fisenko A. V. Vlasov I. I. Semjonova L. F.
Raman and Luminescence Spectroscopy of Meteoritic Nanodiamonds **[#4025]**

12:45 p.m. LUNCH

Wednesday, May 18, 2011
PLANETARY IN SITU APPLICATIONS OF LUMINESCENCE AND RAMAN TECHNIQUES
2:30 p.m. Rocasolano Hall

Chairs: Emilio Nogales
Marc Fries

2:30 p.m. Marc Fries * [INVITED OVERVIEW TALK]
Raman in a Combined Instrument Package: Co-Registered and "Smart Raman" Techniques

3:00 p.m. Pidgeon R. T. * Nemchin A. A. Grange M. Timms N.
Events in the Life of the Oldest Zircon on the Moon: A Combined SIMS, CL, EBSD and Raman Study **[#4002]**

3:15 p.m. Muñoz-Iglesias M. V. * Bonales L. J. Prieto-Ballesteros O.
Characterization of the Differentiation Process by Clathration in Europa Satellite Using Raman Spectroscopy **[#4032]**

3:30 p.m. De Angelis S. * Della Corte V. Baratta G. A. Brunetto R. Palumbo P. Ciucci A. Rotundi A.
Raman Micro-Spectroscopy Performed on Extraterrestrial Particles **[#4059]**

3:45 p.m. Kollegger P. * Zaccarini F. Bakker R. J. Garuti G. Thalhammer O. A. R.
Compositional Analyses of F, Cl and OH by Raman Spectroscopy in Apatite from Mafic-Ultramafic Pipes of the Ivrea Verbano Zone (NW Italy) **[#4018]**

4:00 p.m. COFFEE BREAK

4:45 p.m. Garcia-Guinea J. Tormo L. Azumendi O. Ruiz J.
Luminescent Detection of Active Stress in Melilite-Anorthite CAI Grains of Allende CV3 Chondrite (Mexico) **[#4053]**

5:00 p.m. Caporali S. * Moggi-Cecchi V. Muniz-Miranda M. Pagliai M. Pratesi G. Schettino V.
Adenine Adsorbed on a Martian Meteorite as a Test Case for SERS Investigation of Extraterrestrial Life Traces **[#4041]**

5:15 p.m. Blacksberg J. * Rossman G. R.
In Situ Planetary Mineralogy Using Simultaneous Time Resolved Fluorescence and Raman Spectroscopy **[#4048]**

5:30 p.m. Böttger U. * de Vera J.-P. Fritz J. Weber I. Hübers H.-W.
Raman Microscopy of Samples of Martian Analogue Material with Cyanobacteria **[#4071]**

Wednesday, May 18, 2011
SOCIAL EVENT
6:00 p.m. Rocasolano Hall

Cocktail party in the Meteorite Exhibit Hall of the Museo Nacional of Ciencias Naturales. Attendees will also have access to the historical collections and the geological analytical facilities (including the Raman and spectra cathodoluminescence microscopes).

6:00 p.m. *Group photo at the CSIC main building stairs (meet by the granite columns)*

6:30 p.m. *Group meets in CSIC gardens to walk to the Museo Nacional Ciencias Naturales*

7:00 p.m. *Cocktails in the Geology Exhibition Hall*

Thursday, May 19, 2011
NEW TRENDS AND DEVELOPMENTS IN OPTICAL SPECTROSCOPY AND LUMINESCENCE TECHNIQUES I
9:30 a.m. Rocasolano Hall

Chairs: Emilio Nogales
Ana Cremades

9:30 a.m. Emilio Nogales * [INVITED OVERVIEW TALK]
Confocal Raman and Luminescence Spectromicroscopy Studies of Nano- and Microscale Inorganic Materials

10:00 a.m. Guimbretière G. * Canizares A. Simon P. Tobon-Correa Y. A. Ammar M. R. Corbel C. Barthe M. F.
In Situ Micro-Raman Observation of Uranium Dioxide Weathering in Contact with Water and Under Ion Beam Irradiation **[#4013]**

10:15 a.m. Ammar M. R. * Rouzaud J.-N. Charon E. Aleon J. Guimbretière G. Simon P.
On the Reliable Structural Characterization of Polished Carbons in Meteorites by Raman Microspectroscopy **[#4015]**

10:30 a.m. Bonales L. J. * Muñoz-Iglesias M. V. Sanchez-Román M. Fernandez-Remolar D. Prieto-Ballesteros O.
Quantitative Raman Spectroscopy (QRS), a Potential Tool to Study the Formation Mechanism of Carbonates of Early Earth and Mars **[#4031]**

10:45 a.m. Ujj L. * Hemasinha R. Prayaga C.
Spectral Decomposition Methods for Coherent Raman Spectroscopy **[#4080]**

11:00 a.m. COFFEE BREAK

Thursday, May 19, 2011
NEW TRENDS AND DEVELOPMENTS IN OPTICAL SPECTROSCOPY AND LUMINESCENCE TECHNIQUES II
11:30 a.m. Rocasolano Hall

Moderators: **Emilio Nogales**
Ana Cremades

Panel Members:

Rafael Sanchez (Thermofisher Scientific Spain)
Compact Micro-Raman Microscopes

Vicent Larat (Horiba Scientific Spain)
Raman Equipment

Sebastien Maussang (Renishaw Iberica)
Latest Developments in Raman Spectroscopy

Pedro Toribio (Microbeam S. A.)
Portable Raman Devices

Thursday, May 19, 2011
LUMINESCENCE AND RAMAN SPECTROSCOPY APPLIED TO EARTH SCIENCES
2:30 p.m. Rocasolano Hall

Luminescence and Raman Spectroscopy Applied to Minerals, Gemstones, Rocks, Fossils, and Natural Glasses

Chairs: Elena Crespo-Feo
Lutz Nasdala

2:30 p.m. Lutz Nasdala * [INVITED OVERVIEW TALK]
Raman and Luminescence Images Applied to Study Internal Textures of Minerals and Geological Samples

3:00 p.m. Can N. * Garcia Guinea J. Hatipoglu M. Kibar R. Cetin A.
Luminescence Behaviour and Raman Characterization of Rhodonite from Turkey **[#4001]**

3:15 p.m. Zaccarini F. * Bakker R. J. Garuti G. Thalhammer O. A. R. Proenza J. A. Aiglsperger T.
Raman Spectroscopy Applied to Rare and Tiny Phases: Example from the Study of Platinum Group Minerals (PGM) **[#4019]**

3:30 p.m. Gigler A. M. * Sánchez-Pastor N. Cruz J. A. Fernández-Díaz L.
Raman Spectroscopy and Microprobe Investigation of the Incorporation of Cr(VI) in $CaCO_3$ **[#4034]**

3:45 p.m. Volovetsky M. V. * Averin A. A. Shiryaev A. A.
Raman Spectroscopy Study of Tektites **[#4010]**

4:00 p.m. COFFEE BREAK

4:30 p.m. Brenker F. E. * Schmitz S. Vincze L. Vekemans B. Krebs M. de Nolf W. Janssens K. Stachel T. Harris J.
Trapped High Density Fluids and Melts in Superdeep Diamonds **[#4054]**

4:45 p.m. Cetin A. * Kibar R. Can N.
Luminescence Spectra of Plagioclase (Labradorite) from South Greenland **[#4060]**

5:00 p.m. Kibar R. * Kati M. I. Cetin A. Turemis M. Keskin I. C. Tastekin B. Hatipoglu M. Can N.
Structure and Luminescence Characteristics of Aquamarine from Turkey **[#4061]**

5:15 p.m. Crespo-Feo E. * Hernandez-Ferreiros P. Garcia-Guinea J. Correcher V.
Effects of the Tectonic Stress on Luminescence of Cerussite $PbCO_3$ **[#4081]**

5:30 p.m. Schlueter C. F. * Gigler A. M. Moritz W.
Iron Oxids on Ag(111) — Reversible Switching Between Hematite and Magnetite **[#4076]**

GALA DINNER
8:00 p.m. Rocasolano Hall

Friday, May 20, 2011
LUMINESCENCE AND RAMAN TECHNIQUES FOR GEOSCIENCE-RELATED USES
9:00 a.m. Rocasolano Hall

Luminescence and Raman Techniques for Geoscience-Related Uses Such as Dating and Radiation Dosimetry, Building Heritage, Pigment Preservation, Mortars, and Archaeological Artifacts

Chairs: **Virgilio Correcher**
Chris Burbidge
Angel Fernandez Cortes

9:00 a.m. Chris Burbidge * [INVITED OVERVIEW TALK]
Facets of Luminescence for Dating

9:30 a.m. Fernandez-Cortes A. Cuezva S. Cañaveras J. C. Garcia-Guinea J. Sanchez-Moral S.
Content of Rare Earth Elements in a Speleothem Analyzed by ICP-MS and CL-Spectroscopy **[#4066]**

9:45 a.m. Sanjurjo-Sánchez J. * Vidal Romaní J. R.
Luminescence Dating of Pseudokarst Speleothems: A First Approach **[#4029]**

10:00 a.m. Sanchez-Moral S. Fernandez-Cortes A. Cuezva S. Cañaveras J. C. Correcher V. Miller A. Z. Dionisio A. Marques J. M. Saiz-JImenez C. Afonso M. J. Chamine H. I. Furio M. Garcia-Guinea J.
Uranyl Groups Coupled to Evansite Granite Vein Infills in the Porto Undergrounds (NW Portugal) **[#4023]**

10:15 a.m. López-Arce P. * Zornoza-Indart A. Vázquez-Calvo C. Gomez-Heras M. Álvarez de Buergo M. Fort R.
Evaluation of Portable Raman for the Characterization of Salt Efflorescences at Petra, Jordan **[#4038]**

10:30 a.m. González-Acebrón L. * Barca D. Arribas J. Mas J. R.
Trace Element and REE Leaching During Diagenetic Albitization and Its Relationship to the Cathodoluminescence Colour of Feldspars: The Tera Group, Cameros Basin (NE Spain) **[#4045]**

10:45 a.m. COFFEE BREAK

11:15 a.m. Henner Busemann * [INVITED OVERVIEW TALK]
Spectroscopy Results on Stardust, Interplanetary Dust Particles, and Meteorites

11:45 a.m. Arnold Gucsik *
Proposal of Creation of the European Society of Luminescence

12:15 p.m. Javier Garcia-Guinea *
Proposals for the Next CORALS III Conference 2013

12:30 p.m. LUNCH

Friday, May 20, 2011
POSTER SESSION
3:00 p.m. Church Cloister

Posters may be prepared in vertical format,
and are limited to no more than 75 cm (29 inches) wide and 120 cm (47 inches) high

Bersani D. Mantovani L. Tribaudino M. Lottici P. P.
Raman Investigation on Pigeonite in Ureilite **[#4077]**

Matsuda J. Morishita K. Nara M. Amari S.
Raman Spectroscopic Study of Allende (CV3) and Saratov (L4) Chemical Residues and Its Implication to Phase Q **[#4017]**

Azumendi O. Tormo L. Ruiz J. Garcia-Guinea J.
Madrid L6 Chondrite (Fall 1896): ESEM-Cathodoluminescence Survey **[#4020]**

Ivliev A. I. Alexeev V. A. Kuyunko N. S.
Thermoluminescence and Shock Metamorphism of Ordinary Chondrites **[#4040]**

Glotch T. D. Ferrari M. J.
Raman Microscopy of Shocked and Unshocked Basalts from Lonar Crater, India **[#4049]**

Alba-Aldave L. A. García-Guinea J. Furio M. Jorge-García A.
Cathodoluminescence and Raman Spectroscopic Characterization of Phosphates in Mexican Chondrites **[#4052]**

Aparicio A. Bustillo M. A.
CL-Spectral Characteristics of Quartz and Feldspars in Fresh and Hydrothermal Altered Volcanic Rocks (Cabo de Gata, Almeria, Spain) **[#4008]**

Prieto A. C. Guedes A. Dória A. Noronha F. Jiménez J.
Quantitative Determination of Gaseous Phases in Fluid Inclusions by Raman Microscopy **[#4039]**

Torres D. I. Llopis J.
Luminescence and Raman Scattering of Stabilized Zirconia Crystals **[#4051]**

Prieto-Taboada N. Gómez-Laserna O. Ibarrondo I. Martinez-Arkarazo I.
Olazabal M. A. Madariaga J. M.
Cross-Section Analysis to Establish the Penetration Level of Atmospheric Pollution in Mortars **[#4058]**

Kashkarov L. L. Kalinina G. V. Shilobreeva S. N.
Thermoluminescence as One of the Methods for Determination of the Crystal Lattice Structure of Quartz **[#4070]**

Aramendia J. Gómez-Nubla L. Fdez-Ortiz de Vallejuelo S. Castro K. Madariaga J. M.
New Findings by Raman Microspectroscopy of Inclusions Inside a Libyan Desert Glass **[#4075]**

Sánchez-Pastor N. Gigler A. M. Fernández-Díaz L.
Raman Study of Synthetic $BaCO_3$–$SrCO_3$ Solid Solutions **[#4036]**

Bustillo M. A. Pérez-Jiménez J. L. Alonso-Zarza A. M. Furio M.
Moganite in the Chalcedony Varieties of Continental Cherts (Miocene, Madrid Basin, Spain) **[#4009]**

Vazquez-Calvo C. Martinez-Ramirez S. Álvarez de Buergo M. Fort R.
Preliminary Studies for the Use of Portable Raman in the Identification of Conservation Treatments Applied in the Architectural Heritage **[#4014]**

Sanjurjo-Sánchez J. Blanco Rotea R.
Luminescence Dating of Mortars from Ancient Architectural Elements **[#4030]**

Medialdea A. Porat N. Benito G.
Optically Stimulated Luminescence Response of Modern Flash-Flood Deposits in Small Mountain Catchments **[#4033]**

Prieto A. C. Avella M. Martínez O. Jiménez J. Alonso J. L. Sánchez I. Martín R. Barrera M.
Raman Spectroscopy Analysis of a Playing Card from the XVII Century **[#4046]**

Prieto A. C. Avella M. González M. A. Jiménez J. Romero F. De Pablo R. Górriz C. Sanz C.
Analysis of the Residual in Grave Goods from the Vaccaea Era at the Necropolis of "Las Ruedas" in Pintia **[#4047]**

García-Antón E. Cuezva S. Fernández-Cortes A. Cuevas-González J. Muñoz-Cervera M. C. Benavente D. Sanchez-Moral S. Cañaveras J. C.
Mineral Variations Study of Canelobre Cave Phosphate Stalactite by Raman and Luminescence Methods **[#4056]**

Turemis M. Tastekin B. Kati M. I. Keskin I. C. Kibar R. Cetin A. Can N.
The Influence of Annealing on Thermoluminescence Behaviour in ZnO **[#4062]**

Fdez-Ortiz de Vallejuelo S. Castro K. Martínez-Arkarazo I. Madariaga J. M.
Raman Spectroscopic Characterisation of Green-Blue Stalactites in Lantz Cave (Navarra, North of Spain) **[#4063]**

Gómez-Nubla L. Aramendia J. Fdez-Ortiz de Vallejuelo S. Castro K. Madariaga J. M.
Relations Between Leachated Compounds and Raman Spectrum of Black Slags from EAF in Order to Characterize Them **[#4067]**

Aramendia J. Gómez-Nubla L. Castro K. Martínez-Arkarazo I. Arana G. Madariaga J. M.
The Consequences of the Presence of Urban Atmospherica Particles and Airbornes in CorTen® Steel Surfaces **[#4069]**

Tastekin B. Turemis M. Kati M. I. Keskin I. C. Kibar R. Cetin A. Can N.
Effects of Thermal Annealing on the Thermoluminescence Properties of Ion-Implanted $SrTiO_3$ **[#4082]**

Iordanidis A. Garcia-Guinea J. Correcher V.
Cystine-Apatite Renal Calculi: EPMA, Raman and ESEM-CL Study **[#4005]**

Bower D. M. Steele A. Fries M. D. Kater L.
Micro Raman Spectroscopic Investigations of the Nature and Provenance of Carbonaceous Material in Micro-Fossil Bearing Rocks: Redefining D and G Carbon Band Parameters for the Detection of Biosignatures **[#4016]**

Sanz M. E. González-Acebrón L. Rodríguez-Aranda J. P. Marshall C. P.
Raman Spectra on Fluid Inclusions in Glauberite from Miocene Saline Lakes of the Madrid Basin: Evidence for Microbial Activity **[#4044]**

Saturday, May 21, 2011
FIELD TRIP ACROSS GUADARRAMA MOUNTAINS AND EL ESCORIAL
9:30 a.m. Rocasolano Hall

Field Trip Across Guadarrama Mountains and El Escorial

Guide: Javier Garcia Guinea

9:30 a.m. Bus departs from CSIC Central Campus *(Serrano St., 117)*

10:30 a.m. Visit at Madrid Deep Space Communications Complex *(www.mdscc.org)*

12:00 p.m. Snacks and drinks in the Silla de Felipe II Area (El Escorial, Madrid)

1:00 p.m. Free time in the El Escorial City Center and Monastery

5:00 p.m. Bus departs for evening trip to Guadarrama Mountains—Manzanares—Colmenar Viejo (Geological Park of Rock Monolites)

8:00 p.m. Estimated time of return to Madrid

Cathodoluminesce and Raman Spectroscopic Characterization of Phosphates in Mexican Chondrites

L. A. Alba-Aldave, J. García-Guinea, M. Furio, and A. Jorge-García

Four chondrite meteorites fallen in Mexico (Nuevo Mercurio, Nuevo Mercurio (c), Cuarta Parte, and Cosina) were studied in polished thin sections, using a secondary electron microscope catodoluminesce system (SEM-CL), and Raman spectroscopy (RS). We analyzed and compared the spectra obtained by CL and RS of merrillite and apatite. These meteorites belong to the collection of Institute of Geology of the University of México.

Meteorite description

a) Nuevo Mercurio meteorite, classified as an olivine and bronzite chondrite H5, fell down in december of 1978 near the locality of Nuevo Mecurio, Zacatecas (24° 18' N 102° 08' W).
b) Nuevo Mercurio (c) is a genomict breccia H5/6, with the presence of some H6 clasts, a dark inclusion, and a large grain of metal-troilite. The minerals are olivine, pyroxene and feldspars, while the opaque mineral phases are troilite, kamacite, taenite and chromite.
c) Cosina meteorite, classified as a chondrite of olivine and bronzite H5, fell down near Dolores Hidalgo city, Guanajuato (21° 10' N 100° 52' W) in january of 1844. It is an unusual ordinary chondrite with a highly porous lithology.
d) Cuarta Parte (also known as Silao) meteorite, classified as an ordinary chondrite L4, fell down in april of 1995 in Silao municipality, Guanajuato (20° 56' N 101° 21' W).
Merrilite and apatite are present as accessory minerals in all meteorites.

a) 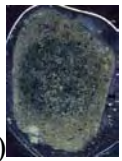 b) 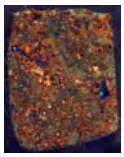 c) 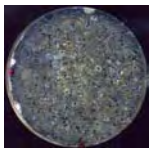 d) 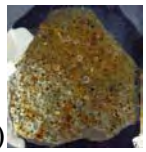

Experimental method

The luminescent images showed the occurrence of plagioclases and phosphates. The phosphates CL spectra show the presence of two different profiles which could be assigned to merrillite and apatite, and this assignment was then confirmed by EDS and Raman spectroscopy studies. The CL spectra of merrillites of the four meteorites were very similar, even though they fell very separated in time and place.

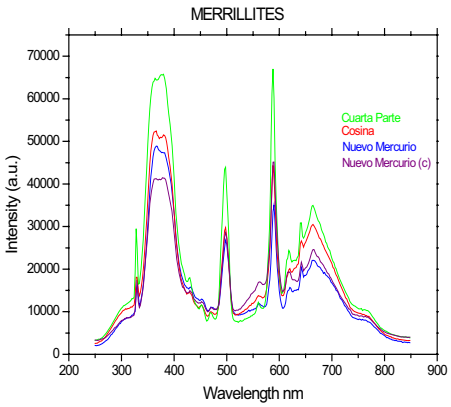

Fig. 1 CL spectra of merrillites

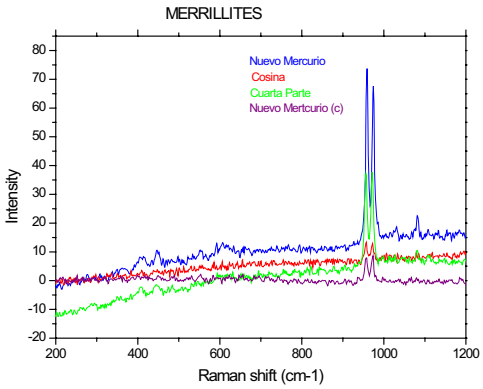

Fig. 2 Raman spectra of the merrillites

Conclusions:

Despite of the differences in mineral composition and texture of the four meteorites, it is remarkable that the merrillite CL spectra are so much alike, indicating the presence of the same RE elements, with similar relative proportions, in all the cases.

On the reliable structural characterization of polished carbons in meteorites by Raman microspectroscopy

M. R. Ammar[1,2,3*], J.-N. Rouzaud[3], E. Charon[3], J. Aleon[4], G. Guimbretière[1,2], P. Simon[1,2]

[1]UPR CNRS 3079, 1D, Avenue de la Recherche Scientifique, 45071 Orléans cedex 2, France. [2]Université d'Orléans, Polytech'Orléans, 8 rue Léonard de Vinci 45072 Orléans, France. [3]Laboratoire de Géologie de l'Ecole Normale Supérieure, UMR CNRS 8538, 24 rue Lhomond, F-75231 Paris cedex 5, France. [4]Centre de Spectrométrie de Masse, CNRS/IN2P3, Univ. Paris Sud, Bât 104, 91405 Orsay Campus France.

*mohamed-ramzi.ammar@cnrs-orleans.fr

Whatever its anthropogenic or natural origin (terrestrial and extra-terrestrial), the carbon multiscale organization (structure, nanostructure) is a fingerprint allowing to reconstruct their formation and to better constraint the parameters such as precursor nature, temperature, pressure .... Raman microspectroscopy becomes nowadays a method of choice to characterize the carbon matter and is sensitive to the full range of the structural states present in this class of materials, from perfectly crystalline to amorphous. In the case of graphitic natural carbons materials, the intensity ratio I_D/I_G has frequently been used as a reliable quantitative parameter of the structural order such as the determination of the mean 'crystallites' diameter **[1]**. As far as the meteorites are concerned, the information can be obtained on the precursor origin, the metamorphism degree **[2-3]**...

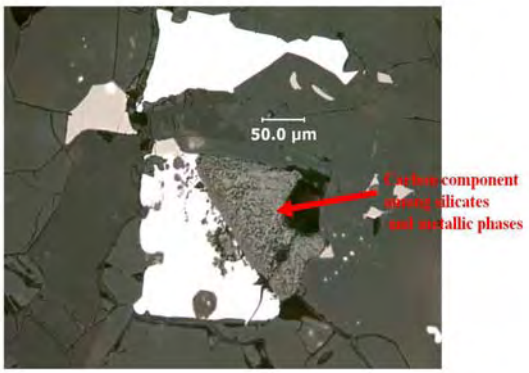

Fig.1: Optical microscopy observation of Acapulco meteorite

In order to characterize various carbons in meteorites and also to discriminate them from opaque components such as metallic phases, the optical observation has to be performed by the reflexion mode on carefully polished sections prior to performing the Raman analysis (Fig. 1). However, the reliability of such I_D/I_G ratio fails when the carbons were polished (Fig.2). This mode of preparation is known to be responsible for a remarkable growth of the D band intensity **[4-5]** and consequently induces prohibitory errors in the structural characterization and the estimation of the intrinsic and original degree of ordering in the meteorite cabons.

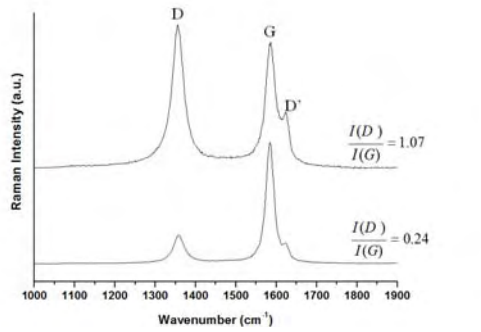

Fig.2: Raman spectra of polished (spectrum on the top) and unpolished (spectrum on the bottom) graphitized carbon obtained after 2900°C heat treatment.

In this presentation, the applicability of Raman microspectroscopy on polished graphitized carbons will be discussed in details. A new and reliable manner to obtain the intrinsic structural order from Raman spectra will be then given. An example of such application will be shown on the graphitized carbons found in the Acapulco primitive achondrite.

[1] Tuinstra F. and Koenig J.L. (1970) J Chem Phys. 53**,** 1126. [2] Le Guillou C. et al. (2010) Geochim. Cosmochim Acta. 74, 4167-4185. [3] Quirico E. et al. (2009) Earth. Planet. Sci. Lett. 287, 185−193. [4] Mostefaoui S. et al. (2000) Geochim. Cosmochim. Acta. 64,1945. [5] Pasteris J.D. (1989), Appl. Spectrosc. 43,567.

CL-SEM SPECTRAL CHARACTERISTICS OF QUARTZ AND FELDSPARS IN FRESH AND HYDROTHERMAL ALTERED VOLCANIC ROCKS (CABO DE GATA, ALMERIA, SPAIN). A. Aparicio[1] and M. A. Bustillo[2]
[1]Depto. de Dinámica Terrestre. Instituto de Geociencias. UCM-CSIC, c/ José Gutiérrez Abascal, nº2, 28006-Madrid, Spain, mcny144@mncn.csic.es ,[2]Dpto. de Geología. Museo Nacional de Ciencias Naturales. CSIC, c/ José Gutiérrez Abascal, nº2, 28006-Madrid, Spain, abustillo@mncn.csic.es

Introduction: The volcanic rocks of the Cabo de Gata are lava flows and domes formed underwater or by air emissions, being sometimes piroclastics hydromagmatic deposits. In some areas, the volcanic rocks are transformed by hydrothermal alteration forming highly silicified and feldspatized rocks, or clay- rich rocks of economic interest. In this study, different samples from outcrops of fresh and altered volcanic rocks have been studied by optical microscopy and scanning electron microscope cathodoluminescence (CL-SEM), with the aim of knowing how the spectral characteristics of quartz and feldspar are modified by the hydrothermal alteration, and characterizing the spectral features of the neoformed minerals.

Metodology: Conventional transmitted-light microscopy data together with a study in scanning electron microscope cathodoluminescence (CL-SEM) was carried out on quartz and feldspar of both fresh and hydrothermal altered volcanic rocks. In the alterated rocks, inherited and neoformed minerals were defined by optical microscopy and were separately studied.

Scanning electron observations were made using a FEI QUANTA 200 microscope (SEM) equipped with an Analytical-Inca (Oxford Instruments) analysis system incorporating an energy dispersive [EDS] X-ray detector. The SEM-CL images and spectra were obtained with a MONOCL3 Gatan instrument to record CL spectra and panchromatic and monochromatic plots. The excitation for CL measurements was provided at 25-kV electron beam. The capability of combining CL with back-scattered electron (BSE) or secondary electron (SE) mode, or energy dispersive spectroscopy (EDS) microanalysis allows us to correlate important features as spectral patterns, growth textures, structural defects, incorporation of trace element…i.e.

Results:

Quartz. The quartz magmatic crystals, from volcanic rocks without alteration, show CL-spectrum with four emission bands at around 400, 430-440, and 480nm. Sometimes, in the hydrothermal altered volcanic rocks, the inherited quartz crystals are differentiated of primary magmatic quartz because they show numerous cracks and small fractures. The inherited quartz crystals show the same bands as the primary magmatic crystals (at 400, 430- 440 and 480 nm), and others at 640 and 775 nm, that are absent or are less intense in the magmatic quartz of the fresh volcanic rock. The inherited quartz crystals from Rodalquilar outcrop have emission bands at 390, 430-440, 475, 630 and 780 nm., showing slight differences and lower intensity, in relation to inherited quartz crystals of other outcrops. In this case, both magmatic and inherited quartz contain small amounts of Al, K and Na, under EDS.

Neoformed quartz shows two types of spectrum: 1) a emission band at 560-580 nm and others with less intensity at 400 and 460nm. Under EDS, these crystals also contain small amounts of Al and K, and 2) emission bands around 589, 400 and 460 , with a new band at 310nm. In this case the amount of trace elements is higher (Al, K, Ti, Na) than the other types of quartz.

Feldspars. Magmatic plagioclase shows quite uniform CL spectra with intense bands at 570, 340-350 nm., and others of lower intensity at 430, 480, 675-710 nm. In the altered volcanic rocks, the inherited plagioclase spectra are similar. The composition of the plagioclase from the fresh volcanic rock (bitownite, labrador) and from the altered volcanic rock (oligoclase, andesine) have no influence in the CL-spectrum, only the intensity of the bands is changing .

Neoformed anorthoclase is scarce founded in some samples of altered volcanic rocks, and their spectra have the same characteristics as those of the magmatic plagioclase with maxima peaks at 570 and 345 -360 nm.

Sanidine show differences in the CL spectra between magmatic and neoformed. The spectra of magmatic sanidine has intense bands at 425, 440 and 490 nm, while the low temperature sanidine has the intense bands at 310 and 570, and others smaller at 370 and 440-460 nm.

Conclusions: The studies by CL-SEM of the minerals that constitute fresh and hydrothermal altered calc-alkaline volcanic rocks show that the CL spectra denote the provenance and origin of the minerals. A magmatic, inherited or neoformed origin could be interpretable through their respective CL spectra.
Financial support: Project CGL2008-05584-CO2-01 from the Spanish Ministry of Science and Innovation.

THE CONSECUENCES OF THE PRESENCE OF URBAN ATMOSPHERICAL PARTICLES AND AIRBORNES IN CorTen® STEEL SURFACES.

J. Aramendia*, L.Gomez-Nubla, K. Castro, I. Martínez-Arkarazo, G. Arana and J. M. Madariaga
University of the Basque Country, Department of Analytical Chemistry, P.O.Box 644, 48080 Bilbao, Spain, +34 946018297, *jaramendia002@ehu.es

CorTen steel is known because it develops a layer composed by iron oxides which protects the surface against the corrosion. The presence of different atmospherical particles and urban-marine airborne in that surface can affect the normal development of the protective rust layer that generates this kind of steel. In an urban-marine atmosphere there are many different particles such as silicates and carbonates and airborne such as NaCl, nitrates, etc. These compounds can change the nature and the composition of the rust layer affecting to the protective properties of this surface. As a consequence, unusual iron oxide phases are formed.

In the present work, several CorTen steel surfaces have been analyzed. These surfaces are exposed in Bilbao (North of Spain) to the same urban–marine atmosphere. For this study, non-destructives techniques like Raman spectroscopy and SEM-EDS (Scanning Electron Microscope coupled to Energy-Dispersive X-ray spectroscopy) have been used. With these techniques, we have been able to observe the changes of the evolution in the rust layer due to the presence of particles and airborne.

It has been detected the presence of akaganeite (β-FeOOH). Akaganeite appears in those environments with high amount of salt airborne [1]. This iron oxyhidroxide has a very porous structure and facilitates the entrance of ions and contaminants in the internal side of the structure [2]. It has been checked also that the massive presence of silicates in the steel surface can delay the passivation of the rust layer. In fact, the presence of this kind of compounds avoids the transformation of the lepidocrocite (γ-FeOOH, active phase) into goethite (α-FeOOH, stable phase) [3]. In addition, the acid gases present in the urban atmosphere affect the steel surface. For example, it has been detected gypsum in all sculptures. This gypsum can be formed by the reaction of calcite particles with SO_2 present in the atmosphere [4]. This reaction can also provide the enough SO_4^{2-} ions to generate iron sulphates with the iron present in the steel. Furthermore, iron nitrates were also identified. Iron nitrates can be formed due to the massive presence of NO_x gases that attack the steel surface.

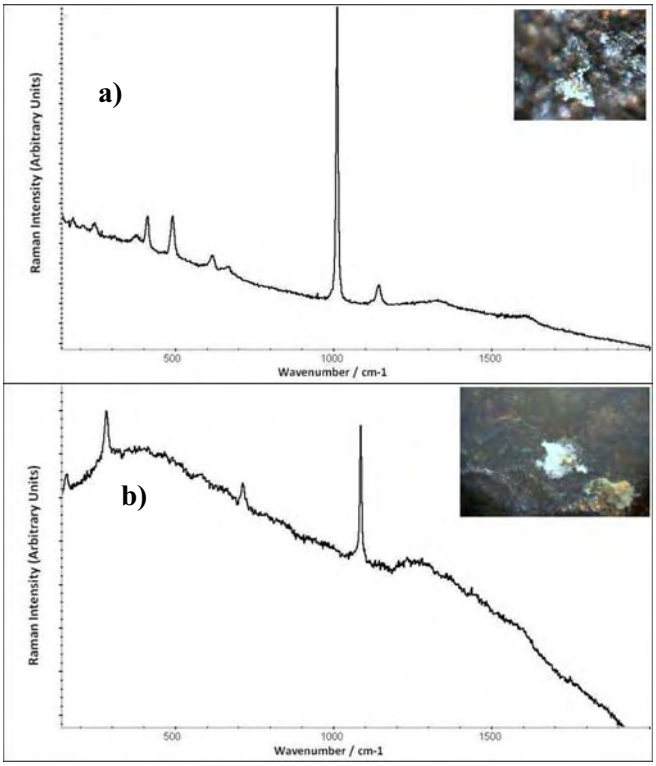

Figure 1. Raman spectra of a) gypsum and b) calcite particles found in the same CorTen steel surface.

References

[1] Kamimura T. et al. (2006) *Corros. Sci*., 48, 2799-2812.
[2] Millan A. et al. (2009) *Polymer*, 50, 5, 1088-1094.
[3] Schwertmann U. and Taylor R.M. (1972) *Clays Clay Miner*., 20, 159-164.
[4] Sarmiento A. et al. (2008) *J.Raman Spectrosc.*, 39, 1042-1049.

Acknowledgments

This work has been financially supported by Spanish Government through IMDICOGU project (BIA2008-06592)**.** J.aramendia and L.Gomez-Nubla are grateful to the Basque Government and to the University of the Basque Country (UPV-EHU) respectively, for their pre-doctoral fellowship.

NEW FINDINGS BY RAMAN MICROSPECTROSCOPY OF INCLUSIONS INSIDE A LIBYAN DESERT GLASS. J. Aramendia[1], L.Gomez-Nubla[1], S. Fdez-Ortiz de Vallejuelo[1], K. Castro[1], X. Murelaga[2] and J. M. Madariaga[1]

[1] University of the Basque Country, Deprt. Analytical Chemistry, P.O.Box 644, 48080 Bilbao, Spain. Tel: +34 946018297. Email: jaramendia002@ehu.es

[2] University of the Basque Country, Deprt Stratigraphy and Paleontology, P.O. Box 644, 48080, Bilbao, Spain

Libian Desert Glass (LDG) has been a mistery for scientist since its discovery in 1932. LDG is a natural glass that is scattered in the Western Desert of Egypt, near the Libyan border. It is estimated to be 28.5 million years old. There is a controversy around the genesis of these glasses. Apparently, they could be created by an impact process or by an airburst [1]. The large volume of the glass and its very high silica content led to the assumption that it formed by shock-melting of quartz sand and/or sandstone during a meteorite impact [2]. This hipothesis would be argued because of the crater absence. Some sciencist affirm that depends on the chemical composition of the LDG it could be known the origin of the glass [3]. Several works studied the composition of LDG, but only a few of them were carried out using Raman spectrometry. This work shows new information about the mineral composition of the inclusions present in LDG.

In this work two samples of LDG were analyzed. The analysis of the samples were carried out with two Raman spectrometers: InnoRam ultramobile B&WTEK$_{inc}$, and Renishaw InVia Raman espectrometer coupled to a DMLM Leica microscope. The last equipement has a 514 nm and a 785 nm excitation laser. In order to complement the information obtained from Raman spectra it was used a portable ArtTax X-ray micro-fluorescence equipment (μ-XRF) by Brucker.

According to Raman data, it has been possible the determination of LDG matrix, supposedly a glassy matrix (≈1370 cm^{-1}, ≈1600 cm^{-1}). This result differs from the data found in other studies that affirm that the bulk material is formed of glassy matrix but with broad Raman bands around 480 cm^{-1} and 820 cm^{-1}. With this technique different inclusions were identified, such as: quartz (SiO_2,), anatase (TiO_2), calcite ($CaCO_3$), Na_2CO_3 and carbonaceus matter (Fig.1). In the case of these samples of LDG the brownish inclusions are composed of pure quartz, with Raman bands 204(m), 263(s), 354(s), 401(vs), 463(vs), 695(vs), 806(s), 1081(vs), 1158(vs) cm^{-1}. With regard to the calcite, it was not identified in other LDG studies and this compound could be related with the anhydrite found in other publications [4].Another compound has been found by Raman spectroscopy, with bands at 513 and 529 cm^{-1}. According to literature it could be a microcline feldspar. The elemental composition of LDG obtained by using the XRF, where the main elements present in the samples are: Si, S, K, Ca, Ti and Fe, would be consistent with the molecular composition obtained by Raman spectroscopy.

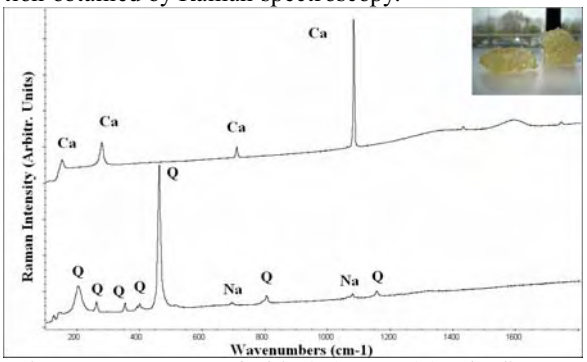

Figure 1. Raman spectra of calcite (Ca), Quartz(Q) and sodium carbonate (Na) found in LDG.

Compound	This study (Wavenumber/cm^{-1})	Other LDG studies (Wavenumber/cm^{-1})
LDG matrix	Silicate: ≈1370(br) ≈1600(br)	Glassy matrix: 480(br) 820(br)
Quartz (SiO_2)	204(m) 263(w) 354(w) 401(vw), 463(vs) 806(w) 1158(vw)	208(w) 465(m)
Anatasa (TiO_2)	143(s)	142(vs) 227(vw) 395(vw), 515(vw) 637(w)
Calcite ($CaCO_3$)	153(w) 279(m) 710(w) 1085(vs)	Not Found
Sodium carbonate (Na_2CO_3)	695(vw) 1081(w)	Not Found
Anhydrite ($CaSO_4$)	However Not Found	418(vw) 1018(vs) 1130(w)
Amorphous carbon	≈1300(br) ≈1600(br)	≈1300(br) ≈1600(br)
Microcline feldspar	513(m) 529(m)	Cristobalite, etc

References

[1] Koeberl C. (2011) *CAG 23,* Abstract #7.

[2] Greshake A. et al. (2010) *Meteoritics & Planet. Sci., 45,* 6, 973-989.

[3] Koeberl C. et al. (2004) *Meteoritics & Planet. Sci., 39,* 8, 1273-1285 .

[4] Swaenen M. et al. (2010) *Anal. Bioanal. Chem., 397,* 2659-2665.

Acknowledgments

J.Aramendia and L.Gomez-Nubla are grateful to the Basque Government and to the University of the Basque Country (UPV-EHU) respectively, for them predoctoral fellowship. This work has been financially supported by the Basque Government through the Environmental Analytical Chemistry Project 2007–2012 (Ref. IT-245-07).

SPECTROSCOPIC CHARACTERIZATION OF FERRUGINOUS CEMENTS IN A TEMPERATE BEACHROCK FORMATION CLOSE TO NERBIOI-IBAIZABAL ESTUARY (TUNELBOKA COVE, BAY OF BISCAY).

N. Arrieta[1]*, A. Iturregi[1], I. Martinez-Arkarazo[1], X. Murelaga[2], J.I. Baceta[2] and J.M. Madariaga[1]. [1] Department of Analytical Chemistry, University of the Basque Country (EHU/UPV), P.O. Box 644, E-48080 Bilbao, Spain. [2] Department of Stratigraphy and Palaeontology, University of the Basque Country (EHU/UPV), P.O. Box 644, E-48080 Bilbao, Spain. *Tel.: +34 94 60182 98, nikole.arrieta@ehu.es

Beachrocks are coastal sedimentary formations mainly occurring along equatorial-tropical coasts that result from a relative rapid cementation of beach sediments by the precipitation of carbonate cements. A series of physico-chemical and biologically-induced processes have been invoked to explain such rapid cementation [1-4]. Beachrock cements are usually dominated by $CaCO_3$ polymorphs which rarely are overlied by non continuous iron-rich dark layers [5].

The present work is focused on the occurrence of an unusual temperate setting (43ºN latitude) beachrock located in Tunelboka cove, close to the Nerbioi-Ibaizabal estuary (Bay of Biscay, North of Spain).

A previous research work carried out on the area and in some adjacent beaches which present these lithified structures, revealed the existence of different cement generations (CG) by means of Raman microspectroscopy, SEM-EDX analyses and petrographic descriptions: CG 1 (aragonite, high-magnesium calcite and silicates), CG 2 (aragonite) and CG 3 ($CaCO_3$ polymorphs and iron oxides) [6].

Besides the $CaCO_3$ cements, some iron containing cements enclosing the beach grains were also observed in several lithified outcrops of the Tunelboka cove. The ferruginous cements appeared in two forms: (i) acompaining carbonate cements as discontinuous an non-homogeneous layers and as (ii) uniform an continuous cements between the beach grains. To our knowledge, the second cementing form has not been described previously in beachrock formations in contrast to the (i) cements.

The characterization of the ferruginous cements have been carried out by means of Raman spectroscopy. For that purpose, an InnoRaman® (B&WTEK$_{INC}$) ultramobile spectrometer, equipped with 20x and 50x focusing lens, an excitation wavelength of 785 nm, a CCD detector (Peltier cooled) and BWSpec 3.26_38 software for the data acquisition was used.

First of all, the effect of laser power was studied in order to avoid decomposition/transformation processes of oxides and hydroxyoxides during measurements [7].

The Raman spectra taken in the (i) cements, showed limonite ($FeO(OH)\cdot nH_2O$, with Raman bands at 241w, 298s, 393vs, 478w, 548m), aragonite ($CaCO_3$, 146w, 205m, 705m, 1085vs) and silicates mixtures (1159br, 1258vs, 1365br, 1837br, 1939br). Exporadically mixtures of limonite and quartz (SiO_2, 205m and 465vs) or hematite (α-Fe_2O_3, 225vs, 292vs, 410s, 496m, 611m) and aragonite mixtures were observed as well.

The Raman spectra got in the continuous ferruginous cements (ii), revealed limonite as the main cementing mineral phase. Frecuently, hematite remains were also identified into the limonite cement (Fig. 1). Moreover, traces of other mineral phases such as wüstite (FeO, 459br, 653br), anatase (TiO_2, 147vs, 199w, 398s, 510m, 638s), magnetite (308m and 668vs) and lepidocrocite (γ-FeO(OH), 213m, 246vs, 304m, 344m, 373vs, 523m, 645m) were also identified. It is remarkable that lepidocrocite appeared as a thin layer covering hematite grains, which suggest the superficial transformation of hematite. Indead, hematite is thought to be the main original iron containing mineral coming from a submarine disposal area located 4 miles north of the mouth of the estuary where old steel factories dumped rubble derived from blast furnace during the first half of the XX century.

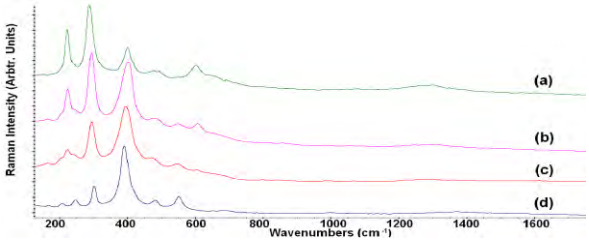

Fig. 1. Raman spectra obtained from the continuous ferruginous cement, (ii). (a) hematite, (b) and (c) different hematite proportions in limonite based cement; (d) limonite.

Taken into account the mineral phases identified by Raman, our hypothesis is that the iron mineral wastes arrived to the beach, cemented and part of them disolved by different mechanisms (including acid aerosols attack) to reprecipitate as limonite.

References

[1] Díez B. et al. (2007) *Appl. Environ. Microbiol, 73*, 3656-3668. [2] Grischler E. et all. (2007) *Geochemical Sediments&Landscapes*, Wiley-Blackwel, UK, 365-390. [3] Vousdoukas M.I. et al. (2007) *Earth Sci. Rev., 85*, 23-46. [4] Vieira M.M., Ros L.F.D (2007) *Sediment. Geol., 192*, 207-230. [5] Strasser A. et al. (1989) *Sediment. Geol., 62,* 89-100. [6] Arrieta N. et al. (2011) *Spectrochim. Acta A*, doi:10.1016/j.saa.2011.01.031. [7] de Faria D.L.A. et al. (1997) *J. Raman Spectrosc., 28,* 873-878.

Acknowledgements

This work has been financially supported by the Basque Government through the Environmental Analytical Chemistry Project (ref. IT-245-07). N. Arrieta is grateful to the University of the Basque Country (UPV/EHU) for her pre-doctoral fellowship.

MADRID L6 CHONDRITE (FALL 1896): ESEM-CATHODOLUMINESCENCE SURVEY. O. Azumendi[1], L. Tormo[2], J. Ruiz[1], J. Garcia-Guinea[2], [1]Departamento de Geodinamica, Universidad Complutense de Madrid. Madrid 28040 Spain. oscarazumendi@yahoo.es, [2]Museo Nacional Ciencias Naturales. CSIC. 28006 Madrid. Spain. ltormo@mncn.csic.es

Introduction: The Madrid meteorite fell in Madrid downtown the 10th of February of 1896, seconds before 9:30 am. Ten samples were recovered in the city, just after a bright white-blue light and a strong explosion scared and advertised the people of the meteorite fallen. The heaviest and lightest weight 143.79 and 1.3 respectively. The meteorites distribution formed an ellipse NW/SE orientated, where the largest meteorites fell in the NW. The compositions of olivines (Fa_{25}) and low-Ca pyroxenes (Fs_{24}) in Madrid meteorite are within the range of equilibrated L chondrite. The amount of troilite (5.02 wt. %) and metallic Fe-Ni (5.95 wt. %) support this classification. The material is highly crystallized and brecciated, with chondrules poorly defined and clearly visible (bigger than 50µm across) feldspars. This classify the meteorite in the petrographic type 6: the Madrid meteorite is therefore an impact melt breccia L6 ordinary chondrite. The main aim of this work is to analyse feldspars and whitlockites from Madrid meteorite by cathodoluminescence and to determine the trap structure. The impact events of this chondrite have also been using the mineralogy and ESEM images interpretations.

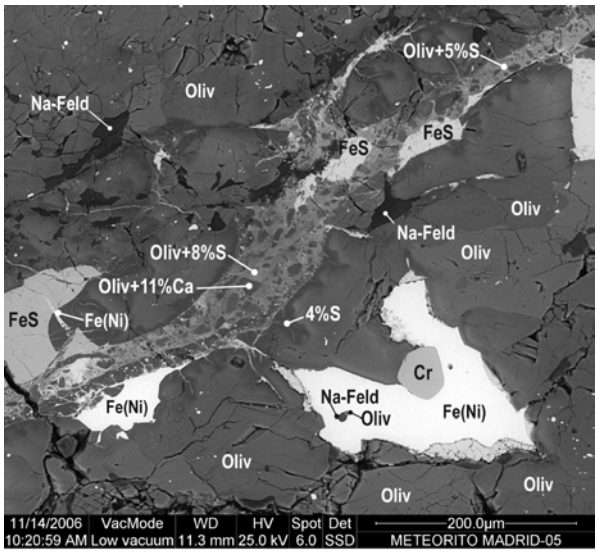

ESEM-BackScattering Image showing a schock vein composed by a mixture of Olivine, Troilite and infilled iron in very thin veins sized from 1 to 3 microns.

Schock veins: In similar cases have been demonstrated: (i) the presence of eutectic Fe and FeS indicates that the temperature during melt formation exceeded 988ºC, (ii) the troillite nodules occurred in many shocked chondrites being characteristic of the shock stage S3-S6. This L6-chondrite suffered two main impacts episodes. The first one produced the breccia, with thick dark areas, very heterogeneous, mixed with the unmelted minerals. This shock is been dated by $^{40}Ar/^{39}Ar$ in 470 Ma, when a big body impacted L6 parent body (all L6 meteorites have the same porphyritic to holocristaline texture, produced by this impact), and a mayor degassing event occurred. The second shock melted the Fe and FeS, propagating the hot liquid and gaseous metals through the breccia, entering into the minerals background in very thin shock veins of few microns.

Merrilite cathodoluminescence: This $CaPO_4$ phase is related with mesostasis processes having a late crystallization. The characteristic emission peaks of the CL spectra from 300 nm to 1000 nm has been associated to specific activators such as Ce^{3+}, Eu^{2+}, Mn^{2+}, Dy^{3+}, Sm^{3+} and Sm^{2+} the two structural positions of calcium.

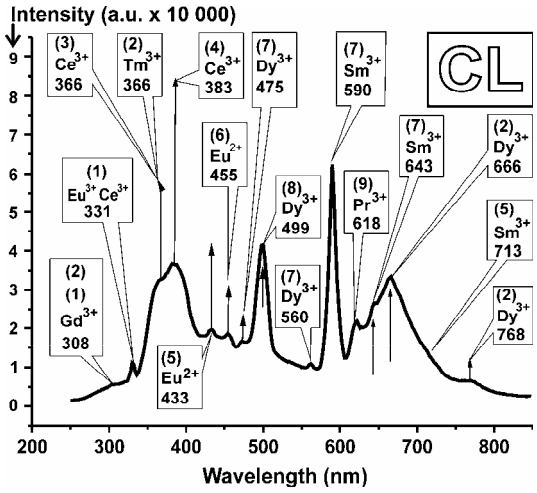

This merrilite ($CaPO_4$) from Madrid L6 Chrondrite emits cathodoluminescence peaks attributed to Ce^{3+} (360-380 nm peak), Dy^{3+} (499 nm peak and 666nm peak), Sm (590 nm peak) and Tm^{3+} (366 nm peak).

RAMAN SPECTROSCOPY IN CORALS AND PEARLS. Laura Bergamonti, Danilo Bersani and Pier Paolo Lottici, Physics Department, University of Parma, Viale G.P. Usberti 7/a, 43124 Parma, Italy.
email: lottici@fis.unipr.it

Introduction: Corals and pearls are organic gem material used for ornamental purposes. Apart from black and gold corals, formed by hornlike organic matter, red to pink corals and pearls consist mainly of calcium carbonate in calcite or aragonite forms. The formation and nature of calcium carbonate have been largely investigated by means of Raman spectroscopy [1], [2], [3]. Raman scattering may be helpful to distinguish between coral and pearl species through the identification of their calcite or aragonite structure, or differences in the pigments.

Experimental: Here we report on the Raman spectra taken at 632.8 nm and at 473.1 nm with a micro-Raman Labram HORIBA Jobin-Yvon instrument equipped with 50x objective on a series of red to pink corals and on natural pearls.

Results: The Raman spectrum of coral identifies the biogenic calcium carbonate phase of the skeleton. The Raman spectrum of natural-color coral typically reveals additional peaks related to organic pigments. Pearls show the aragonite peaks at 206 cm^{-1}, 702-706 cm^{-1} and at 1086 cm^{-1}.

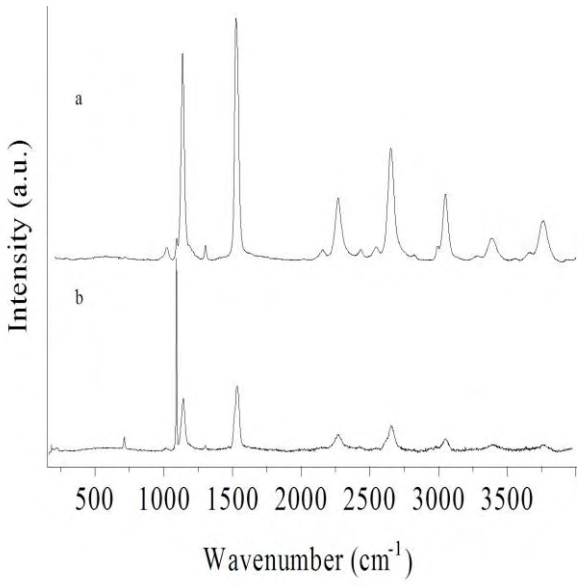

Fig.1 – Raman spectrum taken with 473.1 nm excitation showing the strong carotene features at 1132 cm^{-1} and 1523 cm^{-1} and a series of overtones and combination bands, in addition to characteristic peaks of $CaCO_3$: (a) Corallium rubrum (283, 713, and 1087 cm^{-1}, calcite); (b) pink cultured pearl (aragonite).

The nature of the dyes responsible for the natural color in pink-to-red corals and pearls has been largely investigated by means of Raman spectroscopy [4], but the scientific debate on their nature is still open [5]. Carotenoids or mixtures of polyenes [6] have been proposed. The presence of high intensity overtones and combination frequencies in the Raman spectrum taken with the "resonant" 473.1 nm line (Fig.1) enables the investigation of the characteristic C=C stretching vibrations, whose frequencies seem to depend on the polyenic chain length, and the C–C stretching vibrations, whose frequencies are more influenced by the presence of the $–CH_3$ substituting groups in carotenoids [6], [7], [8]. Here we report additional data on the vibrational frequencies and their combinations as found in the Raman spectrum of different corals and pearls.

Raman analysis can establish conclusively if the color of corals or pearls is natural or obtained by dyeing. The dyed coral samples do not exhibit the Raman spectrum associated with carotene (Fig.2). Some examples with both excitation lines are reported and the dyeing substance has been identified.

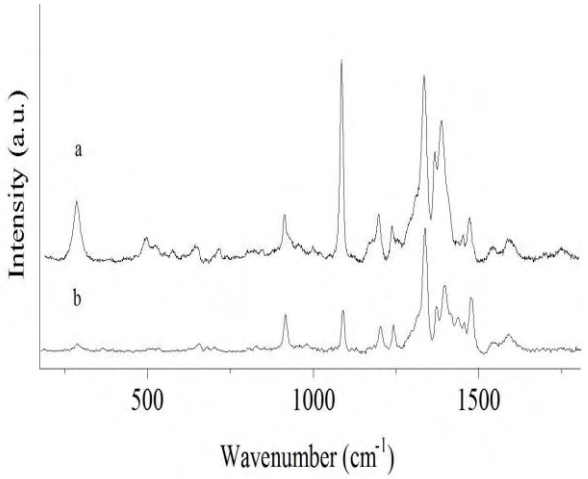

Fig.2 – Raman spectrum taken at 632.8 nm (a) and at 473.1 nm (b) of a dyed "red coral". No carotene features are present.

References: [1] Urmos J., Sharma S.K., Mackenzie F.T. (1991) *Am. Mineral., 76*, 641–646. [2] Kaczorowska B. *et al.* (2003) *Anal. Bioanal. Chem., 377*, 1032–1037. [3] Zakaria F.Z. *et al.* (2008) *J. Raman Spectrosc., 39,* 1204–1209. [4] Barnard W. and de Waal D. (2006) *J. Raman Spectrosc., 37*, 342–352. [5] Karampelas S. *et al.* (2009) *Gems Gemol., 45,* 48-52. [6] de Oliveira V.E. *et al.* (2010) *J. Raman Spectrosc*., *41*, 642-650. [7] Fritsch E., Karampelas S. (2008) *Spectrochim. Acta A, 71*, 1627. [8] Karampelas S. *et al.* (2009) *Eur. J. Mineral., 21*, 85–97.

RAMAN INVESTIGATION ON PIGEONITE IN UREILITE. D. Bersani[1], L. Mantovani[2], M. Tribaudino[2] and P. P. Lottici[1], [1] Dipartimento di Fisica, Viale Usberti 7/A, 43100 Parma, Italy, e-mail: danilo.bersani@unipr.it, [2] Dipartimento di Scienze della Terra, Viale Usberti 157/A, 43100 Parma, Italy

Introduction: The family of ureilites is one of the most studied among achondrites. Ureilites are mainly composed by a mineral assemblage of pyroxene and olivine [1], [2]. Both ortho and clinopyroxenes are present, and clinopyroxenes are mostly pigeonite. Pigeonites have a potential in unraveling the thermal history of the parent body: their composition, TEM microtextures and single crystal site partitioning are therefore widely studied [3], [4], [5]. On the other hand, the potential of spectroscopic methods was little exploited. Raman spetroscopy provides a non-destructive method of investigation, which can be used for on site studies, as well as for laboratory investigations [6]. The Raman technique was used in ureilites to test the presence of diamond [7]: important information are expected also from the study of silicates.

The relation between composition and Raman spectra in pyroxenes was studied in [8] and [9], but very few data were collected in the pigeonite field; recently it was also shown that, as an effect of the $P2_1/c$ to $C2/c$ phase transition, the relation between Raman peak positions and composition does not follow the same trend in pigeonite as in other clinopyroxenes [10]. Therefore for pigeonite a specific calibration is required. Moreover, the analysis of the peak-width can provide further information on the sample microtextures, preliminary to TEM analysis.

First results on the Raman spectra of pigeonite in three ureilites are here reported and compared with those obtained on natural and synthetic samples with different iron content.

Results: Raman spectra of pigeonite in three ureilites (Y791538, ALHA77257 and RKPA80239, Wo respectively 9.4, 6.4 and 6.4, *mg* = 91.2, 86.3 and 84.3 [4]), in an iron free synthetic pigeonite sample ($Di_{15}En_{85}$, Wo7.5 and *mg* = 100 [11]) and in the volcanic iron richer sample BTS308 (Wo10 and *mg* = 52 [12]) were collected (Fig. 1). Peak fitting was done via Lorentian profile functions, and related with composition. The spectra of pigeonites from ureilites are quite similar to the iron free synthetic one, and can be distinguished from Fe richer BTS308 by the two peaks of similar intensity at 670 cm^{-1}, nearly unresoved for Fe richer pigeonite. The wavenumber of the main peaks changes linearily with *mg* (Fig. 2), whereas, due to the small difference in Ca content, no correlation is found with Wo.

Peak-width increases according to Di15< ALHA77257 ≅ RKPA80239<Y791538<BTS308. The result can be related to previous TEM observations: in samples BTS308 and Y791538, few nanometer sized antiphase domains were observed together with mottled textures, indicating compositional heterogeneity. In ALHA77257 and RKPA80239, even if antiphase domains are larger, stacking disorder is present. The synthetic sample $Di_{15}En_{85}$ is homogeneous.

Conclusions: Preliminary results have shown the potential of Raman spectroscoy as a non destructive compositional probe of microstructures in pigeonite. Further studies in ureilic pigeonite are in progress to better define the relationships between composition and peak position and between linewidth and microstructures.

References: [1] Berkley J.L. *et al.* (1980) *GCA, 44*, 1579. [2] Goodrich C.A. *et al.* (1987) *GCA, 51*, 2255. [3] Goodrich C.A. *et al.* (2001) *GCA, 65*, 621 [4] Tribaudino M. (2006) *Meteoritics & Planet. Sci., 41,* 979. [5] Michouki *et al.* (2010) *Meteoritics & Planet. Sci., 45,* A145. [6] Wang A. *et al.* (2004) *JRS, 35,* 504. [7] Ferroir T. *et al.*, (2010) *EPSL, 290,* 150. [8] Huang E. *et al.* (2010) *Am. Min., 85,* 473. [9] Wang A. *et al.* (2001) *Am. Min., 86,* 790. [10] Mantovani L. *et al.* (2010) *89th SIMP meeting,* 262. [11] Pasqual D. *et al.* (2000) *Am. Min., 85,* 953. [12] Tribaudino M. *et al.* (2002) *Am. Min., 87,* 648.

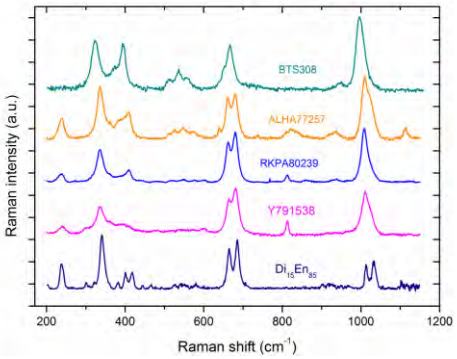

Fig. 1 Raman spectra of the pigeonite samples

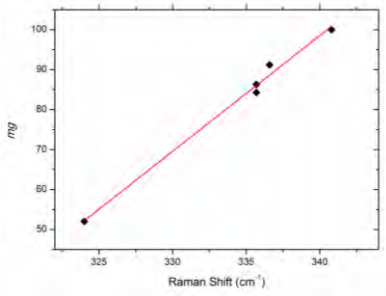

Fig. 2. Raman shift vs *mg* for the peak at 330 cm^{-1}.

IN SITU PLANETARY MINERALOGY USING SIMULTANEOUS TIME RESOLVED FLUORESCENCE AND RAMAN SPECTROSCOPY. J. Blacksberg[1] and G.R. Rossman[2], [1]Jet Propulsion Laboratory, California Institute of Technology, 4800 Oak Grove Dr., Pasadena, CA 91109, Jordana.blacksberg@jpl.nasa.gov, [2]California Institute of Technology, Division of Geological and Planetary Sciences, Pasadena, California 91125, grr@gps.caltech.edu

Introduction: Micro-Raman spectroscopy is one of the primary methods of mineralogical analysis in the laboratory, and more recently in the field. Because of its versatility and ability to interrogate rocks in their natural form (Figure 1), it is one of the frontrunners for the next generation of *in situ* instruments designed to explore adiverse set of solar system bodies (e.g. Mars, Venus, the Moon, and other primitive bodies such as asteroids and the Martian moons Phobos and Deimos), as well as for pre-selection of rock and soil samples for cache and return missions.

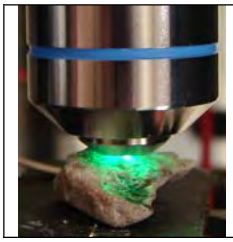

Figure 1. Image of our pulsed 532nm laser focused on a natural mineral sample without prior sample preparation. The Raman and fluorescence spectra are collected and sent to the spectrometer through the same objective lens.

Fluorescence spectroscopy offers complementary information revealing the many impurity and defect states present in minerals[1]. For a typical continuous wave (CW) green Raman measurement, fluorescence is viewed as a nuisance and is often so strong that the weaker Raman signal cannot be distinguished above the background. We discuss the use of time resolution to obtain Raman spectra under even the most extreme fluorescence conditions [2]. Since Raman occurs instantaneously, and fluorescence decay times vary, it is possible to separate them using time resolution (Figure 2). In addition to obtaining fluorescence-free Raman, we can distinguish the fluorescence spectra as well as any other time-dependent phenomena that may be present such laser induced breakdown spectroscopy (LIBS) when performed under appropriate conditions.

Time Resolved Spectroscopy for Planetary mineralogy: Raman spectroscopy is under consideration for a host of landed planetary missions aimed at definitive mineralogical studies. For example on Mars, evidence for an early water rich history is supported by the probable presence of altered minerals such as goethite, jarosite, Fe-, Mg-,and Ca- sulfates, hydrated sulfates (e.g., kieserite), phyllosilicates (e.g., clays), and Fe-, Mg-, and Ca- carbonates [3]. Because many of these altered minerals are known to exhibit strong fluorescence, the use of time resolution would be expected to significantly improve the number of successful measurements on Mars. We demonstrate this

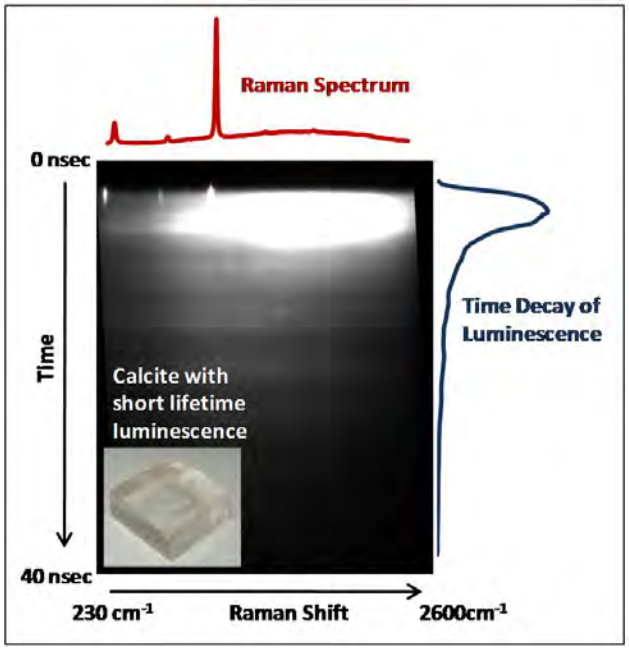

Figure 2. Streak Camera Image taken on a natural calcite sample with short lifetime fluorescence. The Raman spectrum is distinguishable during the laser pulse, and the fluorescence lifetime is ~ 8 ns.

technique using a green pulsed miniature microchip laser synchronized with a streak camera. We will discuss spectra obtained on a variety of strongly fluorescnt altered minerals, with particular relevance to Mars (e.g. sulfates, phosphates, and clays). For many of these minerals Raman spectra were completely obscured by large background fluorescence when using CW Raman. We will conclude with a discussion of the challenges and feasibility of developing an on-surface time resolved spectrometer for planetary exploration.

Acknowledgements: The research described in this publication was carried out at the Jet Propulsion Laboratory, California Institute of Technology, under a contract with the National Aeronautics and Space Administration. CW Raman measurements were performed at the California Institute of Technology, and time-resolved experiments at JPL.

References: [1] M. Gaft et al., Modern Luminescence Spectroscopy of Minerals and Materials, Springer-Verlag, 2005. [2] J. Blacksberg, G. Rossman, and A. Gleckler (2010) *Applied Optics, 49 (26),* 4951-4962, [3] D.W. Ming et al. (2008) in *The Martian Surface: Composition, Mineralogy and Physical Properties, J.F. Bell III, ed.,* 519-540

QUANTITATIVE RAMAN SPECTROSCOPY (QRS), A POTENTIAL TOOL TO STUDY THE FORMATION MECHANISM OF CARBONATES OF EARLY EARTH AND MARS.

L. J. Bonales[1, 2], M. V. Muñoz-Iglesias[1], M. Sanchez-Román[1], D. Fernandez-Remolar[1] and O. Prieto-Ballesteros[1] . [1]Centro de Astrobiología. INTA-CSIC. Torrejón de Ardoz, 28850 Madrid. Spain, [2]Departamento de Química Física I, Facultad de Química, Universidad Complutense, 28040 Madrid, Spain. (bonales@cab.inta-csic.es)

Introduction: Carbonates form an important mineral group for astrobiological/geological studies, since they (1) can directly or indirectly be the result of microbial metabolic processes, (2) are very common in Earth´s geological record, and (3) can remove C from the planetary biogeochemical cycle. Calcite ($CaCO_3$) and dolomite [$CaMg(CO_3)_2$] are the two most abundant carbonate minerals on Earth. This is consistent with equilibrium thermodynamic considerations for the environmental conditions under which most sedimentary carbonate minerals form and persist [1].

In the present study, we focus on the abiotic formation of carbonates and we show that QRS is a good tool to get new insights about their mechanism of formation. Our findings are of fundamental importance for understanding modern environments in which carbonate minerals form as a window into the geologic past, and can explain how their formation can affect the biogeochemical cycles of other planets like Mars.

Materials and Methods: Reactants were purchased from Sigma-Aldrich. Raman spectra were excited with a 532 nm line of an solid laser at power 200 mW. After passing a monochromator (Horiba JobinYvon HRi 550) the scattered light was detected with a CCD. *High Pressure Planetary Environment Chamber* is a facility of Centro de Astrobiologia (Madrid, Spain), and consists of a stainless steel high pressure cell. It has a control temperature system and four ports for making different "in situ" analysis.

Results: Carbonate synthesis can be performed using two-ways. First, formation of MCO_3 from bicarbonate (Eq.1) and second, from $CO_2(g)$, which once is solubilized to $CO_2(aq)$ (Eq.2) and protonated (Eq.3) can react with free M^{2+} to give MCO_3 (Eq. 4).

$$M(ClO_4)_2+2NaHCO_3 \leftrightarrow MCO_3(s)+CO_2(g)+M(ClO_4)_2 \quad (1)$$

$$CO_2\,(g) + H_2O \leftrightarrow CO_2\,(aq) \quad (2)$$

$$CO_2\,(aq) + H_2O \leftrightarrow H_2CO_3 \quad (3)$$

$$H_2CO_3 + M(ClO_4)_2 \leftrightarrow MCO_3\,(s) + H_2ClO_4 \quad (4)$$

where M means Ca, Mg, Fe, Mn, Ba, and/or Sr. These reactions are governed by the concentration of M^{2+} in the medium and several parameters such as pressure (P), temperature (T), ionic strength and pH. The first method can be studied measuring the decreasing in concentration of the bicarbonate ion, while the second one can be analyzed by measuring the solubility of CO_2 (Eq. 2) (Note that the Eq. 2 is the limiting step in the second method). We highlight QRS as a tool to analyze the kinetic of these reactions.

QRS analysis of HCO_3^-: The vibrational spectra (lattice and internal modes) of hydrogen-carbonate in aqueous solution were carried out over a wide range of concentrations (0.01-0.1M), taking into account the concentration of CO_3^{2-} formed by autoprotolysis of HCO_3^-. The HCO_3^- and CO_3^{2-} activities in each solution were determined using the software PHREEQC [2]. The relationship between the calculated HCO_3^- and CO_3^{2-} activities, and the relative area of the most intense bands in the Raman spectra allows us to calculate the activity of HCO_3^- at any time in the Eq. 1, and, therefore the amount of MCO_3 formed as a function of time, T, P and pH.

QRS analysis of $CO_2(aq)$: We performed a systematic study of the aqueous CO_2 in pure water (Eq. 1) at different T and P by using Raman spectroscopy. The vibrational spectra of the gas-water mixture at equilibrium were performed at certain conditions of T and P from which the solubility of CO_2 in water is well know. The existence of an isobestic point in water allows normalizing all the obtained spectra at different physical conditions. We obtained a calibration curve for the $CO_2(aq)$ based on the relative Raman area of the dominate peak of the spectra and the theoretical solubility of CO_2 at each condition. From this calibration curve, it is possible to calculate the amount of $CO_2(aq)$ during the formation process (Eq. 2), and consequently the amount of MCO_3 precipitated at different conditions of T, P and ionic strength.

This study can help to clarify paradigms from the early Earth and Mars environments. We simulate the formation conditions of some ancient carbonates assuming: a) the atmosphere contains high concentration in CO_2 during Hadean-Archean, therefore we use the second method (Eq. 2, 3 and 4) at T >20ºC and P up to 300bar; b) there were some global glacial crisis during Proterozoic, so for this aim we will study the first synthesis method (Eq. 1) at <0ºC and P up to 50bar.

Acknowledgements: This work was supported by MALTA-CONSOLIDER (CSD2007-00045) and QUIMAPRESS (S2009/PPQ-1551) projects.

References: [1] Morse and McKenzie (1990) Geochemisty of sedimentary carbonates. Developments in Sedimentology, 48. Elsevier, New York. 707 pp.[2] Parkhust and Appelo (1999): User´s guide to PHREEQC (V.2) – a computer program for speciation, batch reaction, one-dimensional transport, and inverse geochemical calculations. Water-Resources Investigations Report 99-4259. USGS, Denver, CO.

SHOCK-INDUCED PHASE TRANSFORMATIONS IN MELT POCKETS WITHIN MARTIAN METEORITE NWA 4468. Suporn Boonsue and John Spray, Planetary and Space Science Centre, University of New Brunswick, NB E3B 5A3, Canada. sboonsue@unb.ca, jgs@unb.ca

Northwest Africa (NWA) 4468 is 675 g martian meteorite recovered from the Western Sahara in 2006 [1]. It is an olivine basaltic shergottite, comprising clinopyroxene, olivine, maskelynite, chromite, ilmenite, Ca-phosphate polymorphs, troilite and pyrrhotite. The sample shows both bulk (maskelynite formation) and localized shock effects (excursions in veins and melt pockets). There have been several studies of NWA 4468, including geochronology, petrology and bulk composition. The formation of high pressure polymorphs in melt pockets, however, has been only noted. Here we report the presence of high pressure polymorphs in melt pockets and their relation to the presence of $Ca_3(PO_4)_2$ phases using Field Emission Scanning Electron Microscopy (FESEM) and micro-Raman Spectroscopy, including Raman mapping (Figures 1, 2 & 3). We have discovered three different $CaPO_4$ polymorphs in the melt pockets, and their crystal structure has been confirmed by Raman analysis [2] [3]. The mineral assemblages of the melt pockets are apatite, merrillite, tuite, Fe-rich clinopyroxene, pigeonite, chromite, troilite, stishovite, and hollandite in a microcrystalline matrix comprising pyroxene, apatite, merrillite, Fe-Ti-Cr oxide and silica glass. Ringwoodite is developed at the rims of pockets. The mineral assemblages of the melt pockets are indicative of solid state transformations, nucleation and recrystallization at high temperatures and pressures. The stability fields of these minerals are used to infer the pressure and temperature conditions reached locally in the melt pockets to 23 GPa, and 2000°C [3] [4].

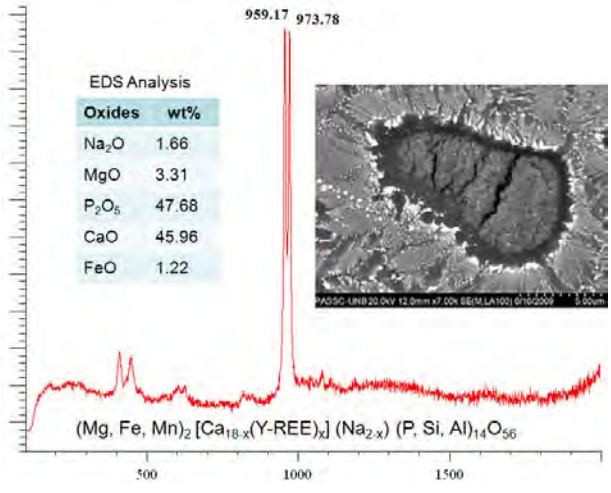

Figure 1. Intense twin peaks at 959 and 974 cm^{-1} and less intense peaks at 410, 577, 637 and 1093 cm^{-1} are characteristic of merrillite (β-apatite) (Xie et al., 2002).

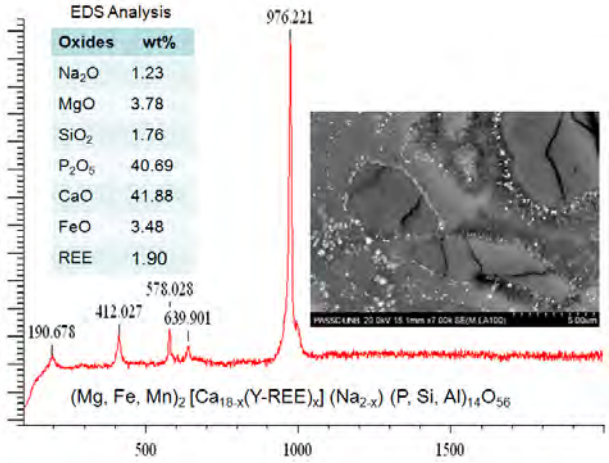

Figure 2. Raman spectrum of tuite (γ-apatite) in the pocket displays only one intense peak at 976 cm^{-1}, and less intense peaks at 1095, 410.8, 577, 639 cm^{-1}. The strong peak at 976 cm^{-1} is induced from symmetrical stretching vibrations of the PO_4 group (Xie et al., 2003).

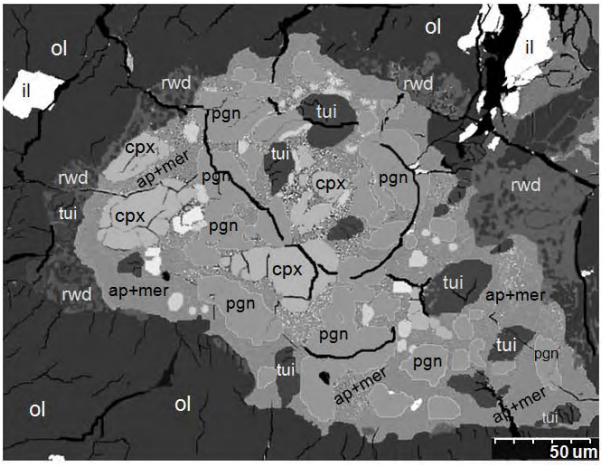

Figure 3. Combined SEM and micro-Raman analysis of a melt pocket and its mineral assemblage (ap- apatite, cpx-clinopyroxene, il-ilmenite, mer-merrillite, ol-olivine, pgn-pigeonite, rwd-ringwoodite, tui-tuite).

References:

[1] A.J. Irving et al., (2007) *LPSC XXXVIII*, Abstr.# 1526. [2] Xie, X., Minitti, M.E., Chen, M., Mao, H.K., Wang, D., Shu, J., Fei, Y., (2002) *Geochim. Cosmochim. Acta, 66*, 2439-2444. [3] X. Xie, , M.E. Minitti, M. Chen, Ho-Kwang Mao, D. Wang, J. Shu and Y. Fei (2003) *Eur. J. Mineral. 15*, 1001-1005. [4] Beck, P., P. Gillet, L. Gautron, I. Daniel, and A. El Goresy (2004), *A Earth Planet. Sci. Lett., 219*, 1 –12.

Raman Microscopy of Samples of Martian Analogue Material with Cyanobacteria.

Ute Böttger[1], Jean-Pierre de Vera[1], Jörg Fritz[2], Iris Weber[3], and Heinz-Wilhelm Hübers[1,4], [1]Department of Experimental Planetary Physics, Institute of Planetary Research, German Aerospace Center (DLR e.V.), Berlin (Ute.Boettger@dlr.de), [2]Museum für Naturkunde, Leibnitz-Institut an der Humboldt Universität zu Berlin, Germany, [3] Institute of Planetology, Muenster, Germany, and [4]Technische Universität Berlin, Institut für Optik und Atomare Physik, Berlin, Germany

Introduction Raman Laser Spectrometer - RLS - onboard ExoMars 2018 will perform measurements on Mars to identify organic compounds and mineral products as an indication of former and recent biological activity. The measurements will be performed on crushed powdered samples inside the Rover's ALD (Analytical Laboratory Drawer). The objective of the presented investigation is to analyze the influence of the crushing process on the Raman spectra. This is done by comparing Raman spectra of polished solid samples with those of crushed samples. The second objective is to study Raman spectra of crushed samples with cyanobacteria in regard to the discrimination of the cyanobacteria from the mineral background. Appropriate measurement parameters (e.g. integration time and number of repetitions) for the determination of the mineral composition as well as the detection of biological material are derived. A measurement regime is proposed for mineral mixtures with cyanobacteria on the basis of the RLS instrument characteristics. **Sample Choice and Preparation** Orbital observations showed that in general the phyllosilicate deposits do not occur together with the sulphate deposits [1]. Thus the Mars simulant mineral mixture is assigned to phyllosilicatic and sulfatic Mars regolith. The minerals and rocks are chosen to be structurally and chemically similar to those identified in Martian meteorites [2] and on Mars by recent orbiter and rover missions [3], [4]. The Martian analogue rocks and minerals are crushed and only fragments smaller than 1 mm are used for the mineral mixtures. The powder is pressed with 4.5 MPa to retrieve pellets with a smooth surface for better sample handling. Cyanobacteria are chosen as candidates for potential life on Mars. **Experimental Setup** The Raman measurements are performed with a confocal Raman microscope Witec alpha300 R system at room temperature under air at ambient pressure. The Raman laser excitation wavelength is 532 nm. The spectral resolution of the spectrometer is 4-5 cm^{-1}. A Nikon 10x objective is used. The spot size on the sample is in focus about 1.5 μm. The laser power of 1 mW on the sample is chosen. This value is proposed for the RLS instrument on ExoMars. Values of integration time are taken between 1 s and 100 s per measurement and 1 to 100 measurement repetitions at one point on the sample. First, measurements are carried out on the polished solid samples. Then measurements are performed on each Martian analogue powder sample without bacteria and on pure cyanobacteria seperately. Third, measurements are made on the pellets with cyanobacteria. **Results and Summary** The Raman spectrum of cyanobacteria is influenced by the Raman signal of the mineral background. If cyanobacteria are present, β - carotene is the dominant feature in the spectrum. To get optimal spectra of the mineral mixtures of phyllosilicatic and sulfatic Mars and the cyanobacteria the integration time needs to be adjusted. Only short measurement time should be used to avoid saturation of the spectrum of β - carotene. If cyanobacteria are not present, a longer integration time can be applied, which is necessary to identify the different mineral constituents of the sample. To propose a measurement regime for mineral mixtures with cyanobacteria the procedure should start with a measurement time of only a few seconds. In a next step the time and the number of repetitions need to be increased until acceptable spectra of minerals are obtained. For a laser power on the sample of 1 mW the measurement time should be selected between 1 s (for cyanobacteria) and 20 s (for minerals). **Acknowledgement** This research has partly been supported by the Helmholtz Association through the research alliance "Planetary Evolution and Life".

References

[1] F. Poulet, J-P. Bibring, J. F. Mustard, A. Gendrin, N. Mangold, Y. Langevin, R. E. Arvidso, B. Gondet, and C. Gomez. Phyllosilicates on Mars and implications for early martian climate. *Nature*, 438:623–627, 2005. [2] H. Y. Jr. McSween. What have we learned about Mars from the SNC meteorites. *Meteoritics*, 29:757–779, 1994. [3] J-P. Bibring, Y. Langevin, A. Gendrin, B. Gondet, F. Poulet, M. Berth, A. Soufflot, R. Arvidson, N. Mangold, J. Mustard, P. Drossart, and the OMEGA team. Mars surface diversity as revealed by the OMEGA/Mars express observations. *Science*, 307:1576–1581, 2005. [4] V. Chevrier and P.E. Math. Mineralogy and evolution of the surface of Mars: A review. *Planetary and Space Science*, 55:289–314, 2007.

Micro Raman spectroscopic investigations of the nature and provenance of carbonaceous material in microfossil bearing rocks: redefining D and G carbon band parameters for the detection of biosignatures. D. M. Bower[1], A.Steele[1] , M.D. Fries[2] and L. Kater[3], [1]Geophysical Laboratory, Carnegie Institution of Washington, 5251 Broad Branch Rd, NW, Washington, DC, 20015, dbower@ciw.edu, [2]Planetary Science Institute, Tucson, AZ 85719, [3]WITec GmbH, Ulm, Germany.

Introduction: The identification of biosignatures and detection of extra planetary life is one of the primary goals in astrobiology. Intrinsic to this goal is the improvement of analytical techniques and protocols used to identify biosignatures. Micro Raman spectroscopy is a non-destructive method that allows for in situ analysis of samples and unambiguous identification of a wide range of minerals and compounds. One of the biggest controversies using this technique, however, is in the use of D (~1350 cm^{-1}) and G (~1580 cm^{-1}) band parameters to determine the biogenicity of carbonaceous materials in ancient rocks [4,6,7]. Not only do carbonaceous compounds from different sources often share the same spectroscopic characteristics, but the absolute nature of the D band is still unclear [1,2,9,10]. To elucidate biogenicity, young samples of known provenance are typically analyzed and used as a baseline for comparison to much older samples or samples that have experienced extreme temperatures and pressures. To this ends we used the high-resolution imaging and geochemical mapping capabilities of micro Raman spectroscopy to investigate the nature and provenance of the mineral and carbonaceous material in samples from the 400 Ma Rhynie chert, 570 Ma Duosnato phophorite, 1.9 Ga Gunflint chert, 2.7 Ga Tumbiana carbonate, and the 3.5 Strelley Pool and Apex cherts. The wide array of morphological microstructures, carbonaceous components, and mineral assemblages in these samples provide the perfect testing ground for these techniques [5, 7, 8]. To further constrain D and G band carbon characteristics, micro Raman analyses were also performed on a suite of well-characterized carbonaceous meteorites. The spectral features of each sample set were quantified and compared. The results give much needed information for biosignature identification in these and other biologically significant rocks.

Method: Raman spectra of the samples were collected using a WITEC Digital Pulse scanning near-field optical microscope (AlphaSNOM) with Scan Control Spectroscopy Plus. The Raman scans were conducted with a a frequency-doubled 532 nm YAG laser with. The laser was focused through a 25µm diameter fiber and a 100x objective lens. The scan speed was 3-5s dwell time per pixel at 30 kW cm^{-2}. Images and virtual maps of the spatial elemental and mineral composition of the microtextures were generated using Witec Project 1.99 software. The collected spectra were deconvoluted and quantified using ACD Labs 12 software.

Results: Comparisons of the Raman data from the microfossils and meteorites studied here show that G and D band parameters for both sample sets overlap, making it difficult to assign a biologic or abiolgic source for the carbonaceous material. The results of one G-band parameter comparison, however, provide a way to confirm the degree of thermal alteration of the carbonaceous matter in geologic samples. Raman spectral maps for each sample also show a wide range of microstructural features and minerals associated with the carbonaceous material.

Conclusions: While the unique mapping capabilities of micro Raman spectroscopy provide a greater view of the spatial relationships between carbonaceous materials and other features in ancient rocks, the D and G band characteristics of the carbonaceous material found in biologically associated structures are similar to those of abiologic origin. Careful analysis and deconvolution of the carbon D and G band parameters should be undertaken in any study involving the origins of carbonaceous meterials. In addition, it is necessary to explore the spatial relationships and spectral characteristics to establish biosignatures for life detection in ancient rocks on Earth and of those on other planets.

Acknowledgments: This work is funded by the NASA Postdoctoral Program, NAI.

References: [1] Beyssac O., Goffe B., Petitet J.-P., Froigneux E., Moreau M., Rouzaud J. -N. (2003) *Spectrochimica Acta Part A, 59,* 2267–2276. [2] Brasier M.D., Green O.R., Lindsay J.F., McLoughlin N., Steele A., Stoakes C. (2005) *Precambrian Research, 140(1-2)*, 55-102. [3] DeGregorio B. T, Sharp T.G., Flynn G.J., Wirick S., Hervig R.L. (2009) *Geology, 37,* 631-634. [4] Javaux E.J., Marshall C.P., Bekker, A. (2010) *Nature 463*, 934-938. [5] Kudryavsvev A. B.,Schopf J.W., Agresti D.G., Wdowiak T.J. (2001) *PNAS, 98*, 823–826. [6] Marshall C.P., Edwards H.G.M., Jehlicka J (2010) *Astrobiology, 10(2),* 229-243. [7] Schelbe R.T., Westall F., Allen C.C. (2004) *Advances in Space Research, 33,* 1268–1273. [8] Schweizer M. (2008) *PhD Thesis*. [9] Steele A., Fries M.D., Amundsen H.E.F., Mysen B.O., Fogel M.L., Schweizer M., Boctor N.Z. (2008) *Meteorics Planet. Sci., 42,* 1549–1566. [10] Tazaki K., Ferris F.G., Wiese R.G., Fyfe W.S. (1992) *Chemical Geology, 95,* 313–325.

TRAPPED HIGH DENSITY FLUIDS AND MELTS IN SUPERDEEP DIAMONDS. **F. E. Brenker[1], S. Schmitz[1], L. Vincze[2], B. Vekemans[2], M. Krebs[1], W. De Nolf[3], K. Janssens[3], T. Stachel[4], J. Harris[1,5]**
[1]Geosciences Institute, Goethe University, Frankfurt/M., Germany, [2]Department of Analytical chemistry, Ghent University, Belgium, [3]Centre for Micro- and Trace Analysis - Department of Chemistry, Antwerp University, Belgium, [4]Department of Earth and Atmospheric Sciences, University of Alberta, Edmonton, Canada, [5]Division of Earth Sciences, University of Glasgow, Scotland, UK, (.brenker@em.uni-frankfurt.de).

Introduction: Diamonds from the transition zone and the lower mantle have attracted considerable attention in recent years [1-6]. Compared to the majority of diamonds worldwide derived from lithospheric and sub-lithospheric sources, these rare samples provide exceptional insights into the chemistry and dynamics of the deepest accessible parts of the Earth. Several occurrences of such "ultra-deep" diamonds have been reported and studied intensively in terms of their chemical characteristics and mineral paragenesis [1-7]. Several aspects, e.g. the C-isotopic composition of the diamond host or Eu-anomalies of pyroxene (former perovskite) inclusions, link to a subduction related origin for several of these ultra-deep inclusions [1-2,6].

Although diamonds and their inclusions may probe the deep Earth only locally they are the only direct source of information available and any finding provides information on the physical conditions (pressure, temperature, composition, oxygen fugacity) of their source region. In addition a minimum size of each chemical heterogeneity is expected because temperature is reasonable high in the deep mantle and the timescales of subduction, storage, capture and exhumation exceed tens to hundreds of millions years. Homogenisation is even faster within the transition zone, where the resistance time (time before complete assimilation) of a ~1m sized object is calculated to be limited to ~1 million years [8].

The diamonds investigated in this study were mined from alluvial deposits in the Juina area of south western Brazil. It is shown that these diamonds contain abundant inclusions derived from sources extending from the deep asthenosphere into the lower mantle [4,5].

Methods: In the present work, the inclusions were studied in situ (inside the unbroken diamond) by the means of confocal Raman spectroscopy, confocal micro x-ray fluorescence [9-11] and micro x-ray diffraction. These techniques allow the investigation of the structure and chemical composition of even very tiny inclusions (< 5µm) with the only sample preparation being the polishing of a window close to the inclusions in the diamond in order to reduce light and x-ray absorption/scattering effects. Keeping a (reduced) diamond layer covering the inclusions prevents the trapped phases from any contamination and allows better distinction between their syn- and epigenetic origin, which was essential for the present study.

Results: Of special interest was a large Kankan diamond containing many Ca-Si-O rich inclusions (KK200). Investigations applying Raman spectroscopy yield $CaSiO_3$ walstromite, $CaSi_2O_5$ titanite and larnite (beta-Ca_2SiO_4) as inclusion paragenesis. The varying proportions of the respected phases indicate a depth of origin within the two phase field of larnite + $CaSi_2O_5$ titanite between 300 and 360km [3].

Detailed trace element tomography of several cubo-octahedral inclusions indicate a Ca,Si-rich source, in the absence of several common mantle minerals, like olivine, garnet and Ca-poor pyroxene. This reservoir may represent metasomatized oceanic lithosphere (rodingites, ophicarbonates), meta-morphosed carbonaceous sediments or a trapped carbonatitic melt. In addition investigations on the surrounding narrow fractures around the inclusions show that contrary to our expectation the fractures are actually filled with material. The fracture filling shows close similarities in trace element composition to the mineral inclusions, in addition to being generally enriched in REE. The former existence of a fluid or melt is required to transport material into these elongated fractures. This interpretation is further confirmed by X-ray diffraction measurements which indicate the presence of florencite and La-cerite crystals within the fracture fills.

The most likely interpretation is the entrapment of a volatile component during diamond growth, probably dissolved at high pressure within the solid inclusion phases. During uplift of the diamonds and associated pressure release this volatile content is expelled from the solid inclusion as a fluid and penetrates into the newly forming fractures.

References: [1] Harte, B et al. (1999) *vol. 6, Geochemical Society, USA,* 125-153. [2] Stachel, T. et al. (2000) *Contrib. Mineral. Petrol.* 140, 16-27. [3] Stachel, T. (2001) *Eur. J. Mineral.* 13, 883-892. [4] Kaminsky, F. et al. (2001). *Contrib. Mineral. Petrol.* 140, 734-753. [5] Hayman, P. et al. (2005) *Contr. Mineral. Petrol.* 149, 430-445. [6] Tappert, R. et al. (2005) *Geology* 33, 565-568. [7] F.E. Brenker, F.E. et al. (2002) *EPSL* 198, 1-9. [8] Chakraborty, S. et al. (1999) *Science* 283, 362-365. [9] Brenker, F.E. et al. (2005) *EPSL* 236, 579-587. [10] Vincze, L. et al. (2004) *Analytical Chemistry* 76, 6786-6791. [11] Vekemans, B. et al. (2004) *JAAS* 19, 1302-1308.

MOGANITE IN THE CHALCEDONY VARIETIES OF CONTINENTAL CHERTS (MIOCENE, MADRID BASIN, SPAIN). M. A. Bustillo[1], J. L. Pérez-Jiménez [1,2], A. M. Alonso-Zarza[3] and M. Furio[1].
[1]Dpto. de Geología. Museo Nacional de Ciencias Naturales, CSIC. c/ José Gutiérrez Abascal, nº2, 28006-Madrid, Spain (abustillo@mncn.csic.es, jlperez@mncn.csic.es and mfurio@mncn.csic.es)
[2]Current address: Centro Tecnológico de Repsol, 28931-Móstoles, Spain.
[3]Dpto. de Petrología y Geoquímica, Facultad de Geológicas, Universidad Complutense de Madrid, 28040-Madrid, Spain (alonsoza@geo.ucm.es).

Introduction: The Miocene of the Madrid Basin includes relatively frequent cherts and opaline cherts, which show different quartz textures under thin section in optical microscopy. This work discusses the amounts of moganite (in relation to quartz) obtained in different quartz textures (calcedonite, quartzine, lutecite, microcristaline quartz mosaics, etc.), using micro-Raman and optical microscopy.

Thermo Fisher DXR Raman microscope, which has a point-and-shoot Raman capability of 1-µm spatial resolution was use with laser source at 532 nm. Moganite shows bands at 128, 141, 220, and 502 cm^{-1}, with the latter being the most intense peak. Variations in the moganite/quartz ratio are revealed by the intensity ratios of the main symmetric stretching-bending vibrations of alpha-quartz (465 cm^{-1}) and moganite (502 cm^{-1}) respectively. This method provides a measure of the moganite content and its spatial variation. The data are interpreted in relation to their genesis and the type and environmental setting (shallow lacustrine carbonates, palustrine carbonates, palustrine gypsums and palustrine clays) of the host rock silicified.

The samples are attributed to the Middle Miocene and can be considered of similar age. It allows ruling out variations in the presence of moganite due to its disappearing with time (ageing). All the samples are formed in surficial environments and dolomite or gypsum are present in most of the cases. Optical microscopy shows many quartz textures are interconnected with opal, and in these cases it can be deduced that they formed by recrystallization of the opal (ageing). When opal does not appear, it is interpreted that quartz varieties could were formed directly by replacement of the host rock.

Results: After the realization of 250 analyses, it has been observed that all the varieties of chalcedony (calcedonite, quartzine and lutecite) contain moganite. The qualitative estimations of moganite/quartz (intensity of peak 502 of the moganite divided between intensity of peak 465 of quartz and multiplied by 100) show interesting data. The values in each texture can change very much (e.g. in the lutecite it can change from 26 to 82% or in calcedonite from 32 to 70%). Therefore, every studied chalcedony will be composed of alternating quartz and moganite domains in all three dimensions, with variable domain sizes. But also these variations can be due to the orientation of the analyzed section. Moganite was always absent in the macrocrystalline and mesocrystalline quartz, and occasionally in some calcedonite cements.

When different chalcedony varieties are found in the same sample, the lutecite shows the highest amounts of moganite (48-59%), followed by calcedonite (36-55%) and quartzine (31-36%). When quartzines are not well formed and show a fibrous or microcrystalline nuclei and a border of elongated and interpenetrated megaquartz/mesoquartz crystals, then moganite only was detected in the nuclei. The opaline zones produce flat spectrums with no peaks, but when microcrystalline mosaic quartz is distinguished in optical microscopy, then moganite is found.

Calcedonite is pervasive in the carbonate sedimentary settings without dolomite or gypsum. The moganite proportion in the chalcedony is variable, with a higher variation in the calcretes (37-77%) and the shallow lacustrine limestones (32-70%) than in the palustrine limestones (25-38%), although these data can only to reflect the orientation of analyzed sections. No discrimination has been possible to make in relation to ageing from opal or cementation in these settings. Length-slow fibrous forms (lutecite and quartzine) are dominant in the palustrine evaporitic and Mg-rich settings (with gypsum and dolomite-magnesic clays respectively). In these settings length-slow fibrous forms have the highest variation in the proportion of moganite (26-82%).

Conclusions: Researchers have proposed that moganite actually is identical to lutecite, and therefore, moganite may prove an important indicator for vanished evaporites. Our results show that all the varities of chalcedony (calcedonite, quartzine and lutecite) can have a composite Raman spectrum of both, quartz and moganite, and it is independent of their genesis by ageing, direct replacement or cementation. The presence of moganite is also independent of the surficial sedimentary setting of the host rocks in which it formed.

Acknowledgments: Financial support was provided by project CGL2008-05584-CO2-01 from the Spanish Ministry of Science and Innovation.

LUMINESCENCE BEHAVIOUR AND RAMAN CHARACTERIZATION OF RHODONITE FROM TURKEY. N. Can[1], J. Javier Garcia Guinea[2], M. Hatipooglu[3], R. Kibar[1] and A. Cetin[1], [1]Celal Bayar University, Faculty of Arts and Sciences, Physics Department, 35140 Manisa-Turkey, email;cannurdogan@yahoo.com
[2]Museo Nacional Ciencias Naturales, Jose Gutierrez Abascal 2, Madrid 28006, Spain, [3]Dokuz Eylül University, İMYO, İzmir Multidisciplinary Vocational School, Gemmology and Jewelry Program, 35140 Buca-İzmir / Turkey.

A large massive-structured pale pink-colored mass, which is an element of the secondary replacement mineralisation paragenesis and is covered and interfered with the massive manganite mass, are found in the Menderes-İzmir region of the western Anatolia, only found in one deposit in Turkey. But, they do not occur as a single mineral. Instead they are polycrystalline and consist of the sub-microscopic mixing of rhodonite, anorthoclase, calcite, and quartz minerals. However, the rhodonite is the main constitutive element having over 60% of total of these masses, since the production of typical pinkish color is due to the presence of the abundance of rhodonite. Therefore, these masses should be stated as silica-rich rhodonite, and formulized as [(Mn,Ca,Fe,Mg)SiO_3]. These rhodonite masses consist of some unusual major components of SiO_2 (67.01%), Mn (18.61%), CaO (6.77%), Fe_2O_3 (0.97%), Al_2O_3 (0.37%), and MgO (0.36%), as well as a lot of trace elements. The crystal structure of the sample were analysed by X-ray diffraction (XRD) measurement. Samples of rhononite display some distinctive dispersive (visible) confocal micro-Raman shifts and spectral luminescence emissions of cathodoluminescence (CL), photoluminescence (PL), and radioluminescence (RL). As might be expected it is impossible to show all spectra here. Therefore we will give CL data as an example as rhodonite exhibits strong CL which is very rare (see Fig. 1). We suggest that the important amount of manganese must destroy the CL emission. Fig. 1 shows CL emission spectra of rhodonite at room temperature. As seen from the figure, rhodonite exhibits luminescence maxima at 310, 425 and 626 nm. The Fe^{3+} and Mn^{2+} ions are isoelectronic with $3d^5$ configuration. Their absorption and luminescence are well known.

The optical absorption and Raman spectroscopy of rhodonite were reported earlier [1-2] and studies of the surface properties using glancing X-ray techniques undertaken [3-4]. As far as we are aware no previous work on rhodonite luminescence has been performed. If the assumption is made that rhodonite structure is similar to an orthosilicate and that a large cation perturbs the tetrahedral SiO_4 units, then an analysis of the Raman spectra of rhodonite should be able to be undertaken. Indeed a comparison between rhodonites from different origins has been made [2] but there is no work on Turkish rhodonite. A tetrahedral SiO_4 molecule not involved in distortion should have four vibrational modes. An intense band at around 668 cm^{-1} was assigned to the ν_4 bending mode and showed additional bands exhibiting loss of degeneracy of the SiO_4 units. The low wave number region of rhodonite is complex. A strong band at 408 cm^{-1} is attributed to the ν_2 bending bond. Our results are in good agreement with earlier work [2] but some subtle differences have been observed. We suggest that these differences depend on the cationic substitution of Mn by Ca and/or Fe^{2+} and Mg.

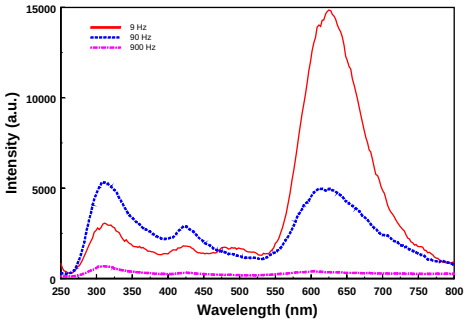

Fig.1 CL spectra for rhodonite at modulation frequencies ranging from 9 to 900 Hz at room temperature

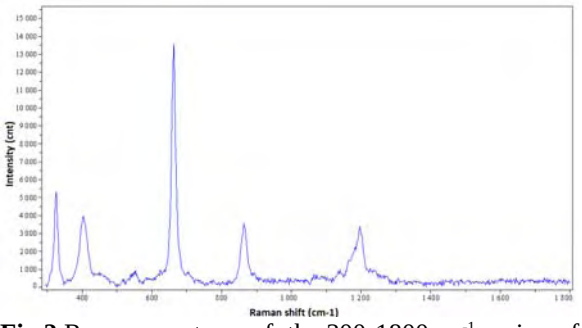

Fig.2 Raman spectrum of the 300-1800cm^{-1} region of rhodonite from Turkey.

References: [1]Lakshman S.V.J. et al. (1973*) Physica*, *66(3),* 601-610. [2]Mills S.J. et al. (2005) *Spectrochimica Acta Part A, 62*, 171-175. [3]Farquhar M.L. et al. (2003) *Min. Mag., 67(6),* 1205-1219. [4]Petit P.E. et al. (2001) *J. Synch. Rad., 8*, 952-954.

ADENINE ADSORBED ON A MARTIAN METEORITE AS A TEST CASE FOR SERS INVESTIGATION OF EXTRATERRESTRIAL LIFE TRACES. S. Caporali[1,2], V. Moggi-Cecchi[1], M. Muniz-Miranda[2], M. Pagliai[2], G. Pratesi[3], V. Schettino[2], [1] Museo di Scienze Planetarie, Via Galcianese 20/h, I-59100 Prato, Italy, [2] Dipartimento di Chimica, Università degli Studi di Firenze, Via della Lastruccia 3, 50019, Sesto Fiorentino, Italy, e-mail stefano.caporali@unifi.it, [3] Dipartimento di Scienze della Terra, Università degli studi di Firenze, Via G. La Pira 4, I-50123 Firenze, Italy, e-mail g.pratesi@unifi.it

Introduction: Surface Enhanced Raman Scattering (SERS) is a powerful technique for the chemical and structural analysis of minerals and organic molecules. This technique provides a huge enhancement of the Raman signal by means of the interaction with silver, gold or copper nanoparticles [1]. In recent years, owing to its high sensitivity, this technique has gained an increased attention especially for the study of trace biological molecules.

Since microbial life, if extinct or extant on Mars, would give rise to the formation of biomolecules that could be adsorbed on rocks and sediments, the SERS investigation of nucleic acids is important to understand if and how primitive life originated in extraterrestrial environments. Two main limitations usually impair the employment of the conventional Raman technique for this purpose, the low sensivity and the occurrence of fluorescence, which could interfere with the observation of vibrational bands. Even if SERS spectroscopy allows overcoming these issues [2,3] its suitability to be used as "in situ" technique for direct investigation on Mars surface still remains to be assessed [4].

In this contribution we report the results of a SERS investigation on DAG 670 meteorite [5] (Martian shergottite) where adenine, a nucleobase detected in several meteorites [6-7], has been deposited.

Experimental: A thick slide of the meteorite was polished with diamond slurry down to 0.25µm, ultrasonically cleaned with water, rinsed with bidistilled water and air dried. Then, a drop of dilute (~ 10^{-2} mol.dm^{-3}) water solution of adenine was deposited on the surface. Once the solvent was evaporated a drop of silver colloidal nanoparticles were add.

Results: Aiming to find the optimal experimental conditions for the detection of adenine in a real Martian rock we carried out SERS investigation on three mineralogical phases constituting the main part of the meteorite (olivine, orthopyroxene and ilmenite) by means of three different excitation laser lines; two in the red light region (632.8 nm and 785 nm) and one in the green light region (514.5 nm). In such a way we collect an accurate owerview of the Raman signal as function of the substrate as well as the excitation laser wavelength. The results show adenine can be unambiguously identified by detecting the intense SERS band located at ~735 cm^{-1}, which frequence results practically unaffected by the nature of the substrate. However, silicate substrates (olivine and orthopyroxene) result more prone to give intense and sharp peaks respect to the oxides (ilmenite) and therefore they should be preferred for analytical purposes. On the other side, fluorescence phenomena were greately enhanced when short excitation wavelength were employed turning in a much lower analytical performace for the green light region excitation laser respect to the red ones.

Furthetmore, we extend these investigations also to salted silver nanoparticles. Adding salt (LiCl) to the Ag hydrosols results in the increase of the colloid zero potential. It turns in the enhanced solution stability (many months under Earth's gravitational attraction without marked aggregation) respect to the unsalted one. Experimental evidence show no appreciable differences between the two types of silver colloidal nanoparticles.

Conclusion and Perspectives: Experimental evidence of the capability of SERS technique to detect traces of adenine on Martian-type rock (Martian shergottite, DAG 670) were provided allowing a clear identification of this nucleobase as small trace (about $10^{-12} \div 10^{-13}$g). We also demonstrated the use of red-light laser excitation helps to limit the fluorescence phenomena, while the use of LiCl-stabilised silver nanoparticle does not infer in the thecnique analytical performance allowing the use of this more stable Ag hydrosol.

References: [1] K. Kneipp et al. (Eds) (2006), Surface-Enhanced Raman Scattering: Physics and Applications; [2] W. Kiefer, J. Raman Spectrosc. (2004), 35, 427; [3] M. Muniz-Miranda et al., J. Raman Spectrosc. (2010) 41, 12–15; [4] S. Caporali et al. (2011) LPSC XLII, Abstract #1401; [5] L. Folco et al., Met. Plan. Sci. (2000) 35, 827-839; [6] Z. Martins et al., Earth Plan. Sci. Lett. (2008) 270, 130-136; [7] P.G. Stoks, A. W. Schwartz, Nature (1979) 282, 709–710.

Acknowledgements: The authors would like to thank Regione Toscana for financial support of the project LTSP through the fund POR FSE 2007-2013 (Obiettivo 2, Asse IV).

Luminescence spectra of plagioclase (labradorite) from South Greenland

A.Çetin, R.Kibar and N.Can, Celal Bayar University, Faculty of Arts and Sciences, Department of Physics, 45140 Manisa-TURKEY, (somacetin@yahoo.com)

Minerals and materials can luminescence when they are exposed to an electron, X-ray, ion, or photon beam. Luminescence is generally associated with light in the ultraviolet (UV) to infrared (IR) region and can exhibit both broad and narrow band spectra. From the spectra it is possible to identify both the activators responsible for the luminescence and their charge states. Whatever the nature of the incident energy, energy cascades associated with the subsequent luminescence is often similar and hence different forms excitation/stimulation explore subtly different aspects of luminescence centres within materials. A large number of research groups routinely employ luminescence and optical analysis as a key macro and micro-characterization techniques in the study of minerals and materials

Results are presented for the time resolved Cathodoluminescence (CL), Optical Absorption (OA), X-Ray Diffraction Analysis (XRD) and SEM of plagioclase (labradorite) from South Greenland. CL spectrum of plagioclase exhibit three emission bands at around 443 nm in the blue region, 580 nm in the yellow-green region and 770 nm in the red-infrared (IR) region, which can be assigned to Al⋯O⋯Al or Ti^{4+} , Mn^{2+} and Fe^{3+} centers, respectively (Fig 1). The Optical Absorption spectra were measured using a Perkin-Elmer Lambda 950 spectrophotometer in the wavelength range of 200–800 nm. The Optical Absorption spectrum showed an absorption band centered at approximately 500 nm (Fig. 2).

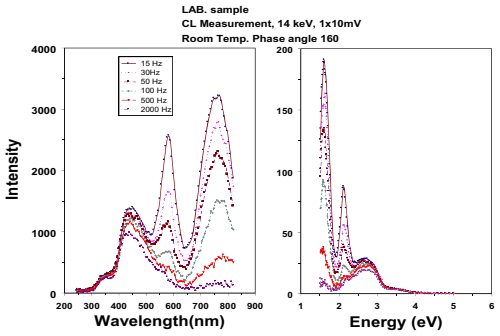

Fig.1 CL spectra for plagioclase at modulation frequencies ranging from 15 to 2000 Hz at room temperature

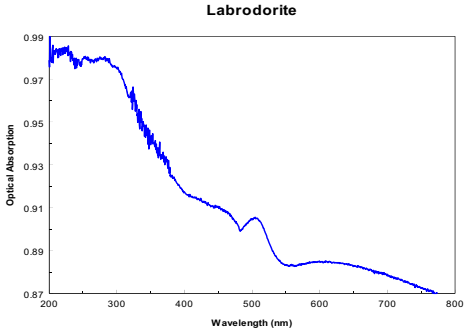

Fig.2 Optical Absorption spectrum measured at 300 K.

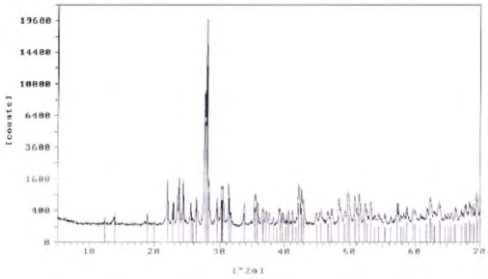

Fig.3 XRD spectra of plagioclase from South Greenland

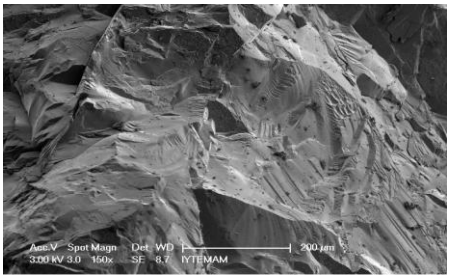

Fig.4 SEM image of plagioclase from South Greenland

References:

[1] Telfer DJ, Walker G (1978) Ligand field bands of Mn2+ and Fe3+ luminescence centres and their site occupancy in plagioclase feldspars. Modern Geol 6:199-210. **[2]** Huntley, D. J., Godfrey-Smith, D. I., Thewalt, M. L. W. and Berger, G. W. (1988) Thermoluminescence spectra of some mineral samples relevant to thermoluminescence dating. J. Luminescence 39, 123-136. **[3]** Finch, A. and Klein, J. (1996) EPR and the cathodoluminescence of alkali feldspars. In International Conference on Cathodoluminescence and Related Techniques in Geosciences and Geomaterials, Nancy, France, Abstracts, pp. 45±46.

Thermal Effect on The Cathodo- and Thermoluminescence Emission of Natural Topaz ($Al_2SiO_4(F,OH)_2$). Correcher, V.[1] , Garcia-Guinea, J[2], Martin-Fernandez, C[2]., Can, N[3]. [1]CIEMAT. Av. Complutense 22. Madrid 28040, Spain. [2]Departamento de Geologia y Geoquimica. Museo Nacional Ciencias Naturales. CSIC. 28006 Madrid. Spain. [3]Celal Bayar University, Faculty of Arts and Sciences, Physics Department, 35040 Manisa-Turkey. Correspondence author: v.correcher@ciemat.es

Introduction. Most of gemstones, being natural materials (silicates, carbonates, phosphates, etc.), exhibit luminescence emission. Such property is of great interest since could be potentially employed, not only for dating purposes, but also as personal dosimeters in case of radiation accident or radiological terrorism where conventional monitoring was not established. For these purposes the laboratory routine is mainly based on the analysis of the blue emission (at about 400 nm) of natural materials. This emission, that is strongly dependent of the temperature, is produced by the incidence of the radiation on the aluminosilicates lattices that induces mobility of the alkalis causing a high number of electron–hole pairs in the lattice. Alkali self-diffusion through bulk and interfaces gives rise to a continuous alkali–oxygen bond splitting–linking processes with continuous formation–destruction of $[AlO_4]^o$ centres. Some holes can be trapped, forming $[AlO_4/M^+]$ centres. When the supplied energy is enough, the recombination of the electrons with the hole trapped adjacent to Al-M^+ reduces the presence of ionic charge compensators at the Al sites and induces the blue luminescence emission to $[AlO4]^o$ centres (aluminium–hole centres). In this sense, this paper reports about the influence of the temperature on the thermoluminescence (TL) and cathodoluminescence (CL) behaviour of a well-characterised topaz from Badajoz (Spain). TL provides information about the trapped charge recombination sites related to metastable defects inside the lattice depending on whether the detrapping process is due to heat. CL is a process whereby light is created from an energetic electron beam. CL supplies data about transient defects after irradiation on the surface of the lattice. CL is used in the identification of the migration and diffusion of some luminescent centres from the emission bands.

Results. The CL spectra all clearly show two features viz., a shoulder emission band at near 340 nm (3.64 eV) and a sharp emission at 450 nm (2.75 eV). Since the excitation efficiency of CL is not uniform with depth one possibility is that the defect centre which is responsible for this particular emission, could be present closer the surface. For the low temperature CL measurements the 450 nm emission disappeared but the 340 nm emission becomes sharper. In addition to these features, another broad band is featured between 650 nm (1.91 eV) and 750 nm (1.65 eV). Comparison of signals with other silicates may be helpful and these features are similar to those observed in thermally treated quartz where they have been attributed to $(AlO_4)^o$ and $(H_3O_4)^o$ centres.

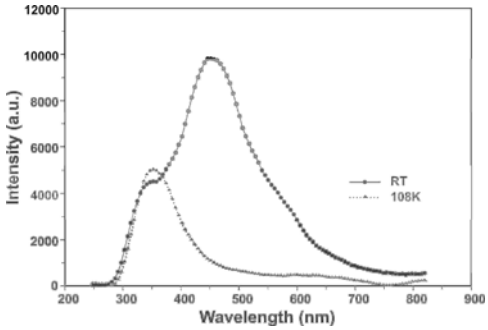

Fig 1. CL of natural topaz taken at room temperature and low temperature

TL glow curves of different aliquots of natural topaz are shown after the preannealing treatment. In the whole natural TL glow curve a broad peak is appreciated at 240°C followed by a second structure consisting on a wide broad distribution peaked at 450°C. In the whole curve the TL features typically involve a gradual and progressively shift of the maximum peak up to higher temperatures and a change in the shape and intensity of the TL distribution in accordance with the thermal pre-treatment. The thermolabile broad band of blue emissions shows TL glow curves of multi-order kinetics involving continuous processes of trapping-detrapping. These thermal phenomena of TL could be involved in consecutive breaking and linking of bonds of Al-O, Si-O, redox reactions and also losses of fluoride ions.

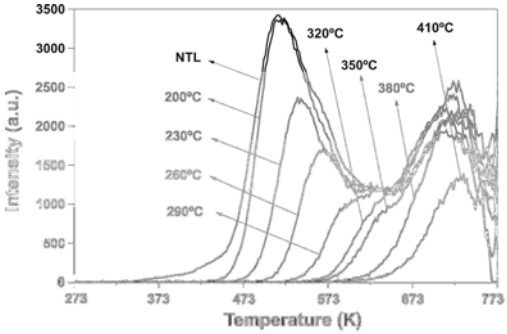

Fig 2. TL glow curves taken after preheating with temperatures from 200 to 410°C.

PRELIMINARY STUDIES ON THE SPECTRA LUMINESCENCE OF BRENKITE $Ca_2F_2CO_3$. E. Crespo-Feo[1], J. Garcia-Guinea[2], V. Correcher[3], and A. Nieto-Codina[2], [1]Dpt. Cristalografia y Mineralogia. Fac. CC. Geologicas-UCM. C/ Jose Antonio Novais 2. Madrid 28040 Spain, correspondence autor: ecrespo@geo.ucm.es. [2]Museo Nacional de Ciencias Naturales-CSIC. C/ Jose Gutierrez Abascal, 2 Madrid 28006 Spain, [3]CIEMAT. Av. Complutense 22. Madrid 28040 Spain.

Introduction: Brenkite ($Ca_2F_2CO_3$) is an orthorhombic mineral with *Pbcn* space group that is reflected in its external habit, radiated agregate fibers (Fig.1a) with well developed crystal faces at the top of the laths (Fig.1b).

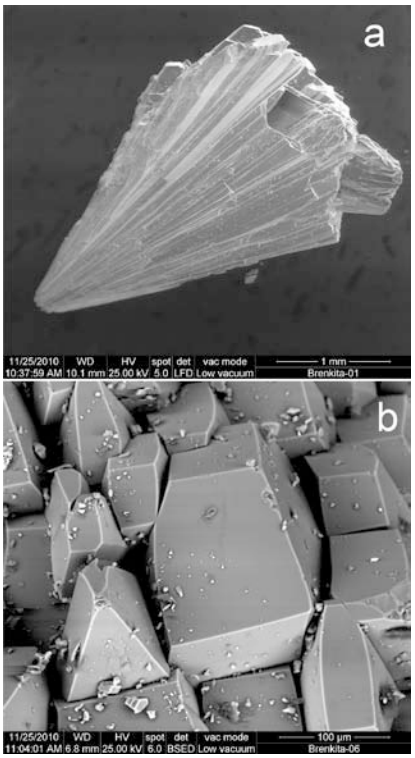

Fig.1. *Scaning Electron Microscope (ESEM) images of the studied brenkite: (a) radial intergrown of prismatic crystals; (b) detail of the crystal faces from the top of the fibers.*

It was first described in 1978 [1] and, since brenkite is not a common mineral, very few papers have dealed on this carbonate [1-3]. No previous works on its luminescence has been developed therefore this is the first aproched to its luminescence features.

Methods: Brenkite was characterized by means of X-ray powder difracction (XRD) using a Phillips PW1710/00 difractometer with a CuKa radiation source, equipped with a graphite monochromator. Chemical analyses, together with the scaning electron microscope images, were obtained by enviromental scaning electron microscopy and energy dispersive X-ray spectrometer (ESEM-EDS) using an Inspect-S of the FEI Company. CL spectra were performed in low vacuum mode without coating, using a Gatan MonoCL3 detector and PA-3 photomultiplier attached to the ESEM. The PMT covers a spectral range of 185 nm–850 nm. The excitation for CL measurements was provided at 25 kV electron beam.

Results and Discussion: By XRD the mineral seems to be pure brenkite and the chemical analyses (Ca 44%, F 23% and C 6%) fit very closely with the theoretical composition of the mineral [1,4], although some Yb has been observed (1%). CL spectra were performed in four different point along the brenkite fiber. If we consider the aggregate as a part of a spherical morphology, the analyses were located as follows: close to the inner part of the radial aggregate, in the middle of the fiber length, at the upper part of the fiber, and on the well developed crystal faces at the top. Spectra show similar features except the intensity variability. The main luminescence response is located in the blue part of the spectrum with most intense peak situated at ~380 nm. Slighter signals are recorded at ~660 and ~760 nm. These could be related to some impurities as well as the blue region could be intrinsic although more detailed analysis are requireed. Also, it is needed to understand the Yb implication on the brenkite luminescence.

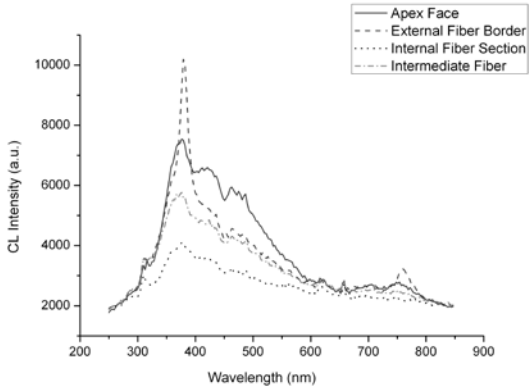

Fig.2. *CL spectra of 4 different points along the brenkite fiber. See text for a detailed description.*

References: [1] Hentschel G. et al. (1978) *Neues Jahrb.Min.,Mh.*, 325-329. [2] Leufer U. and Tillmanns E. (1980) *Tschermaks Mineral. Petrog. Mitt*., *27*, 261–266. [3] Grice J. D. et al. (2007) *Chem. Rev., 107,* 114–132. [4] Anthony J. W. et al. (2003) *Handbook of mineralogy (Volume V-Borates, Carbonates, Sulfates): Mineral Data Publishing, Tucson, Arizona, 813 p.*

EFFECTS OF THE TECTONIC STRESS ON LUMINISCENCE OF CERUSSITE $PbCO_3$. E. Crespo-Feo[1], P. Hernandez-Ferreiros[2], J. Garcia-Guinea[2], and V. Correcher[3], [1]Dpt. Cristalografia y Mineralogia. Fac. CC. Geologicas. UCM. C/ Jose Antonio Novais, 2 Madrid 28040 Spain, corresponding autor: ecrespo@geo.ucm.es, [2]Museo Nacional de Ciencias Naturales-CSIC. C/ Jose Gutierrez Abascal, 2 Madrid 28006 Spain, [3]CIEMAT. Av. Complutense 22. Madrid 28040 Spain.

Introduction: Luminescence of cerussite is commonly associated to the Pb^{2+} present in the own mineral structure. Though Pb^{2+} is coordinated with CO_3^{2-}, luminescence features have been assigned to isolated Pb^{2+} ions [1]. Neither impurities nor structural features have been related to luminescence properties of the mineral since the two observed emission bands at ~310 and ~450 nm are generally ascribed to $^3P_{0,1} \rightarrow {}^1S_0$ transition of Pb^{2+} (A-transition) and a higher level transition called D-transition, respectively [2].

Sample and Experimental Procedure: The studied mineral is a cerussite from Mibladen Mine (Morocco). The $PbCO_3$ occurs as a common alteration mineral, disseminated in carbonate rocks heavily faulted and brecciated. Several periods of tensional tectonic processes have affected the rocks containing lead mineralization [3].

Cerussite was characterized by means of X-ray powder difracction (XRD) using a Phillips PW1710/00 difractometer with a CuKa radiation source, equipped with a graphite monochromator. Scanning electron microscope images were obtained by environmental scanning electron microscopy (ESEM) using an Inspect-S of the FEI Company. CL spectra were performed in low vacuum mode without coating, using a Gatan MonoCL3 detector and PA-3 photomultiplier attached to the ESEM. The PMT covers a spectral range of 250 nm–800 nm. The excitation for CL measurements was provided at 30 kV electron beam.

Results and Discussion: CL panchromatic image shows different luminescence areas (Fig.1). An anomalous high emission of light is situated in a small fragment close to a fracture whereas the rest of the surface has a lower intensity. CL spectra of both zones (darker and brighter areas, marked on Fig.1 as points 1 and 2) show the same characteristics (Fig.2). A broad luminescence area can be observed with two different peaks (~440 and ~470 nm), both related to the ~470 nm peak assigned to Pb^{2+} D-transition [2]. A-transition is hardly noticed in our results although a slight peak is detected at ~310 nm (Fig.2).

No different composition occurs in the studied area, then another explanation must be developed for that anomalous luminescence. As it can be seen on the Fig.1, the fissures indicate movements due to, probably, tensional stress. Areas rounded by white circles are also pointing to this hypothesis and the direction of movement is marked by the white arrows. As cerussite hosted-rock is faulted and brecciated due to tectonic strain, it seems that part of the tensional stress has affected the mineral increasing its luminescence.

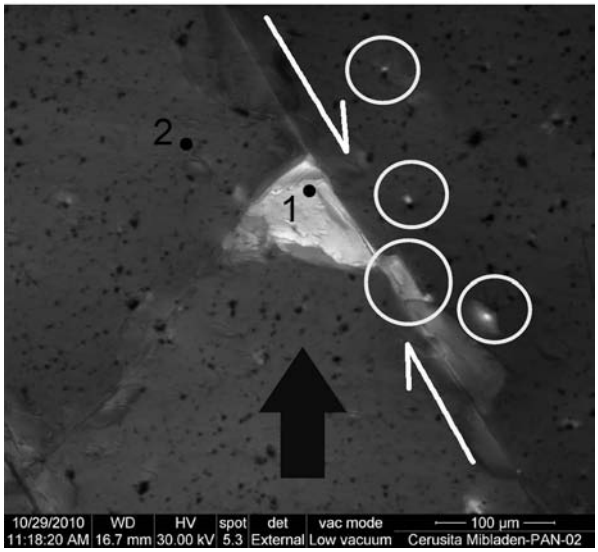

Fig.1. *CL panchromatic image (CL-ESEM). See text for more description.*

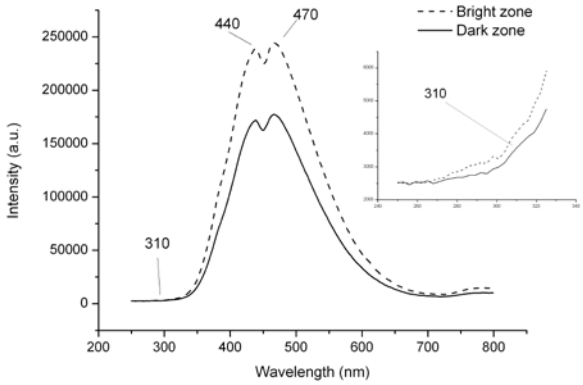

Fig.2. *CL spectra of cerussite from the high luminescence and low luminescence area (points 1 and 2 from the Fig.1, respectively).*

References: [1] Lammers M. J. J. and Blasse G. (1986) *Mat. Res. Bull., 21,* 529-534. [2] Folkerts H. F. and Blasse G. (1996) *J. Chem. Solids, 57,* 303-306. [3] Dagallier G. and Macaudiere J. (1987) *Bull. Soc. Geol. France, 3,* 387-394.

VATERITE STABILITY IN THE PRESENCE OF Cr (VI). J.A. Cruz[1], N. Sánchez-Pastor[1], A. M. Gigler[2], and L. Fernández-Díaz[1]. [1]Departamento de Cristalografía y Mineralogía. Universidad Complutense de Madrid. 28040, Madrid (Spain), [2]CeNS and Department for Earth and Environmental Sciences, Ludwig-Maximilians-Universität. 80333, Munich (Germany).

Calcium carbonate phases are relevant in numerous scientific disciplines due to their abundance in both inorganic and biotic media and for a wide range of industrial applications. Many studies demonstrate that vaterite is thermodynamically unstable with respect to the aragonite and calcite. However, Navrotsky pointed out that calcite, aragonite, and vaterite are close enough in free energy such that small changes in their surface properties and/or concentration of impurities can determine stability crossovers.[1] It has been shown experimentally that vaterite can become temporarily stabilized when it forms in the presence of different ions [2, 3].

This investigation was focused on the effect of Cr (VI) stabilizing the polymorph vaterite. The crystallization of vaterite was carried out using a double diffusion system [4] which consisted of two vertical branches separated by a column of silica hydrogel. The vertical branches were filled with 0.5 M $CaCl_2$ and 0.5 M Na_2CO_3 solutions, and different amounts of a Na_2CrO_4 solution were added to the silica gel during its preparation (0.1, 0.15, and 0.2 M). The vaterite aggregates were recovered from the gel after 30 days and were studied by scanning electron microscope and Raman spectroscopy. Figure 1 shows examples of vaterite aggregates grown in silica gel bearing Cr (VI) concentrations ranging from 0.1 M (a) to 0.2 M (c), where their characteristic morphology can be observed.

The Raman spectra collected from those aggregates formed in gels containing ≥ 0.15 M Cr(VI) (Figure 1b and 1c) show the typical vaterite triplet at 1074, 1081, and 1094 cm^{-1} and an additional line at 750 cm^{-1}. Further translational and rotational lattice modes can be observed between 100 and 300 cm^{-1} consistent with vaterite [5]. However, in contrast to the external morphology of the aggregate shown in Figure 1a, its Raman spectrum shows peaks at 1085 cm^{-1}, 208 cm^{-1} and 711 cm^{-1}, all of them characteristic of calcite [6]. A closer examination of this sample (see the inset of Figure 1a) shows that it is, in fact, a vaterite pseudomorph that consists of small calcite rhombohedra. The facts that: i. Cr-free experiments did not yield any other $CaCO_3$ polymorph than calcite and ii. Vaterite transformed into calcite when the concentration of Cr (VI) in the growth medium was lower than 0.15 M, indicate that the presence of Cr (VI) promotes the formation of vaterite. However, only high Cr (VI) concentrations in the growth medium can prevent its transformation into calcite after a relatively short time.

References:

[1] Navrotsky, A. (2004) *Proc. Natl. Acad. Sci*. 101, 12096–12101. [2] Nassrallah-Aboukais, N., et al. (1998) *J. Chem. Soc*. 94, 2399-2405. [3] Fernández-Díaz, L. (2010) *Geochimi. Cosmochimi. Acta*. 74, 6064-6076. [4] Henisch, H.K. and García-Ruíz, J.M. (1986) *J. Cryst. Growth*. 75, 195-202. [5] Urmos, J. et al. (1991) *Am. Mineral*. 76, 641-646. [6] Bischoff et al. (1985) *Am. Mineral.* 70, 581-589.

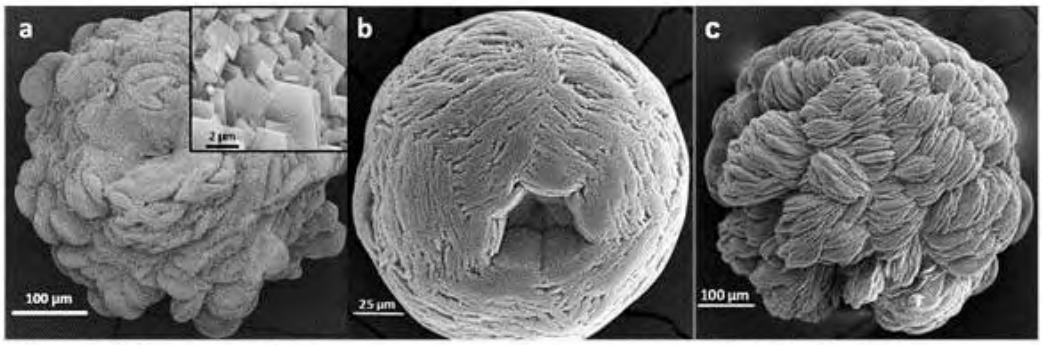

Figure 1. SEM micrographs of aggregates extracted from experiments with: (a) 0.1 M, the close up reveals small calcite crystals, (b) 0.15 M and (c) 0.2 M chromate concentration.

Raman Micro-Spectroscopy performed on Extraterrestrial Particles. S. De Angelis[1,2], V. Della Corte[1], G. A. Baratta[3], R. Brunetto[4], P. Palumbo[1], A. Ciucci[1], A. Rotundi[1]
[1] *Dip. Scienze Applicate, Università Parthenope, Centro Direzionale, Isola C4, 80143, Napoli (Italy) (dangelis@na.astro.it, v.dellacorte@gmail.com, palumbo@na.astro.it, alessandra.ciucci@gmail.com, rotundi@uniparthenope.it)*
[2]*Dip. Ingegneria Aerospaziale, Università Federico II, Piazzale Tecchio, 80, 80125, Napoli (Italy)*
[3]*INAF-Oss. Astrofisico di Catania, Via Santa Sofia 78, 95123, Catania (Italy) (gbaratta@oact.inaf.it)*
[4]*Institut d'Astrophysique Spatiale, CNRS, Universitè Paris-Sud, UMR8617, F-91405, Orsay FRANCE (rosario.brunetto@ias.u-psud.fr)*

Introduction:

We performed Raman measurements on stratospheric particles collected by the balloon-borne DUSTER (Dust in the Upper Stratosphere Tracking Experiment and Retrieval) instrument (Della Corte et al. 2011).

DUSTER is designed to collect particles, with sizes between 0.1 and 40 microns, in the upper stratosphere, at altitudes of 35-40 km; the aim is to collect micron-size cosmic particles settling in the terrestrial atmosphere. The DUSTER instrument has flown in 2006 from Kiruna-Esrange (Sweden, technical flight), in 2008 and 2009 from Svalbard (Norway, scientific flights) and a new scientific flight is planned from Kiruna-Esrange for the end of February 2011. The particles on which we performed Raman measurements were collected during the DUSTER 2008 flight, at an altitude of 37±1 km in the polar stratosphere. The particles analyzed by Raman micro-spectroscopy, (sizes 3 – 12 micron) have been previously characterized by IR micro-spectroscopy, Field Emission Scanning Electron Microscopy (FESEM) and Energy Dispersive X-ray analyses. The Raman spectra are characterized by an intense signal due to amorphous carbon, with the typical D and G peaks at 1361 cm^{-1} and 1580 cm^{-1} superimposed to a fluorescence continuum. In two spectra, relative to particles D08C_006 and D08C_008(b), we can tentatively recognize the presence of a weak peak at 1080 cm^{-1} that could be due to calcite. The peak is hardly distinguishable from the noise of the relatively strong fluorescence background due to the presence of amorphous carbon. The presence of calcite ($CaCO_3$) is confirmed by IR micro-spectroscopy and by EDX analyses results. To support Raman spectra reduction, we developed a program (LabVIEW environment) able to fit many spectra simultaneously, choosing between Gaussian, Lorentzian or BWF curves for the fits.

We compared the Raman results obtained on DUSTER particles, whose origin has been classified as extraterrestrial, with two other sets of Raman analyses performed on extraterrestrial dust: 1) Interplanetary Dust Particles (IDPs), collected by the high flying aircraft stratospheric NASA programm; 2) cometary particles collected during the fly-by of the NASA/Stardust spacecraft in the coma of the comet 81P/Wild 2.

The Raman NASA/IDPs measurements show the presence of the D and G peaks of amorphous carbon, together with the evidence of iron-oxides (magnetite, maghemite and hematite) for all particles except one, in which the intense amorphous carbon signal dominates on possible minerals contribution. The presence of iron-oxides, combined with FESEM images and IR micro-spectroscopy, suggests that these IDPs could have undergone pyrometamorphism because of the flash-heating during atmospheric entry.

The Raman spectra of 81P/Wild 2 samples are dominated by condensed aromatic hydrocarbons (or "disordered carbonaceous material"). The D and G Raman parameters span a range similar to that observed in IDPs and in most primitive meteorites.

Raman analyses were performed at the INAF-Laboratorio di Astrofisica Sperimentale, Catania, Italy.

Thermoluminescence Studies of Dergaon Meteorite

P. Dutta[1] and K. Duorah[2]

1. Department of Physics, Dimoria College, Khetri-782403, Assam, India
2. Department of Physics, Gauhati University, Guwahati-781014, Assam, India

ABSTRACT:

A multiple fall of stony meteorite occurred near the town of Dergaon in Assam, India, on March 2, 2001. Preliminary Mineralogical and Petrologic studies suggested that the meteorite belongs to the H5 Group. Here in this paper we represent Thermoluminescence studies of Dergaon meteorite in order to have its thermal history. The given work consists of an estimation of the quantitative characteristics of thermal and /or shock thermal influence on substance of this meteorite as well as degree of structural change in matter during formation and subsequent evolution of their parent bodies. Here we get the intensity of TL glow in equilibrium changes more than two order of magnitude.

Keywords: Meteorite, Thermoluminescence

PACS: 91.65 Sn, 96.30 Za

RAMAN SPECTROSCOPIC CHARACTERISATION OF GREEN-BLUE STALACTITES IN LANTZ CAVE (NAVARRA, NORTH OF SPAIN). S. Fdez-Ortiz de Vallejuelo*, K. Castro, I. Martínez-Arkarazo and J.M. Madariaga,

Department of Analytical Chemistry, University of the Basque Country (UPV/EHU), P.O. Box 644, E-48080 Bilbao, Basque Country, Spain *Corresponding author. Tel.:+34 94 601 54 45 *E-mail address:* silvia.fernandez@ehu.es.

Speleothems, including stalactites, stalagmites and columns, are typically associated with mineral precipitation in the dark, enclosed environments of caves, and theirs growth is related to climatic controls as temperature, precipitation and vegetation cover [1,2].

Cave of Lantz is located between a large number of relatively small Roman mines caves, 2.5 Km far away from the Lantz village (Navarra, north of Spain). It is considered one of the most perfect manifestations of green speleothems in the world.. The cave's speleothems (stalactites, stalagmites, etc.) vary widely in their morphology and mineralogy causing different shades. In our case, this study was focused on green surface coloration of stalactites.

For the characterization of speleothem samples from Lantz cave, directly on the surface, different analytical techniques were used: X-ray Micro-Fluorescence (μ-EDXRF) using portable ArtTax μ- EDXRF equipment by Rontec (nowadays Brucker AXS; Berlin, Germany) to determine the elemental composition and Raman spectroscopy using InnoRam ultramobile spectrometer (B&WTEK$_{INC}$, Newark, USA) provided with a 785 nm excitation laser with a nominal laser power of 225 mW and a CCD detector, for the characterization of the molecular composition. Treatment and interpretation of the results was carried out with Omnic Nicolet software (Madison, Wisconsin, USA).

In addition to the predominantaragonite (small and large crystals), calcite (columnar, fiber, and grain coating mats) and dolomite [3,4], other minerals were identified. These minerals were cuprite (copper(I) oxide, Cu_2O), hollandite (barium manganese oxide, $BaMn_8O_{16}$) and azurite (basic copper carbonate, $2CuCO_3{\cdot}Cu(OH)_2$). In these samples, quartz and carbon particles were also found.

The Raman spectra of the aragonite and dolomite minerals are shown in Figure 1.

Apart from the elements involved in the mentioned minerals, As, Co and Fe were identified by X-ray microfluorescence as trace elements. The results were correlated with mineral compositions found by Raman measurements.

Water samples were measured by Inductively coupled plasma mass spectrometry (ICP-MS) for interpreting trace elements (Al, Ti, V, Cr, Mn, Fe, Co, Ni, Cu, Zn, As, Cd, Sn, Sb, Ba and Pb) ratios of speleothems and freshwater deposits.

According to the results, trace element concentrations vary between drip waters of these green stalactictes and waters from other parts of the cave.

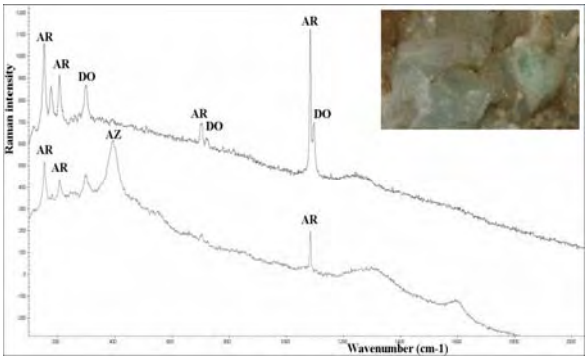

Figure 1. Raman spectra of samples of green-blue stalactite from cave of Lantz; AR: aragonite, $CaCO_3$; DO: dolomite, $CaMgCO_3$ and AZ: azurite, $2CuCO_3{\cdot}Cu(OH)_2$.

References

[1] Jones B. (2010) *Sedimentary Geology, 23,* 15-34.

[2] Collister C., Mattey D. (2008) *Journal of Hydrology*, 358, 259-267.

[3] Martínez-Arkarazo I., Angulo M., Zuloaga O., Usobiaga A., Madariaga J.M. (2007) *Spectrochimica Acta Part A: Molecular and Biomolecular Spectroscopy*, 68, 1058-1064.

[4] Alonso-Zarza A.M., Martin-Perez A. (2008) *Sedimentary Geology*, 205, 160-164.

Acknowledgements

This work has been financially supported by the Basque Government through the Environmental Analytical Chemistry Project 2007–2012 (Ref. IT-245-07). Authors thanks Esteban Faci and Gobierno de Navarra (Departamento de obras Públicas, Transportes y Comunicaciones) for their support.

CONTENT OF RARE EARTH ELEMENTS IN A SPELEOTHEM ANALYZED BY ICP-MS AND CL-SPECTROSCOPY. Fernandez-Cortes, A.[1], Cuezva, S. [1], Cañaveras, J.C. [2], García-Guinea, J[1]., Sanchez-Moral, S[1]. [1] Museo Nacional Ciencias Naturales. CSIC. 28006 Madrid. Spain. [2]Laboratorio de Petrología Aplicada, UA-CSIC, 08040-Alicante, Spain

In the framework of a pilot study to search radiation sources and uranyl groups associated to the host rock and sediments, in a cavity with very high radon levels (Castañar cave, Spain) some Rare Earth Element (REE) mineralization's have been detected in a carbonate stalactite. REE contents of the analyzed host-rock slates [1] by ICP-MS displayed spatially-heterogeneous concentrations, ranging from 20-44 ppm, 9-22 ppm, 8-23 ppm for Ce, La and Y, respectively. The REE signal is smoothed in the speleothem sample; ≤1 ppm, 0.2-0.9 ppm, 0.1-4.2 ppm for Ce, La and Y, respectively, values much higher than in other studied speleothems [2]. Cathodoluminescence (CL) analyses have allowed to obtain the whole spatially resolved spectra of the REE pattern along a concentric sequence of mineral precipitation of calcium-carbonate phases (Fig. 1). CL-spectra shows a wider range of spectral luminescence emissions corresponding to others REEs for B layer (calcite 90%, aragonite 10% by XRD), compared with the more external layer A (calcite ± phyllosilicates) where the intensity of the maximum CL-emissions are smoothed and Ce^{3+} prevails and hide others REE's emissions. Fig. 2 shows a detailed CL spectrum for the growth layer B with a high density of REE: Sm^{3+}, Sm^{4+}, Dy^{3+}, Ce^{3+}, Eu^{3+} or Tb^{3+}. The periodic enrichment of some REE (La, Ce) within the laminations of a speleothem reflect times of more intense weathering that usually correspond to relatively warm and humid climatic phases [2—3]. According with these authors, the higher concentration of Ce, La and Y in the external calcite layer (A) could indicate its growth during a phase with stronger weathering and more dynamic hydrology. REE mobilizations from the host-rock to this growth band corresponded to these major REEs. Simultaneously, the $CaCO_3$ solubility could increase linked to a lower ratio of mineral precipitation due to REE-inhibition. An opposite pattern could be inferred for the inner layer B where the hydrodynamic conditions probably favored long times residence of seepage water and a higher interaction with the siliceous host-rock. This predominant REE-source entailed the incorporation and concentration of other REEs (Dy, Sm, Eu) and SiO_4^-, Si-O groups into the $CaCO_3$ lattices producing CL emission. The relative decrease of La, Ce and Y seems to be coeval to a more pronounced CL-anomalies of these minors REEs, as well as a uranium accumulation in this growth layer (19.3 ppm, 5 times higher than layer A).

An additional CL-spectrum of the growth layer nearest to fed conduit (Fig. 1,C) shows an intermediate pattern of REE's emissions with respect to A and B layer. Thus, the CL-anomalies of the minors REEs are smoothed, except for Sm^{3+} and Dy^{3+}. Originally, the REE's contribution in this growth layer could be associated to similar hydrodynamic conditions of B layer but corresponding to an early stage.

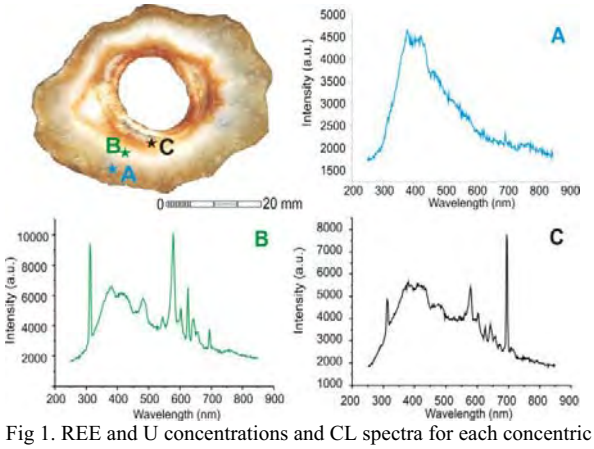

Fig 1. REE and U concentrations and CL spectra for each concentric layer of calcium-carbonated phases.

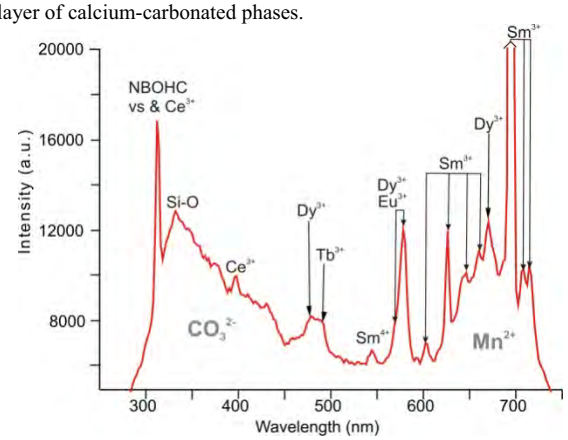

Fig 2. Detailed CL spectrum with high REEs' density corresponding to layer B.

References

[1] Alonso-Zarza et al., (2011). Structural and host rock controls on the distribution, morphology and mineralogy of speleothems in the Castañar Cave (Spain).Geological Magazine 48: 211 - 225.

[2] Zhou et al., (2008). Distinct climate change synchronous with Heinrich event one, recorded by stable oxygen and carbon isotopic compositions in stalagmites from China. Quaternary Research 68, 306–315.

[3] Richter et al., (2004). REE^{3+} and Mn^{2+} activated cathodoluminescence in late glacial and Holocene stalagmites of central Europe: evidence for climatic processes?. Holocene, 14(5): 759-767.

OLD AND MODERN PIGMENTS IDENTIFICATION FROM A 14th CENTURY SCULPTURE BY MICRO-RAMAN. M.L. Franquelo[1], A. Duran[1], D. Arquillo[2] and J.L. Perez Rodriguez[1], [1]Materials Science Institute of Seville, Americo Vespucio 49, 41092 Seville, Spain jlperez@icmse.csic.es [2]Fine Arts Faculty of Seville, University of Seville, Laraña 3, 41003 Seville, Spain

Introduction: Pigments identification in polychromed sculptures is very important for understanding the history of the works of art and the resolution of problems related to its conservation, restoration treatments and author attribution. Portable systems (XRF, Raman, XRD) only provide information from the external layers of the artifact, so in polychromies with a high number of layers, it is necessary to use other experimental techniques. The full identification of the pigments within the artworks requires collecting samples with all the layers, from the varnish to the support. If a sample contains all the layers, it will provide wide information about the way in which the polychromy and the repaint/restoration treatments were carried out. Micro-Raman spectroscopy can be used for the identification of pigments within the cross-sections containing all the layers of the polycromy [1-3]. The purpose of this work is to full characterize the different layers of cross-sections performed on samples from a 14th century polychromed sculpture that had suffered subsequent restoration treatments by using micro-Raman spectroscopy. Also a chromatic study was carried out.

Fig 1: Santa Ana triplex sculpture

Experimental: A triplex polychromed sculpture of Santa Ana, the Virgin and the Child, dating from the Spanish Gothic period, has been studied. The dispersive integrated Horiba Jobin-Yvon LabRam HR 800 system was employed for recording the Raman spectra. The experiments were performed directly on the cross-sections performed from sculpture samples. Two external visible diode lasers are available in this apparatus: at 532.1 nm (green) and at 784.6 nm (red). An optical microscope is coupled confocally to the Raman spectrometer. The chromatic characterization was performed *in situ* using a portable spectrometer Dr. Lange Neurtek model LMC3/DIAM5.

Results: Five red layers were found together with the preparation layer in one of the cross-sections. The Raman spectra of the internal layers showed characteristic bands of vermilion (bands at 251, 289 and 343 cm^{-1}). The presence of red lead was also detected (bands at 118, 147, 221, 307, 386 and 546 cm^{-1}). The amount of red lead is higher than vermilion. The external red layer showed the characteristic bands of vermilion and also those of red ochre: iron oxides mixture with clay minerals (bands at 221, 289, 406 cm^{-1}). Also gypsum (1004 cm^{-1}) and lead white (1049 cm^{-1}) were detected.

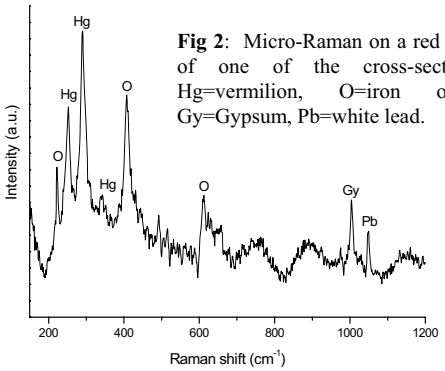

Fig 2: Micro-Raman on a red layer of one of the cross-sections: Hg=vermilion, O=iron oxide, Gy=Gypsum, Pb=white lead.

Titanium oxide (bands at 141, 447 and 609 cm^{-1}) was detected in the external layers of white colour. The shoulder that appear at 438 cm^{-1} could be attributed to zinc white. Zinc was found by XRF (using a portable system) in most areas of the external part of the sculpture. Two blue color layers have been found in one of the stratigraphies, the internal layer is constituted by lazurite (bands at 258, 549, 810 and 1098 cm^{-1}); this pigment accompanied by titanium oxide appeared in the external layer. Other old and modern pigments have been identified using this technique.

Chromatic characterizatyion of the different zones of the sculpture showed heterogeneous values of L*, a*, b*, according with the different colors visually observed. The composition was also confirmed by other techniques such as chemical analysis (SEM-EDX), micro-X ray diffraction and IR spectroscopy.

Conclusions: The micro-Raman spectroscopy study of cross-sections from a sculpture from 14th century has shown the presence of old pigments such as vermilion, lazurite, lead white, red lead, red ochre or red lac in the internal layers and zinc white, titanium oxide, litopon, ultramar blue as modern pigments in the external layers attributed to subsequent restoration/repaint treatments.

References: [1] Clark R.J.H. (2007) *J. Mol. Struct.*, 834-836, 74-80. [2] Franquelo M.L., Duran A., Herrera L.K., Jimenez de Haro M.C., Perez-Rodriguez J.L. (2009) *J. Mol. Struct.*, 924-926, 404-412. [3] Duran A., Jimenez de Haro M.C., Perez-Rodriguez J.L., Franquelo M.L., Herrera L.K., Justo A. (2010) *Archaeometry*, 52, 286-307.

FRANCEVILLITE [(Ba,Pb)$(UO_2)_2(V_2O_8)\cdot 5H_2O$] ON THE HYDROXYPAPATITE BOND FOSSILS OF LORANCA (CUENCA, SPAIN): SPECTRUM CATHODOLUMINESCE OF URANYL-VANADATES

M. Furio, Merino, L., L. Tormo, A. Jorge, J. Garcia-Guinea [1]Electron Microscopy and Spectroscopy Laboratory. Museo Nacional Ciencias Naturales. CSIC. 28006 Madrid. Spain.
Author for correspondence: mfurio@mncn.csic.es

Geological Frame: The palaeontological deposit of fossil vertebrates Loranca-1 is located in the town of Loranca del Campo, Cuenca province, Spain. It is placed in the geological basin of Loranca in the Iberian Range. The basin is recognized as a non-sequenced foreland basin containing continental Tertiary deposits folded along with the underlying Mesozoic rocks. From the Late Oligocene to the Early Miocene the Loranca Basin was filled by two coalescing depositional systems, the Tortola and the Villalba de la Sierra fluvial fans and associated environments. These depositional systems constitute the Upper Detrital Unit with a thickness of up to 900 m, which was formed during the major compressional tectonic phase of the Iberian Range. Tectonic activity during the deposition of the Upper Detrital Unit is evident because of progressive unconformities on the flanks of some anticlines, and along the basin margins. Detailed stratigraphic correlations may be hazardous due to the complex nature of fluvial deposits. During the Tertiary period the Loranca Bassin was filled with beds of terrigenous and chemical sediments such as carbonates and gypsum up to reach 1000 m of thickness. Here we analyze the vertebrate fossils outcrops of Loranca-1 (LO-1) dated as Rambliense (Low Miocene) which is an irregular boudine-shape sized 11 m composed by heterogeneous sands modified by post-sedimentary processes. These sands host fossil bonds with uranium minerals. This Loranca deposit was formed by transported fluvial sands containing fossil bonds. Later, the post-sedimentary tectonic and diagenetic processes break the bonds and remobilize several elements such as vanadium, uranium, iron and barium. Here we studied fragments of the fossil rhino *Protaceratherium minutum,* i.e., enamel, dentin, metapode, by X-ray Diffraction, being hydroxyapatite the enamel and francolite the dentine and metapode. The mineralogical composition of the sediment is quartz (77%), microcline (22%) and calcite (1%). The radioactive yellow mineral sited on fossil bonds and sediment was identified by XRD as Francevillite [(Ba,Pb)$(UO_2)_2(V_2O_8)\cdot 5H_2O$] and was selected to be analyzed under ESEM-CL to learn on the combined effect of the uranyl (UO_2) and vanadyl (V_2O_8) groups with barium and lead cations in comparison with other similar phosphates, arsenates and vanadates with uranyl groups and other cations.

ESEM-CL: The francevillite mineral is a phosphorecent yellow coating onto the Loranca fossil bond [$Ca_5(PO_4)_3(OH)$] (Figure a). Under the ESEM Francevillite looks as perfect euhedric rhomboedral plates (Figure b). The fossil background, ie., hydroxyapatite and collagen, also contain vugs stuffed with baryte ($BaSO_4$) (Figure c). Several spectra CL were recorded from franceville crystals (Figure c) exhibiting the characteristic uranyl emission peaks at circa of 527, 545, 576, 596 nm with the low intensity attributable to the presence of large amounts of vanadium.

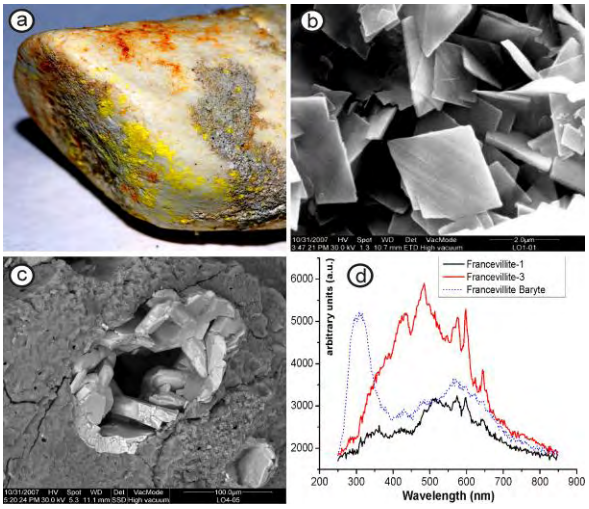

The tetravalent vanadium belongs to $3d^1$ ions being isoelectronic with Ti^{3+} an emission spectrum attributed to V^{4+} consists of broad band peaking at 625nm and narrow lines at approximately 528 and 529nm.

References: Daams, R., Lacomba, J.L. & López, N. (1986). Nuevas faunas de micromamíferos del Terciario continental de la Depresión Intermedia (Provincia de Cuenca, España centrooriental). *Estudios Geol*., 42: 181-196.

Gómez, J.J., Díaz Molina, M. & Lendínez, A. (1996). Tectono-sedimentary analysis of the Loranca Basin (Upper Oligocene-Miocene, Central Spain): a "non sequenced" foreland basin. En *Tertiary basins of Spain* (P. Friend y C.J. Dabrio, ed.). Cambridge University Press, 285-294.

MINERAL VARIATIONS STUDY OF CANELOBRE CAVE PHOSPHATE STALACTITES BY RAMAN AND LUMINISCENCE METHODS. García-Antón, E.[1], Cuezva, S.[2], Fernández-Cortes, A[1], Cuevas-González, J.[2], Muñoz-Cervera, M.C.[2], Benavente, D.[2], Sanchez-Moral, S.[1], Cañaveras, J.C.[2]. [1]Museo Nacional Ciencias Naturales. CSIC. 28006-Madrid. Spain. [2]Laboratorio de Petrología Aplicada, Unidad Asociada UA-CSIC, 08040-Alicante, Spain

Phosphate minerals are relatively abundant in caves although do not form spectacular free-standing speleothems. Phosphate stalactites found inside Canelobre cave (SE Spain) are here studied by hyperspectral Raman and Cathodoluminescence (CL). Together with XRD and EDS analyses we characterized the complex phosphate paragenesis present in these precipitates.

The studied stalactites show a typical concentric structure (Fig. 1b), with layers (50- 500µm thick) of phosphates in their inner zone showing massive to radial fibrous textures. Contact with calcite layers are irregular, indicating dissolutional processes. Hydroxylapatite [$Ca_5(PO_4)_3OH$] and brushite [$Ca(HPO_4) \cdot 2H_2O$] are the main phosphate minerals in the stalactites. XRD analyses also reveals the presence of taranakite [$(K,NH_4)Al_3(PO_4)_3(OH) \cdot 9H_2O$] and carbonate-hydroxylapatite [$Ca_5(PO_4,CO_3)_3(OH,O)$]. XRD patterns of most of these minerals are similar, so the distinction between the two phosphates relies on Raman and luminiscence analyses.

CL analysis show as different curves as spot analysis were done. Calcium phosphate characteristic red luminescence between 574 and 582 nm have been obtained in several points with changeable intensity (Fig. 1a). That marks variability in concentration of Mn^{+2} replacing Ca II and presence of quenching agents (as Fe^{2+}) that decrease luminescence [1]. Also calcite Uv-blue calcite structural emission near 360 nm peak [2] has been found at the interface zone (Fig. 1a). Raman curves confirms these mineralogical attributions: the 1080 peak corresponding to CO_3^{-2} vibration in calcite and the apatite 960 peak associated with carbonate substitution in A and B structural sites [2,3] (Fig. 1e). Raman line scan have been extracted from interface zone between two different phases showing the change in Raman spectra obtained from calcium phosphate to calcium carbonate (Fig 1 c, d and e). Both kind of analyses, CL and Raman, extract not easily interpretable spectra indicating the complex distribution of phosphate minerals. That reflects alteration or mixing of minerals presence. As bands of a Raman spectrum relate directly to the bond strengths and atomic masses, molecular groups such as the carbonate ion, the hydroxyl ion, and water of crystallization could be recognized in subsequent work as well as different phosphate mineral phases also could be distinguished. Brushite and taranakite form under acid conditions, on the contrary hydroxylapatite species indicates a slightly alkaline environment, so the coexistence of the described minerals within the phosphate staslactite gives information about changes in the pH and relative humidity of the environment.

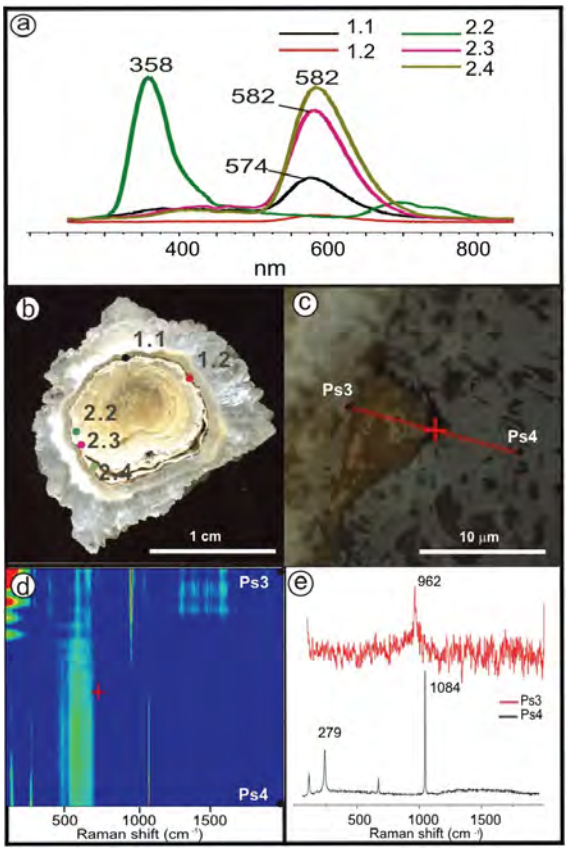

Fig 1. : a) Cathodoluminscence spectra obtained. **b)** sample images and spot analyses localitation. **c)** optical microscope image from the sample. **d)** Raman spectra line-scan from Ps3 to Ps4 image. **e)** Raman spectra from points Ps3 (phosphate minerals) and Ps4 (calcite).

Acknowledgements: Financial support by CGL2008-05929/BTE MEC project.

References

[1] Gaft, M. et al. (2005) *Modern Luminiscence Spectroscopy of Mynerals and Matherials*, 50-55 and 58-62. [2] Porto, S.P.S. (1966) *Depolaritation of Ramman Scatering in Calcite,* Physical Review, Vol. 147, num 2, 608-611. [3] Awonusi, A. (2007) *Carbonate Assignment and Calibration in the Raman Spectrum of Apatite*, Calcified Tissue International, Vol. 81, Num. 1, 46-52.

LUMINESCENT DETECTION OF ACTIVE STRESS IN MELILITE-ANORTHITE CAI GRAINS OF ALLENDE CV3 CHONDRITE (MEXICO).

Garcia-Guinea J.[1], Tormo L.[1], J., Azumendi, O.[2], Ruiz J.[2], Museo Nacional Ciencias Naturales. CSIC. 28006. Madrid. Spain. Dept. Geodinamica. Fac. C. Geologicas. Univ. Complutense 28040. Madrid. Spain
Author for correspondence: guinea@mncn.csic.es

Introduction: Calcium–aluminum-rich inclusions (CAIs) are the oldest known materials formed in the Solar System (Petaev & Jacobsen, 2009). FoBs are important forsterite-bearing Type B CAIs because of their intermediate chemistry and refractory inclusions. The studied Allende CAI has Forsterite (Fo) grains Al-rich clinopyroxene (Cpx), spinel (Sp), Mg-rich melilite (Mel) and minor anorthite (An) intergrown with Cpx forming a core surrounding Fo-Cpx as a discontinuous Al-rich mantle of Mg-depleted melilite. Many melilite grains are almost completely pseudomorphed by grossular (Gr) and monticellite (Mo). Anorthite-melillite grains shows zonings of extreme mineral chemical disequilibrium between their cores and mantles which could be producing the inferred Si–O strained structures as probable responsible emission-defects of the 340 nm CL emission peak.

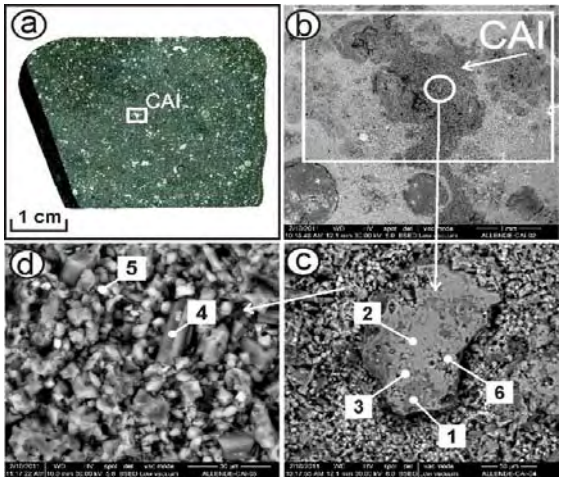

Figure 1.- (a) Allende CV3 chondrite (b) FoB-CAI (c) Melillite-Anothite grain (b) Matrix with Fo, CPx, Sp, An, Me, Mo, Gr.

Spectra blue luminescence : We previously published on the luminescence emission band at 340 nm of stressed tectosilicate lattices (Garcia-Guinea et al., 2007) observed just only in stressed silicon–oxygen lattices. The non-bridging-oxygen or silicon vacancy-hole centers associated with Si–O strained structures are the probable responsible emission-defects. The 340 nm CL emission is rarely detected in stressed aluminum-silicates and quartz with large amounts of Al^{3+}--alkali^{+} substituying silicon. At low temperature silicates enhance its 340 nm peak by cryogenic stress. The 340 nm emission peak can be observed in microcline with hatch-cross texture (Correcher et al., 1999).

ESEM-EDS analyses taken on the CL spots

	1	2	3	4	5	6
Na_2O	1,85	0	0,35	9,82	1,17	0,98
MgO	1,82	2,35	2,13	2,65	10,08	11,17
Al_2O_3	33,96	32,92	26,23	35,48	26,72	45,57
SiO_2	41,82	25,08	38,04	39	35,19	19,93
CaO	18,85	38,45	30,83	8,85	18,75	16,93
Fe_2O_3	1,7	1,2	1,9	2,12	3,89	5,1
TiO_2	0	0	0,52		4,2	0,32
K_2O	0	0	0	2,08	0	0
	100	100	100	100	100	100

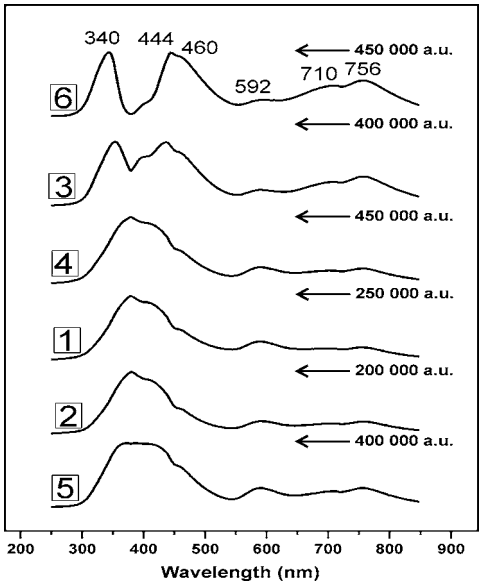

Spectra CL plots of melilite-anorthite grains of FoB-CAI in the Allende CV3 Chondrite (Mexico).

References: Petaev M. I., Jacobsen S. B. (2009) Petrologic study of SJ101, a new forsterite-bearing CAI from the Allende CV3 chondrite. Geochim. Cosmochim. Acta, 73 5100–5114.

Correcher V., Garcia-Guinea J., Delgado A. and Sanchez-Muñoz L. (1999) Spectra thermoluminescence emissions and continuous trap distribution of a cross-hatch twinned low microcline. Rad. Protec. Dosim. 84, 503–506.

Garcia-Guinea J., Correcher V., Sanchez-Munoz L., Finch A.A., Hole D.E., Townsend P.D. (2007) Luminescence emission band at 340nm of stressed tectosilicate lattices. Nucl Instr Meth Phys Res A 580, 648–651.

NATURAL EARTH PIGMENTS FROM ROMAN AND ARABIC WALL PAINTINGS REVEALED BY SPECTROSCOPIC TECHNIQUES. I. Garofano[1], A. Duran[1], J.L. Perez-Rodriguez[1] and M.D. Robador[2]
[1]Materials Science Institute of Seville, Americo Vespucio 49, 41092 Seville, Spain adrian@icmse.csic.es [2]Technical Architecture Faculty, University of Seville, Reina Mercedes 4, 41002 Seville, Spain

Introduction: Natural earths and minerals have been used as pigments since prehistoric times. They have been found in works of art everywhere and in any historical period due to their availability, high colouring capacity and stability [1]. The main aims of this work are the identification and comparative study of the pigments used in Roman and Arabic wall paintings by only using spectroscopic methods. In this form, a multi-analytical approach including micro-Raman, FT-Infrared and UV-visible, accomplished by chromatic studies, provided complete information on the compositions of the paintings, which can be regarded as a powerful tool for conservators, restorers, art historians and archaeologists.

Experimental: Fragments from Roman wall paintings of Reales Alcazares Palace in Seville (1st century B.C.) and Pompeii Houses (2nd century B.C.) were studied. In addition, we studied some Arabic wall painting fragments (11th century A.D.), also collected from Reales Alcazares Palace. The dispersive integrated Horiba Jobin-Yvon LabRam HR 800 system was employed for recording the Raman spectra directly on the fragments. Lasers emitting at 532.1 nm (green) and at 784.6 nm (red) were used. An optical microscope was coupled confocally to the Raman spectrometer. FTIR spectra were collected using a Jasco FT-IR-6200 FV spectrometer (DTGS detector). KBr was mixed with powder samples for performing these experiments. UV-Vis spectra (Cary 100, Varian) were recorded in the diffuse reflectance mode. Powder samples were mixed with $BaSO_4$ that does not absorb in the UV-Vis range. The chromatic characterization was determined over the fragments using a Dr Lange Neurtek model LMC3/DIAM 5 portable spectrometer that produces normalized D65 light.

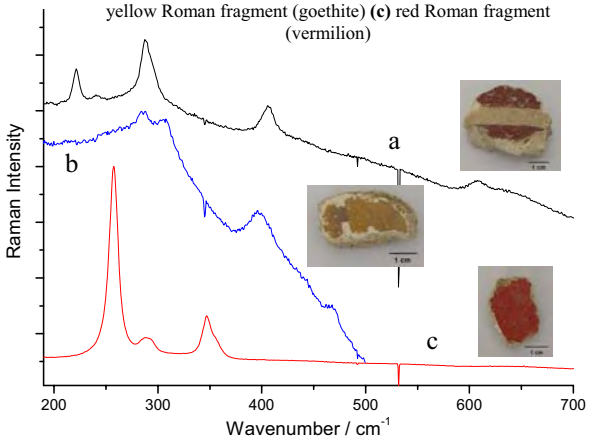

Fig 1: Raman spectra of: **(a)** red Arabic fragment (hematite) **(b)** yellow Roman fragment (goethite) **(c)** red Roman fragment (vermilion)

Results: Raman spectroscopy allowed the indistinguishable identification of the majority of the pigments found in the paintings: hematite (bands at 227, 245, 294, 300, 409, 610 cm^{-1}), goethite (287, 303, 397, 469 cm^{-1}), vermilion (257, 290, 347 cm^{-1}), carbon black (1325, 1592 cm^{-1}), Egyptian blue (431, 1085 cm^{-1}), calcite (277, 710, 1083 cm^{-1}).

We used infrared spectroscopy to distinguish the presence of ochre colours (clays mixed with hematite or goethite) by the detection of bands associated to clays (hydroxyl ions: 3695, 3648, 3617, 3352, 3418, 3185 cm^{-1}, and aluminosilicates: 1032 cm^{-1}). Green earth was also identified by FTIR due to the detection of absorption bands assigned to celadonite (3601, 3556, 3531, 1106, 1075, 961, 799, 683 cm^{-1}) and glauconite (3615, 3531, 979, 962 cm^{-1}). However, poor Raman spectra were obtained for the green colour fragments. FTIR band-shoulder at 1025 cm^{-1}, observed in the black fragment, could be attributed to the presence of phosphate groups (ivory black).

Red ochre, yellow ochre, vermilion, green earth, carbon black, ivory black, Egyptian blue and calcite were the compounds detected in the Roman wall paintings, while hematite and calcite were observed in the Arabic ones (the ornamentation palette of all Islamic buildings is dichromatic, usually red and white).

UV-Vis and chromatic studies agree with the results found with the other experimental techniques. λ_{dom} (dominant wavelengths) are in the adequate zone within the visible region (400-800 nm) in all the cases, and CIE L*a*b* parameters match with those from pigments described in the literature. These latter studies permitted to identify slight variations of hue attributed to mixtures of pigments, such as in the case of blue and green fragments.

Conclusions: The combined application of the above mentioned spectroscopy methods allowed a full characterization of the pigments employed by Romans and Arabs in the wall paintings studied. Natural earths and minerals were the pigments mainly employed by both civilizations although some differences were found. The identification could help in tracing the possible routes of pigments origin and diffusion. The present work is one of the first articles devoted to the study of both Roman and Arabic wall paintings by using exclusively spectroscopic methods.

References: [1] Genestar C., Pons C. (2005) *Anal. Bioanal. Chem.* 382, 269-274.

RAMAN SPECTROSCOPY AND MICROPROBE INVESTIGATION OF THE INCORPORATION OF Cr (VI) IN $CaCO_3$. A. M. Gigler[1], N. Sánchez-Pastor[2], J. A. Cruz[2], and L. Fernández-Díaz[2]. [1] CeNS and Department for Earth and Environmental Sciences, Ludwig-Maximilians-Universität. 80333, Munich (Germany), [2] Departamento de Cristalografía y Mineralogía. Universidad Complutense de Madrid. 28040, Madrid (Spain).

Introduction. Due to its high mobility and toxic effects even in low concentrations, hexavalent chromium (Cr (VI)) is known as one of the most common environmental contaminants resulting from its widespread use in industrial applications. Cr (VI) compounds are used mainly because of their acidic properties and their ability to form intensely colored and insoluble salts.

Experimental. The crystallization experiments were performed in a double diffusion system [1]. Different concentrations of Na_2CrO_4 (0.1, 0.15, and 0.2 M) were added to the sodium silicate solution during the gel preparation. Two months after the nucleation, crystals comprising a representative range of morphologies with different intensities in yellow color were hand-picked from the gel. Their morphology was studied by scanning electron microscopy and the Cr concentration of the crystals and the development of zoning were analyzed by electron microprobe. A confocal Raman microscope was used to identify the $CaCO_3$ polymorphs and to investigate the zoning in the crystals.

Results and discussion. All spectra revealed the characteristic peak of calcite at 1085 cm^{-1} which is caused by the symmetric stretching vibration of the carbonate group. Furthermore, we observed peaks at 280 cm^{-1} and 711 cm^{-1} corresponding to the translational and rotational lattice mode vibrations and to the internal translational modes of in-plane bending of the carbonate ions, respectively. In Figure 1, a close up of the ν_2 region (peaks between 700 and 1100 cm^{-1}) of these samples together with the main vibrational modes for chromatite as a reference is shown. The chromatite spectrum was obtained from a natural sample. In addition to the calcite bands mentioned above, some weak Raman bands appear between 850 and 925 cm^{-1}. As mentioned by Urmos et al. [2], the ν2 band at 875 cm^{-1} is not allowed in the Raman spectra of crystals with calcite structure. However, this vibrational mode at 875 cm^{-1} is the most intense in chromatite and could be assigned to the ν1 symmetric stretching vibration of CrO_4. Some additional weak bands are also present. Frost and Weiner described the Raman spectra of the CrO stretching region of some chromate-bearing minerals [3] In this region the band position varies from 825 to 972 cm^{-1} depending on the mineral. We found three main bands at 855, 875, and 975 cm^{-1}. The first two agree well with those enunciated by Frost and Weiner and subsequently, the new bands represent the incorporation of Cr (VI) into the calcite structure as chromate groups. Furthermore, Wang et al. conducted a Raman spectroscopic study to distinguish the chromate species on Cr-MCM-41 synthesized by a direct hydrothermal synthesis method [4] In this work, the band at 980 cm^{-1} was assigned to the Cr-O vibration stretching of the dehydrogenated monochromate species (CrO_4^{2-}). Thus, the third more intense band found in our spectra can be also correlated with the presence of Cr (VI) in the structure. These hypotheses are supported by the fact of the different intensities of the new bands. As can be observed in Figure 1, the intensity of the new peaks can be correlated to the content of Cr (VI) in the gel medium.

To investigate the possible zoning of the calcite crystals, a yellow crystal from the experiments with higher Cr concentration (0.2 M) was analyzed in detail by Raman and microprobe mapping. The electron microprobe showed that the inner part is Cr rich, while pure calcite is present in the outer regions. Moreover, a Raman profile was obtained from the same crystal and the analysis is perfectly correlated with the micropobe analysis.

Conclusions. i. Our results confirm the suitability of Raman spectroscopy to characterize the incorporation of impurities in carbonate phases and, ii. The incorporation of Cr is evidenced by the appearance of new vibrational bands in the calcite spectrum, which are consistent with the substitution of carbonate groups by chromate groups.

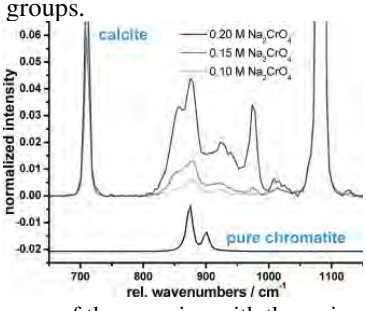

Figure 1. Close up of the ν_2 region with the main vibrational modes for chromatite superimposed.

References.

[1] Henisch, H.K. and García-Ruíz, J.M. (1986) *J. Cryst. Growth*. 75, 195-202. [2] Urmos, J. et al. (1991) *Am. Mineral*. 76, 641-646. [3] Frost, R.L., and Weier, M. (2004) *Neues Jahrbuch Min*. 12, 575-594. [4] Wang, Z. et al. (2002) *J. Biol. Chem.* 277, 24022-24029.

RAMAN MICROSCOPY OF SHOCKED AND UNSHOCKED BASALTS FROM LONAR CRATER, INDIA. T. D. Glotch[1] and M. J. Ferrari[1], [1]Stony Brook University, Stony Brook, NY 11794-2100, tglotch@notes.cc.sunysb.edu

Introduction: Mars, the Moon, and other planetary bodies have been subjected to intense bombardment by meteorites throughout their histories. Understanding the effects of this bombardment on the crystal structures of target materials is a first-order problem in planetary science that has important implications for planetary remote sensing and *in situ* mineralogical studies.

Within the the ejecta of Lonar Crater are basaltic rocks shocked at intermediate pressures of 20-80 GPa [1]. Other terrestrial impact craters primarily occur in typical continental crust or sedimentary settings. The basaltic composition of the Lonar impact crater makes it the only terrestrial impact analog suitable for understanding the effects of impact on the composition of the Martian basaltic crust and lunar mare.

Several studies have detailed the mid-IR spectroscopic properties of synthetically shocked plagioclase feldspar and pyroxene-rich samples and basalts [2-4]. Recent studies have also detailed the macroscopic mid-IR spectral properties of naturally shocked basalts from Lonar Crater [1,5]. Here, we provide micro-Raman data for both shocked and unshocked basalts from Lonar Crater. These data provide a detailed view of the petrography of Lonar samples and indicate that the effects of shock are not homogenous throughout the material undergoing shock compression.

Samples and Methods: We analyzed several samples of shocked and unshocked basalt from Lonar Crater collected by S. P. Wright and described further in [6]. Three samples, LC09-206, LC09-207, and LC09-284 were selected for analysis. LC09-206 and LC09-284 are shock class 2 samples (20-40 GPa shock pressure) [7], while LC09-207 is an unshocked basalt collected in the same suevite breccia outcrop as the other two shocked basalts that displays a minor amount of weathering. Samples were cut and polished into thick sections with a roughness of 0.25 μm.

Each sample was examined using the Stony Brook University Vibrational Spectroscopy Laboratory (VSL) WiTEC alpha300R confocal Raman microscope system equipped with a 50 mW frequency doubled 532 nm Nd:YAG excitation laser. This Raman imaging spectrometer is capable of acquiring spectra from ~8000-150 Δcm^{-1} and is equipped with multiple objective lenses enabling spatial resolutions between several microns and 260 nm/pixel.

Results and Discussion: Both LC09-206 and LC09-284 contain abundant maskelynite (feldspathic glass) formed as a result of the shock process. These samples also contain unshocked clinopyroxene and and melt glass, either in veins or pockets**.** Figure 1 shows background-removed labradorite and augite spectra (705 nm spot size) from the unshocked LC09-207 sample and maskelynite and melt glass spectra from the shocked LC09-206 sample. The maskelynite and melt glass Raman spectra differ, with maskelynite displaying broad peaks between 500 and 600 Δcm^{-1} and ~900-1100 Δcm^{-1}. The melt glass spectrum displays a comparatively sharp peak centered at 590 $\Delta cm^{-1}$and a weaker, broader peak centered at 1090 Δcm^{-1}. Both spectra differ markedly from the crystalline spectra from the unshocked sample. Future work will concentrate on creating Raman maps with sub-μm spatial resolution in an effort to determine the effects of shock on potential accessory minerals and to study the effects of aquesous weathering on these samples and corellating results with micro-FTIR studies of the same samples [8].

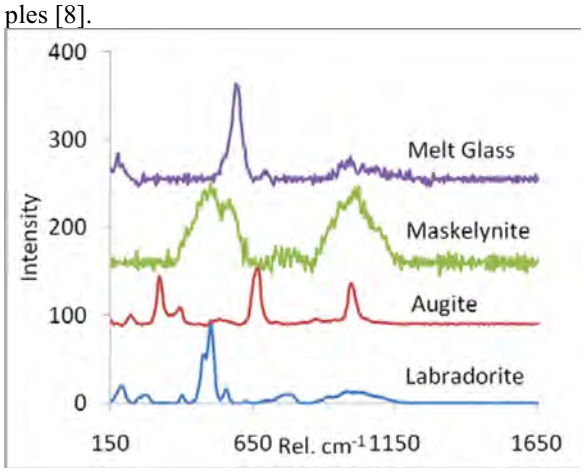

Figure 1. Micro-Raman spectra acquired from samples LC09-284 (labradorite and augite) and LC09-206 (maskelynite and melt glass). Spectra were acquired using a 532 nm excitation laser and a 20 X, 0.46 N.A. objective, leading to a 705 nm spot size.

References: [1] Wright S. P. et al. (2008) *LPS XXXIX,* Abstract 2330. [2] Johnson J. R. et al. (2002) *JGR*, 107(E10), 5073. [3] Johnson J. R. et al. (2003) *Am. Miner.*, 88, 1575-1582. [4] Johnson J. R. et al. (2007) *Am. Miner*, 92, 1148-1157. [5] Wright S. P. et al. (2011) *JGR*, in review. [6] Wright S. P. and H. E. Newsom (2011) *LPS XLII*, Abstract 1619. [7] Kieffer S. W. (1976) *LPS VII*, 1391-1412. [8] Glotch, T. D. et al. (2011) LPS XLII, Abstract 1566.

ANALYSIS OF HEALTH AND ENVIRONMENTAL RISK ASSESSMENT OF AN ABANDONED Zn-Pb MINE THROUGH THE WEATHERING PROCESSES OF THE LOCAL MINERALS. N. Goienaga[1,*], J.A.-Carrero[1], I. Arrizabalaga[1], J. Bustamante[1], L.A. Fernández[1] and J.M. Madariaga[1].
[1] Department of Analytical Chemistry, University of the Basque Country (UPV-EHU), 48080 Bilbao, Spain.
* E-mail: naiara.goyenaga@ehu.es

Introduction: Hardrock mining activities are long-term industrial activities that take place in the natural environment potentially disturbing large amounts of material and land areas. Closure of a mining operation often implies a continuous leaking of risky trace metals into the surrounding environment [1].

The present research aim is to determine the concentration of pollutants in different media as a way to assess the impact of potential sources of contamination. The chemical analysis of their concentrations in different environmental compartments (i.e., soil, air, vegetation) may be an interesting indirect methodology for human health and environmental risk assessment. Thus, the migration of such pollutants should be monitorized in order to avoid a long-term cronic impact of soil, surface and ground water qualities.

Experimental: Ten effluorescence samples were collected along the main gallery of the abandoned mine. Once their physico-chemical characterization was carried out, more exhaustive analytical techniques were used: ICP-MS to know the soil composition and Raman for determining its molecular characteristics.

Movility tests were also performed in order to have a notion of the movable and, consequently, bioavailabe fraction. These solutions were measured by ICP-MS and Ion-Chromatography.

Results and discusion:

The movility test applied showed how easily some ions were able to dissolved in hugh amounts. Not only the most common anions present in soils were obtained (i.e. phosphates, sulphates) but also environmentallly risky heavy metals (Zn, Pb, Cu, As, Hg, etc.).

The present study tried to understand the behaviour that the mine-soil polluting components may have under natural weathering conditions. To achieve this, the molecular structures present in the effluorescences were identified by Raman spectroscopy. Besides, the minerals found were classified into primary (geologically natural minerals) and secondary (non-stable phases derived form the weathering of the primary ones)[2].

The primary mineral list observed included galena (PbS), sphalerite (ZnS), calcite ($CaCO_3$), etc. while the secondary mineral list incorporated calomel (HgCl), olivenite ($Cu_2AsO_4(OH)$), getchellite ($SbAsS_3$), tinticite ($Fe_5(PO_4)_4(OH)_4{\cdot}7H_2O$), otavite ($CdCO_3$), wolfeite ($Fe_2(PO_4)(OH)$), claudetite ($As_2O_3$) etc.

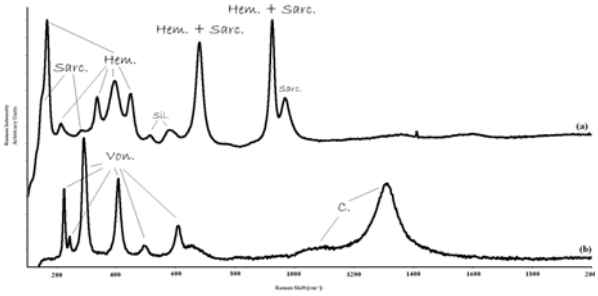

Fig.1. (a) Mixed spectrum of sarcopside (Sarc.) and hemimorphite (Hem.). (b) Mixed spectrum of black charcoal (C.) and vonseite (Von.).

Conclusions:

The concern resulting from the potential exposure to contaminants was the starting point to develop new methodologies in order to evaluate the consequences that those might have over both the environment and human health. Among these methods, risk assessment has been one of the most widely used [1,3]. As it has been shown, environmental monitoring is basic in order to carry out a correct evaluation of the exposure.

The knowledge of the ions' solubilities mixed with the several mineral phases found per metal (i.e. oxide, sulphide, phosphate, etc.), provide a better understanding of the leaching processes for each metal that may have taken or will take place. Furthermore, considering that the studied area is mainly karstic, such processes become crucial in the groundwater protection. Therefore, such research can be included as a first step within the set of tools for risk assessment that governmental policy makers should consider.

Acknowledgements: This work has been financially supported by the ETORTEK Programme of the Basque Government through the BERRILUR II Project (ref. IE06-179). N. Goienaga, J.A. Carrero and J. Bustamante are grateful to the University of the Basque Country for their pre-doctoral fellowships.

References:

[1] EPA (2000). *Abandoned mine site characterization and cleanup handbook.*

[2] N.G. et al. (2011) *Spectrochim. Act. A,* doi 10.1016/j.saa.2011.01.032.

[3] EEA (1998) *Environmental Risk Assessment*.

RELATIONS BETWEEN LEACHATED COMPOUNDS AND RAMAN SPECTRUM OF BLACK SLAGS FROM EAF IN ORDER TO CHARACTERIZE THEM. L. Gómez-Nubla [1], J. Aramendia, S. Fdez-Ortiz de Vallejuelo, K. Castro and J. M. Madariaga. Department of Analytical Chemistry, University of the Basque Country (UPV/EHU), P.O. Box 644, E-48080 Bilbao, Basque Country, Spain. Tel.:+34 94 601 82 97; Fax: +34 94 601 35 00
[1]E-mail address*:* leticia.gomez@ehu.es

The black slags are a by-product of the steel fabrication. In this case they are produced in the fusion process by means of Electric Arc Furnace (E.A.F.). This type of material has a high strength and due to its durability and chemistry has been used as construction material and more recently, as a cement additive, landfill cover material, and for agricultural applications [1-3]. In spite of this fact, they present some difficulties due to their volume instability and leaching of elements from them. So it should be considered the possible impact in soils and nearby drinking or surface waters where black slags have been used [4, 5] or deposited in dumping sites.

In this study have been analyzed samples from two different industries: ordinary steel industry and special steel industry. In both cases, original and treated black slags were provided us. The ordinary steel treatment consisted of outdoor cooling, water, crushing, sifting and magnetic separation of ironed materials. In the case of special steel treatment, it was only based on cooling outdoor and water. Apart from these, some black slags were picked up in two locations of Vizcaya (Basque Country, Spain). These samples were considered treated due to were collected in construction works, and in order to be used they must be subject of treatment according to the legislation [6].

It was carried out a molecular characterization of all these black slags through Raman Spectroscopy Renishaw RA 100, (Oxford, UK) and an InnoRaman ultramobile spectrometer (B&WTEK$_{INC}$, Newark, USA). The spectrums indicated a bigger presence of hydroxides in treated slags than in the slag without treatment: lepidocrocite, goethite, limonite, etc.

Moreover, it was realized a leaching with Milli-Q water as extractant to reproduce the conditions that are given in the nature. The concentrations of released elements from the black slags were obtained by means of Inductively Coupled Plasma Mass Spectrometry (ICP-MS) and ionic chromatography (CI). With these data was made a statistical treatment: correlation analysis between cations (Al, Ba, B, Cr, Cu, Fe, K, Li, Mg, Mn, Mo, Na, Ni, Pb, Sb, Sn, Sr, Ti, V, W, Zn and Ca) and anions (F^-, Cl^-, NO_3^- and SO_4^{2-}). It was compared which cations and anions were relationated with the compounds identified in the Raman spectrums obtained previously. It was observed, among others, a high correlation between iron and calcium, boron and barium, nickel and iron, sulfate and calcium… This last correlation corroborated the presence of gypsum ($CaSO_4$) appeared in the Raman spectrum .

Finally, it was made a parallel valoration with H_2SO_4 and NaOH, in order to determinate the carbonates contained in the black slags. After that, it was speculated about the acid gas attack over these carbonates, forming compounds that with the leaching could arrive to unbalance the environmental where the black slags had been deposited [7].

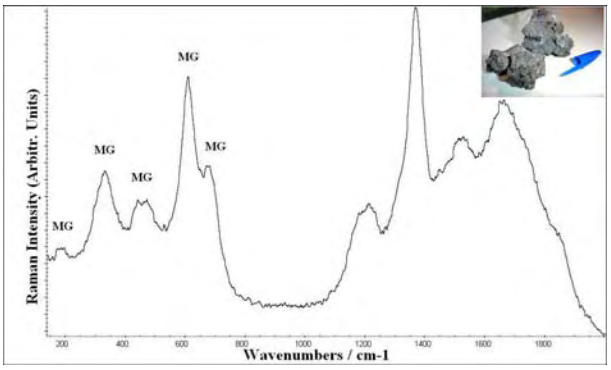

Figure 1. Raman spectrum of magnesioferrite (MG) together with typical silicates Raman bands of the black slags (right side).

References

[1] Tsakiridis P.E. et al. (2008) *J. Hazard Mater.* 152, 805-811. [2] Sofilic T. et al. (2010) *J. Radioanal. Nucl. Chem.* 284, 73-77. [3] Van der Waals J.H. and Claassens A.S. (2003) *Mining and the Environment III*. [4] Tossavainen M. et al. (2007) *Waste Manage*. 27,1335-1344. [5] Proctor D. M. et al. (2000) *Environ. Sci. Technol*, 34, 1576-1582. [6] BOPV, 2003. N4. Decreto 34/2003 (Comunidad Autónoma del País Vasco) (http://www.euskadi.net). [7] Sarmiento A. et al. (2008) *J.Raman Spectrosc*. 39, 1042-1049.

Acknowledgements

This work has been financially supported by Basque Government through ETORTEK BERRILUR 3 project (ref. IE10-273).
L. Gomez -Nubla and J. Aramendia are grateful to the University of the Basque Country (UPV-EHU) and Basque Government respectively, for them predoctor fellowship.

Trace Element and REE leaching during Diagenetic Albitization and its relationship to the Cathodoluminescence colour of Feldspars: the Tera Group, Cameros Basin (NE Spain)

Authors: González-Acebrón, L.[1], Barca, D. [2] Arribas, J.[3]; Mas, Ramón[1]

[1] Dpto. Estratigrafía, Facultad de Ciencias Geológicas (UCM)- IGE, IGEO (CSIC), C/ Jose Antonio Novais 2, 28040 Madrid (Spain)

[2] Dipartimento di Ciencias de la Terra, Università de la Calabria (Italy).

[3] Dpto. Petrología y Geoquímica, Facultad de Ciencias Geológicas (UCM)- IGE, IGEO (CSIC), C/ Jose Antonio Novais 2, 28040 Madrid (Spain)

Corresponding author: Tel: (34)913944785. E-mail: lgcebron@geo.ucm.es (L. González-Acebrón)

This study deals with the diagenetic albitization of both plagioclases and K-feldspars in the Tithonian fluvial sandstones of a rifted basin (Cameros Basin). A cathodoluminescence (CL) study of feldspars was performed using a cold instrument on sandstone thin sections. Trace elements and REE were studied on 300 μm-thick sections involving simultaneous laser ablation and inductively coupled plasma mass spectrometry (ICP-MS).

The sandstones in the lower part of the rift record have not suffered the albitization process. A clear relationship is observed between sodium contents, as the main element of some feldspars, and their CL colour (the higher the sodium content, the lower is their CL). In addition, very different profiles are obtained when comparing trace elements of non-albitized feldspars in sandstones of the lower part of the rift record to those of albitized feldspars in sandstones of the infill top. Non-albitized K-feldspars show Rb, Sr, Ba, Pb contents up to 1000 ppm. In contrast, very flat profiles of trace element contents (<250 ppm) are recorded in albitized feldspars (both K-feldspars and plagioclases). Thus, albitization implies feldspars impoverished in trace elements, including REE. This impoverishment suggests leaching of most of the initial trace elements. In addition, partially albitized grains show albitized areas related to weak zones such as cleavage and fracture planes.

Albitized plagioclases show higher REE contents than albitized K-feldspars. According to the literature, non-albitized plagioclases are richer in REE than non-albitized K-feldspars. We report here that REE patterns partly depend on the initial composition of the feldspar (K-feldspar or plagioclase) as a useful geochemical criterion for distinguishing albitized detrital plagioclases from K-feldspars.

Albitized plagioclases are ridded with primary fluids inclusions, mainly all-liquid. Around 20% of the fluid inclusions feature a gas bubble, with liquid to vapour ratios between 95:5 and 85:15. Homogenization temperatures of cogenetic fluid inclusion assemblages indicate minimum albitization temperature around 83-115ºC. This temperature allowed the leaching of trace elements and REE during the albitization, interpreted as a dissolution and reprecipitation process. Additional work is carrying on determining CL colour relationship with CL spectra.

A COMBINED CATHODOLUMINESCENCE AND MICRO-RAMAN STUDY OF PLANAR DEFORMATION FEATURES IN QUARTZ. A. Gucsik[1,2], T. Okumura[3], M. Kayama[3], H. Nishido[3], K. Ninagawa[4], [1]Department of Earth and Planetary Materials Science, Graduate School of Science, Tohoku University, Aoba 6-3, Aramaki, Aoba-ku, Sendai, 980-8578, Japan (E-mail: ciklamensopron@yahoo.com); [2]Konkoly Observatory of the Hungarian Academy of Sciences, H-1121, Budapest, Konkoly Thege Miklós út 15-17., Hungary; [3]Research Institute of Natural Sciences, Okayama University of Science, 1-1 Ridai-cho, Okayama, 700-0005, Japan; [4]Department of Applied Physics, Okayama University of Science, 1-1 Ridai-cho, Okayama, 700-0005, Japan;

Introduction: The question of whether shock metamorphic effects may modify the luminescent nature of quartz under subsequent compression has been addressed in a pioneering study of Boggs et al. [1]. Here, we report the first systematic experiments by means of the micro-Raman spectroscopy and Scanning Electron Microscopy-Cathodoluminescence microscopy that investigate the effect of shock-induced amorphization to the electronic transitions in the high-pressure phase transitions. Up to now, phase transition studies of quartz have only used high-pressure polymorph of quartz (i.e., coesite, stishovite, etc.), not typical of shock-induced microdeformations (for instance, Planar Deformation Features-PDFs) in quartz as it is found in the target rocks of the terrestrial impact craters.

Experimental Procedure: The Raman spectra were obtained using a Thermo Nicolet Almega confocal micro-Raman spectrometer with a Nd:YAG-laser (20 mW at 532 nm) laser excitation system and a cooled CCD detector at 223K. SEM-CL images were collected using a Scanning Electron Microscope (SEM-JEOL 5410LV), equipped with a CL detector (Oxford Mono CL2), which comprises an integral 1200 grooves/mm grating monochromator attached to a reflecting light guide with a retractable paraboloidal mirror.

Results and Discussion: Raman spectra of shocked quartz exhibit a dominant peak at around 459 cm^{-1}, whereas typical high-quartz has a sharp and intense peak at 464 cm^{-1}, which can be assigned to O-Si-O stretching vibrational mode [2]. This frequency shift is related to a distortion of structural configuration such as formation of high density diaplectic SiO_2 glass and/or amorphization associated with the occurrence of glass-filled PDFs [2] as designated as green or blue stripes of Figure 1.

CL spectrum of shocked quartz contains two broad bands centered at 450 to 650 nm, which are assigned to presence of defect centers on, e.g., SiO_4 groups. The dominant observed defects occur in the short-range order involving the slightly distorted SiO_4 tetrahedra, which are common to both the crystalline and amorphous SiO_2 structures [3]. We observed that the CL emission, which is enhanced at a lower temperature (-192 °C), several hundred times more intense than that at room temperature (25 °C) due to temperature quenching effect. It gives a strong broad peak in the blue region with doublet apexes at 455 and 465 nm, which could be assigned to intrinsic emission bearing on the E'_1 and E'_2 centers [3].

Conclusion: The displacive phase transformation of quartz (i.e., trigonal-hexagonal transition at low temperature and high pressure) occurred in the PDFs has small symmetry and electronic structure-breaking displacements of atoms resulting non-radiative processes in the luminescence emission. This indicates that the non-luminescence of the PDFs will increase with decreasing temperature and increasing shock pressure. We noted that the combination of SEM-CL and micro-Raman techniques is a useful tool for the evaluation of the shock stages and identification of shock-induced microdeformations in the shock-deformed minerals, especially for the rock-forming minerals.

References:

[1] Boggs et al. (2001) *Meteoritics & Planet. Sci., 36,* 783-793. [2] Champagnon et al. (1996) *J. Non-cryst. Solids* 196, 221-226. [3] Kalceff et al. (2000) In Cathodoluminescence in Geosciences (eds. Pagel M., Barbin, V., Blanc, Ph. and Ohnenstetter, D.), Springer, p. 193-224 (2000).

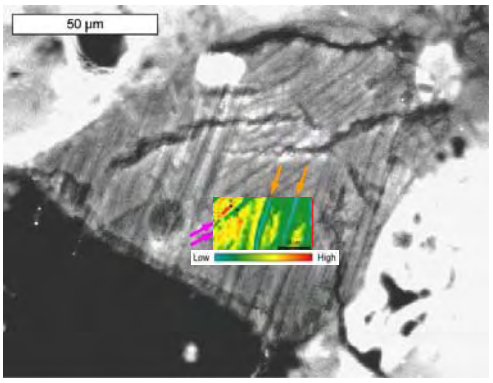

Figure 1. SEM-CL image and a 2D Raman image (inlet) of PDFs in quartz from Ries meteorite crater, Germany.

IN SITU µ-RAMAN OBSERVATION OF URANIUM DIOXIDE WEATHERING IN CONTACT WITH WATER AND UNDER ION BEAM IRRADIATION

G. Guimbretière*, A. Canizares, P. Simon, Y.A. Tobon-Correa, M.-R. Ammar, C. Corbel and M. F. Barthe
CNRS UPR 3079, Conditions Extrêmes et Matériaux – Haute Température et Irradiation, 45071 Orléans Cedex 2
* guillaume.guimbretiere@cnrs-orleans.fr

Earth and space environment are sometimes the frame of extreme conditions of temperature, pression and irradiation. I*n situ* characterizations are necessary for a better understanding of the structural and chemical changes induced by such extreme environmental conditions. This paper deals with *in situ* Raman characterization of a material exposed to ionic irradiation.

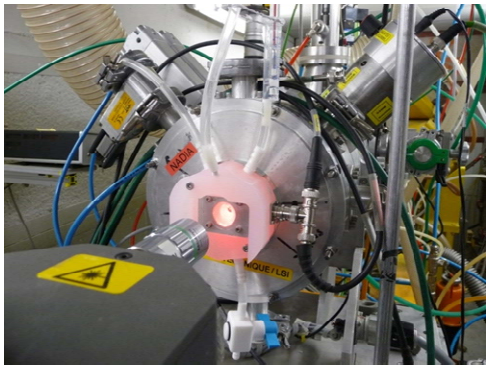

Fig.1 : In situ irradiation µ-Raman head with the cyclotron beam radiolyse cell.

One topic where the irradiation effect is a key-point is the study of the uranium mobility in the geosphere: Naturally, uranium exists in concentrations of a few ppm in soil, rock and water (more than 4 10^7 t as ore and 4.5 10^{12} t in sea water). Besides, the human activities induces a release of uranium ores and secondary weathering products to the surface environment.
It is well known that exposed to oxidizing conditions, tetravalent U(IV) present in uraninite and UO_2 spent nuclear fuel is incorporated in common alteration products as U(VI) –phases, up to form an assemblage of secondary uranyls minerals with chemical compositions indicative of the local environment. These uranyl phases are more soluble than U(IV) material and thus, this leads to an increase in mobility of uranium to groundwater and soil. For these reasons, the impact studies of the environment on the hydration-oxidation weathering of uranium minerals is of first importance.
For uranium compounds, deal with the environmental condition mean dealing with irradiation [1]: Indeed, uranium is naturaly weakly α radioactive with more than 100's million years half-life. Then, uranium products are the most often exposed to self-irradiation or irradiation from neighbouring active actinide products. Unfortunatelly, the possibilities to observe over time the effects of weak radio-activity as in the natural fission reactors of Oklo (Gabon) are infrequent. Effects of ionic irradiation can then be simulated by accelerator ionic beam, where high flux allows to simulate in a short time the dose and fluence of long time natural exposure. The sparsity of appropriate natural conditions and the experimental complexity of *in situ* ion beam characterization may explain the only few works on this topic.

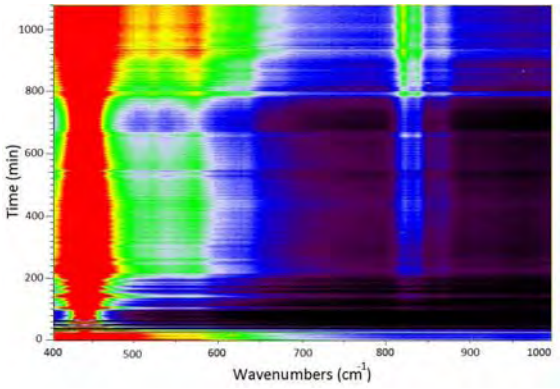

Fig.2: In situ Raman kinetic of the UO_2/water interface during and after irradiation. Colors represent Raman intensity and y-axis the time (one spectrum by 2 min).

Therefore, a significant part of this paper, is dedicated to the original *in situ* Raman spectrometer coupled with an ionic beam of a cyclotron accelerator (see figure 1). In a second part we present and discuss the Raman monitoring Uranium U(IV) dioxide / water interface under He ions irradiation. The figure 2 shows the evolution of the Raman spectra with time. One can distinguish the evolution of hydroxide and peroxide uranyl U(VI) compounds exhibiting signature in the 800-900 cm^{-1} range. Stability of these uranyl oxide hydrates versus the environmental conditions are widely discussed [2,3], and the irradiation effect clearly needs to be taken into account [4].
Our results provide, in part, a foundation for developing predictive models of U(IV) ↔ U(VI) natural cycles.

[1] Utsunomiya S. et al. (2005) *Earth planet. Sci. Lett. , 240,* 521–528. [2] Sowder A.G. et al. (1999) *Environ. Sci. Technol. , 33,* 3552–3557. [3] Kubatko K-A.H. et al. (2003) *Science, 302,* 1191–1193. [4] Corbel C. et al. (2006) *J. Nucl. Mater., 348,* 1-17.

THE SUITABLE CAROTENE AND XANTHOPHYLL IDENTIFICATION IN *LECANORA* LICHENS: RESONANCE RAMAN SPECTROSCOPIC STUDY. I. Ibarrondo*, N. Prieto-Taboada, I. Martínez-Arkarazo and J. M. Madariaga, Department of Analytical Chemistry, Faculty of Science and Technology, *University of the Basque Country* (UPV/EHU), Bº Sarriena s/n 48940 Basque Country, Spain. *corresponding author: iratxe.ibarrondo@ehu.es.

Introduction: Lecanora lichen species have been recognized as air pollution resistant due to their ability in acquiring new knowledge to protect themselves from high concentration of acid gases and metals [1, 2].

Carotenoids, ubiquitous compounds in lichens, are often classified as protective pigments because they dissipate the light energy used in photosynthesis and inhibit the formation of harmful reactive oxygenated species [3].

Raman Spectroscopy has been used widespread for characterization purposes of lichen metabolites, especially in the characterization of lichen acids and pigments such as carotenoids. But sometimes the Raman assignments are not clear, are into controversy and the majority of the authors do not reach agreement [4, 5].

The Raman spectra of carotenoids present three major bands in the following order: in the regions of 1500-1550 cm^{-1} and 1150-1170 cm^{-1} appears two strong bands specific to the conjugated polyene chain of the carotenoids. The first one (ν_1) belongs C=C bonds in main skeleton and the second one (ν_2) related the C–C bonds of the same skeleton. In the 1000-1020 cm^{-1} region another peak (ν_3) appear related to the -CH_3 groups attached to the polyene chain. For instance, low number of conjugated double bonds shifts ν_1 band to major wavenumbers and vice versa [6].

The selection of the incident laser wavelength is an important aspect that influences the absorption of the chromophore. When maximum absorption is achieved, the analyses are said to be done in resonance conditions, where the Raman peaks of the chromophoric compound are enhanced significantly respect to other compounds presented [5].

The aim of this work is to characterize by Resonance Raman Spectroscopy a *Lecanora* lichen colonies to make proper Raman asignments in the path of the differentiation of both carotenes and xanthophylls.

Experimental: The measurements were done by using a Renishaw InVia Raman spectrometer, joined to a Leica DMLM microscope. The spectra were acquired with the Leica 50x N Plan (0.75 aperture) lens. The spatial resolution for the 50x lens is 2 μm. The laser of 514 nm was used in all the measures to obtain the resonance effect of the carotenes and xanthophylls.

Results: Different areas of the Lecanora Muralis lichen were distinguished according to the colour provided by the main photosintethic pigment present. For instance, astaxanthin was the mayor pigment in brown areas, whereas zeaxanthin and β-carotene were the responsibles for the black colour. The figure below displays some of the Raman signatures obtained in the lichen colony. The main band ν_1 of the carotenoid allows to differentiate between astaxanthin (ast, 1507cm^{-1}) and β-carotene (beta, 1521 cm^{-1}). However, none of the three bands normally used for carotenoid identification are enough as to distinguish zeaxanthin from β-carotene. Therefore, Raman signatures between 3100-3500 cm^{-1} corresponding to O-H bonds that are observed under resonance conditions are needed. Moreover, those additional Raman bands can guarantee sometimes the correct carotenoid assignment when Raman features of other lichen compounds such as scytonemin are observed in the same spectrum.

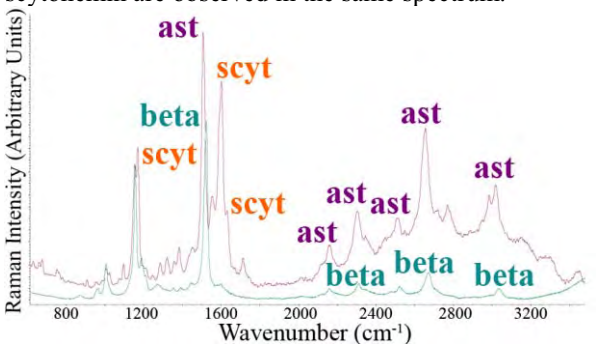

Fig. Resonance Raman spectra of Astaxanthin (ast) and scytonemin (scy) in comparison with β-carotene (beta) in black and brown areas, respectively, of the Lecanora Muralis lichen.

References: [1] Saxena S, Upreti D. K. and Sharma N., (2007) *J. Environ. Biol*. 28, 49-51. [2] Pandey, V., D.K. Upreti, R. Pathak and A. Pal (2002) *Environ. Monit. and Assess*., 73, 221-223. [3] Baranski R, Baranska M., Schulz H., (2005), *Planta,* 222, 448-457. [4] Jorge-Villar S.E., Edwards H.G.M. (2010) *J.Raman Spectrosc.,* 41, 63-67. [5] Robert B. (2009) *Photosynth. Res.,* 101, 147-155. [6] Schulz H, Baranska M, Baranski R, *Biopolymers*, (2005), 77, 212-221.

Aknowlegments: This work was financially supported by the Spanish Government (MICINN) through IMDICOGU project (ref. BIA2008-06592). Technical support provided by the Raman-LASPEA laboratory of the SGIker (UPV/EHU, MICINN, GV/EJ, ERDF and ESF) is gratefully acknowledged. I. Ibarrondo is grateful to the University of the Basque Country (UPV/EHU) for her pre-doctoral fellowship.

CYSTINE-APATITE RENAL CALCULI: EPMA, RAMAN & ESEM-CL STUDY. A. Iordanidis[1], J. Garcia-Guinea[2], V. Correcher[3], [1]Department of Geotechnology and Environmental Engineering, Technological Educational Institute (TEI) of Western Macedonia, Kila, 50100 Kozani, Greece, aiordanidis@yahoo.co.uk, [2]Museo Nacional Ciencias Naturales, CSIC, Abascal 2, 28006 Madrid. Spain. [3]CIEMAT. Av. Complutense 22, Madrid 28040, Spain.

Cystine stones are produced by an inherited disorder of the transport of amino acid cystine that results in excess of cystine in the urine (cystinuria). Cystinuria is characterized by the elimination in the urine of increased amounts of L-cystine which can provoke clinical manifestations. Cystine is a rare renal stone (less than 2% of the patients forming urinary stones), an organosulphur amino-acid compound with a chemical formula $(SCH_2CH(NH_2)CO_2H)_2$. During the last few years, systematic examinations have been undertaken in certain districts of northern Greece in order to detect the incidence of cystinuria among local population. These studies have been focused on diagnosis and treatment of cystinuric patients with stone formation. This study focuses on special hydroxyapatite-collagen-cystine calculi formed in the kidneys of humans living in such areas of the northern Greece. A comprehensive analytical study took place, employing the following analytical techniques: Electron Probe Micro-Analysis (EPMA), Raman microspectroscopy and Environmental Scanning Electron Microscopy (ESEM) coupled to a Cathodoluminescence (CL) tube. A characteristic concentric texture is clearly shown under the Electron Microprobe and the ESEM, with thick cystine layers inter-bedded with thin calcium hydroxyapatite layers.

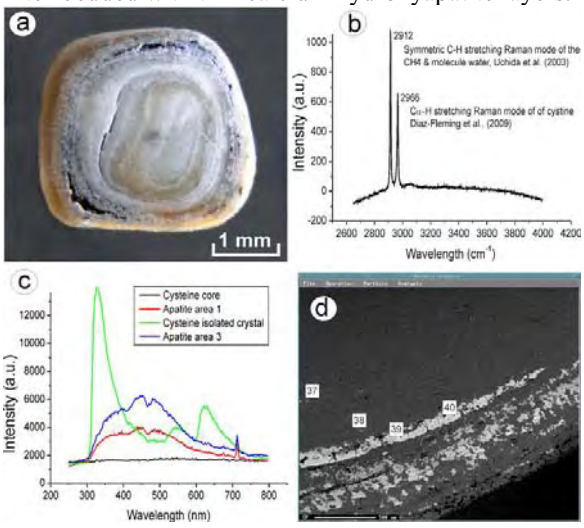

Figure 1. a) Macroscopic view of a cystine-apatite calculus, b) Raman spectrum of cystine crystals, c) CL spectra of cystine and apatite areas, d) ESEM image of cystine core and apatite layers (see Table 1 for chemical spot analyses).

The ESEM pictures exhibit larger concentration of hydroxyapatite and collagen in the external ring and only cystine in the internal core with minor composed mixtures. The elevated concentrations of sulphur are clearly shown under electron microprobe, while calcium and phosphorous prevail within the apatite regions. Cathodoluminescence and Raman spectra were obtained from several areas of the stone [1,2]. The observed features might suggest that the human kidneys isolate the undesirable S-S sulphur bonds encapsulating the cystine with an external bond container. In conclusion, the application of powerful analytical techniques could substantially help the physicians to determine precisely the stone composition and recommend an appropriate prophylactic therapy for the patient and thus prevent or delay the cystine stone recurrence.

Table 1. EPMA spot analyses on the cystine calculus

Element	37	38	39	40
SiO_2	0.025	0.024	-	0.027
Al_2O_3	0.016	0.008	0.074	0.057
MnO	0.046	-	0.046	0.013
MgO	0.032	0.008	2.749	2.272
CaO	0.159	0.042	44.661	45.696
Na_2O	0.012	0.051	1.154	1.102
K_2O	0.008	0.015	0.068	0.048
TiO_2	0.006	0.003	-	0.010
Cr_2O_3	0.035	0.004	0.029	0.050
P_2O_5	0.180	0.067	39.495	39.413
SO_3	98.757	99.327	0.415	0.357
CuO	0.013	0.016	-	-
SrO	0.019	0.054	0.121	0.129
F	-	-	0.822	0.811
Cl	0.022	0.059	0.145	0.095
Total	99.330	99.678	89.779	90.080

References:

[1] Diaz Fleming G. et al. (2009) *J. Raman Spectrosc. 40*, 632–638.

[2]Uchida T. et al. (2003) *Can. Jour. Phys., 81 (1-2),* 359-366.

MOLECULAR CHARACTERIZATION OF A TEMPERATE BEACHROCK FORMATION IN THE NERBIOI-IBAIZABAL ESTUARY (ARRIGUNAGA BEACH, BAY OF BISCAY). A. Iturregi[1*], N. Arrieta , I. Martínez-Arkarazo, X. Murelaga, J.I. Baceta[2], A. Sarmiento[3] and J.M. Madariaga. [1] Department of Analytical Chemistry, University of the Basque Country (UPV/EHU), P.O. Box 644, E-48080 Bilbao, Spain. [2] Department of Stratigraphy and Palaeontology, University of the Basque Country (EHU/UPV), P.O. Box 644, E-48080 Bilbao, Spain. [3] Raman-LASPEA laboratory, SGIker, University of the Basque Country (EHU/UPV), P.O. Box 644, E-48080 Bilbao, Spain. *Tel.: +34 946018298, e-mail address: aiturregui005@ikasle.ehu.es

Beachrocks are well-cemented coastal sedimentary formations resulting from the precipitation of carbonate cements in the intertidal zone. The cementing agents of beachrocks are composed predominantly of $CaCO_3$ polymorphs, high magnesian calcite (HMC) and low magnesian calcite (LMC).Several processes have been described for beachrock cementation, such as, precipitation of carbonates from evaporation of sea water, precipitation from ground water, precipitation in the salt and fresh waters mixing zone and CO_2 degassing from beach ground waters [1-4]. The majority of beachrocks are found predominantly in tropical/subtropical and low latitude coasts (0º - 40º latitude). Nevertheless, there are some evidences of beachrock occurrence at upper latitudes [5]. This work is related to a beachrock formation in Arrigunaga beach (43º21'N-3º1'W) located in the Nerbioi-Ibaizabal Estuary. The purpose of this work was the characterization of the cements of those beachrock outcrops so as to continue a research programme aiming to clarify the processes involved on the cementation of the beaches located in the vicinity of the Estuary.

Different samples were gathered along the beach and classified depending on their relative location in the intertidal zone, distinguishing between high, mid and low intertidal zone. At first instance, the granulometric characterization on the disgregated beachrock samples showed that the majority of the grains belonged to the 250µm and 2mm diameter fractions, although in the hardest (most compacted) samples the amount of the grains corresponding to the diameter less than 75µm was substantially higher. Two raman equipments with different laser wavelengths were used for the molecular characterization: (i) an InnoRaman ($B\&WTEK_{INC}$) ultramobile spectrometer, equipped with 20x and 50x focusing lens, an excitation wavelength of 785 nm (nominal laser power 255 mW), a CCD detector (Peltier cooled) and BWSpec 3.26_38 software for data acquisition. (ii) A Renishaw InVia microRaman spectrometer coupled to a DMLM Leica microscope with 5x, 20x, 50x and 100x long-distance lens, a 514 nm as excitation source (nominal laser power 50 mW) and CCD detector (Peltier cooled). Spectra treatment was performed with the Wire 3.2 software (Renishaw, United Kingdom) in both cases.

Researches carried out in an adjacent beach, describe different types of cement generations within the beachrock formations. The first generation was mainly HMC, followed by aragonite and mixtures of $CaCO_3$ polymorphs, silicates and iron oxides in high amounts [6]. Nonetheless, the Raman analyses of this work revealed that the vast majority of the cement in the study area is aragonite in the whole intertidal zone. HMC is only occasionally found acting as cement in the low intertidal zone and no evidences of the iron oxide based cements are observed. Concerning to the low intertidal zone, calcite was also found sporadically (Fig. 1). Furthermore, the studied beachrock is less cemented than the outcrops analized in the previous work.

These all differences found regarding the cement generations could be attributed to the location of the beaches; that is, to be situated in the interior or out of the Estuary.

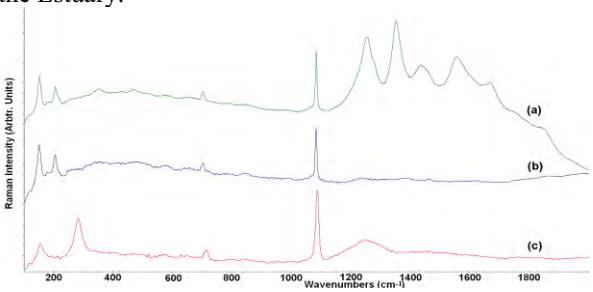

Figure 1. Raman spectra of different points in the intertidal zone: (a) HMC appearing occasionally in the low intertidal zone (b) aragonite (mid); (c) aragonite and silicates (mid).

Apparently, the studied beachrock is less cemented than other outcrops analized nearby, so more analyses must be carried through it to understand the processes of beachrock formation in each setting.

References [1] Beier J.A. (1985) *J. Sediment. Petrol. 55,* 755-761.[2] Russell R.J. (1963) *J.Trop.Geogr. 17,* 24-27. [3] Hanor J.S. (1978) *J. Sediment. Petrol. 48,* 489-501.[4] Milliman J.D. (1974) Marine Carbonates, Springer-Verlag, 375 .[5] Kneale D. et al. (2000) *Sediment. Geol. 132,* 165-170. [6] Arrieta N. et al. (2011) *Spectrochim. Acta A.* doi:10.1016/j.saa.2011.01.031.

Acknowledgements. This work has been financially supported by the Basque Government through the Environmental Analytical Chemistry Project (ref. IT-245-07). Technical support provided by the Raman-LASPEA laboratory of the SGIker (UPV/EHU, MICINN, GV/EJ, ERDF and ESF) is gratefully acknowledged. N. Arrieta is grateful to the University of the Basque Country (UPV/EHU) for her predoctoral fellowship.

THERMOLUMINESCENCE AND SHOCK METAMORPHISM OF ORDINARY CHONDRITES.

A.I. Ivliev, V.A Alexeev, N.S Kuyunko Vernadsky Institute of Geochemistry and Analytical Chemistry, Russian Academy of Sciences, 119991, Kosygin str. 19, Moscow, Russia; e-mail: *cosmo@geokhi.ru*.

Introduction. The collision processes obviously played a leading role in the formation of meteorites. Shock and thermal metamorphism accompanying the collisions is considered therefore as the most fundamental process in the evolution of the primordial matter. The experimental study of this process has undoubtedly the crucial importance, especially with respect to the search for quantitative criteria in the estimation of the effects of shock-thermal metamorphism. One of the most sensitive methods of determination of the degree of structural changes in a matter is the thermoluminescence (TL). The intensity of a TL glow in equilibrium ordinary chondrites (peak height of glow or area under peak) changes more than on two orders of magnitude [1]. The main TL phosphor in these meteorites is feldspar, which one is present at all H, L, and LL chondrites approximately in identical proportions and has a similar composition (Ab_{74}, An_{20}, and Or_6). The investigations of TL in minerals affected by experimental loading in spherically converging shock waves [2-4] have shown that TL characteristics were highly sensitive to changes in the crystal lattice. The shock stage of ordinary chondrites usually is determined by a petrographic method [5]. The purpose of the present investigation was carrying out of the TL investigations of chondrites with a petrographically identified shock stage. And, on the basis of obtained results, carrying out of an estimation of a degree of a shock metamorphism in chondrites with a unknown degree of a shock load.

Experimental method. The method of the sample preparation and the TL measuring is similar to a procedure surveyed in [2-4, 6].

Results of TL measurements.

On the results of recording of X-rays and γ-rays induced TL, there were calculated intensity of glow TL (Sp). The obtained results were compared to a degree of a shock load [6, 7]. The dependence of values Sp from a shock class of meteorites was found. However, at examination of TL induced by a X-rays, it was found, that the most sensing indicators of a degree of a shock load are the value of area under a curve of glow in a temperature region 40 -350 ^{O}C (Sp). The results of these calculations are listed in table. In accordance with these data, the increase of values Sp is observed at the increase of shock pressure up to 10 GPa (stages S1-S2), and subsequent their sharp decrease up to two orders of magnitude is seen at further increase of shock pressure from ~10 up to 90 GPa (stages S3-S6). Using the results of our measurements and values of shock pressures of different classes of meteorites [5], we have received the approximate formulas for an estimation of a value of a shock load, which one have undergone chondrites at collisions in space. For shock classes S1-S2 it was obtained: P = 1.93 x ln (Sp) - 5.57, and for S3-S6: P = -12.28 x ln (Sp) + 91.74. The results of evaluations under these formulas are given in the last column of the table.

Table. Results of calculations of a area under the peak of glow (Sp) and value of a shock load (P).

N п/п	Meteorite	Shock klass	Sp	P, GPa
1	Dhajala H3	S1	222±13	4.9±0.3
2	Pribram H5	a-b	261±10	5.2±0.2
3	Saratov L4	S2	310±16	5.5±0.3
4	Biurboele L4	S1	326±20	5.6±0.3
5	Elenovka L5	S2	355±9	5.8±0.1
6	Tugalin-Bulen H6	S1	575±25	6.7±0.6
7	Nikolskoe L4-5	S2	671±67	7.0±0.7
8	Kunya-UrgenchH5		928±100	7.6±0.8
9	Barwell L5	S3	590±35	13.5±0.8
10	Kunashak L6	e	300±28	21±2
11	Pultusk H5	S3	285±24	22±2
12	Ochansk H4	S3	279±32	23±3
13	Kilabo LL6	S3	262±10	23±1
14	Dalgety Downs L5		142±14	31±3
15	Malakal L5	e	45±2	44±2
16	Kyushu L6	S5	34±3	46±5
17	Pervomaisky L6		7.6±0.6	60±5

Conclusions. The investigation of the TL induced by X-rays in equilibrium ordinary chondrites has shown a high response of values Sp on a shock load, which one was undergone by these meteorites in space. However for precise identification of shock classes S1 - S3 under the TL data, the preliminary petrographic examinations is necessary. The estimation of a shock load of 17 meteorites was executed. The shock classes of meteorites of Kunya-Urgench (S2), Dalgety Downs (S4), and Pervomaisky (S6) were determined.

References. [1] Sears D.W.G. (1988) *Nucl. Tracks Radiat. Meas 14*. 5-17. [2] Ivliev, A.I. et al. (1995) *Geokhimiya.* 9. 1368-1377. [3] Ivliev, A.I. et al. (1996) *Geochemistry International* 34. P. 912-919. [4] Ivliev A.I. et al. (2002) *Geochemistry International*. 40. 739-750. [5] Stöffler D. et al. (1991) *Geochim. et Cosmochim. Acta*, 55. 3845-3867. [6] Alexeev V.A. et al. (2001) *Geochemistry International.* 39. 1043-1055.

SPECTRA CATHODOLUMINESCENCE AND CRYSTAL LATTICE: CERITE VERSUS WHITLOCKITE

Jorge, A., Garcia-Guinea J., Tormo L., Furio M., J. Fernandez-Cortés, A., Cuezva, S. Sanchez-Moral S., Museo Nacional Ciencias Naturales. CSIC. 28006 Madrid. Spain. ***Author for correspondence***: guinea@mncn.csic.es

Introduction: We record more that 10 whitlockite cathodoluminescence (CL) spectra from 10 different chondrites exhibiting very similar and characteristic spectral CL patterns. Following to Gotze (2009) the CL spectra of whitlockite (merrillite) are dominated by strong emission peaks of several rare earth elements **(e.g., Figure 1).**

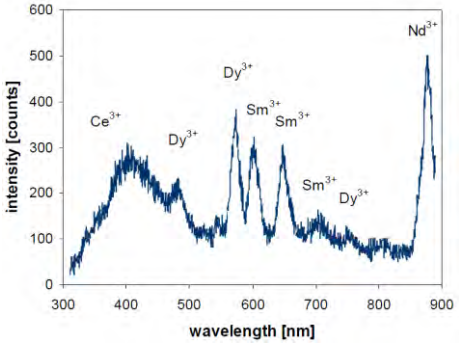

Figure 1.- Spectra CL plot of Götze (2009) of a Lunar whitlockite and REE associated to the main emission peaks.

In addition, we also found this characteristic whitlockitic CL pattern in a natural cerite specimen of a terrestrial slate collected in Castañar de Ibor (Cáceres, Spain) **(Figure 2).**

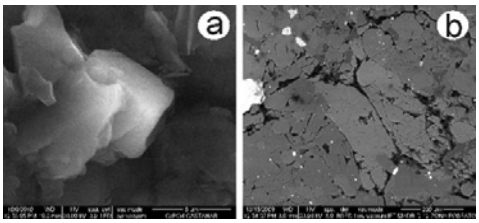

Figure 2.- ESEM images. (a) Cerite crystal sized 5 µm in Paleozoic slate matrix (Castañar de Ibor, Cáceres, Spain) (b) Couple of whitlockite crystals in the L6 Chondrite Madrid.

In accordance with Noore & Shen (1983) Cerite Ce_9 Fe^{3+} $(SiO_4)_6$ (SiO_3) $(OH)_4$ is nearly isostructural to whitlockite Ca_9 $Mg_{0.7}$ $Fe^{2+}{}_{0.5}$ $(PO_4)_6$ (PO_3OH) having the same crytallographic space group R*3C*. Matching the X-ray Diffraction (XRD) patterns of the structural data of this Cerite specimen with the whitlockite specimen of the Tip Top Pegmatite, Custer County, South Dakota studied by of Hughes J.M. et al. (2008) we detect very close X-ray diffraction patterns with an angular difference of just only of five 2θ angle. The EDS chemical analysis of the meteoritical whitlockite is: Na_2O % 0.76, MgO % 2.11, Al_2O_3 % 0.41, SiO_2 % 3.49, P_2O_5 % 40.01, SO_2 % 0.52, K_2O % 0.14, CaO % 44.58, Fe_2O_3 % 3.10 while the EDS analysis of the terrestrial cerite is: MgO % 2.09, Al_2O_3 % 5.70; SiO_2 % 16.89; P_2O_5 % 26.56; K_2O % 0.75; CaO % 1.44; Fe_2O_3 % 2.00; Y_2O_3 % 1.87; La_2O_3 % 9.02; Ce_2O_3 % 19.06; Pr_2O_3 % 1.09; Nd_2O_3 %7.25; Sm_2O_3 % 0.86; Gd_2O_3 % 0.97; ThO_2 % 4.45 in which a minor slate contamination can not be disregarded, i.e, elements Al, Si, K, Fe from the intrinsic EDS spot analysis measurement of a little grain sized 5 µm inlaid in the slate matrix.

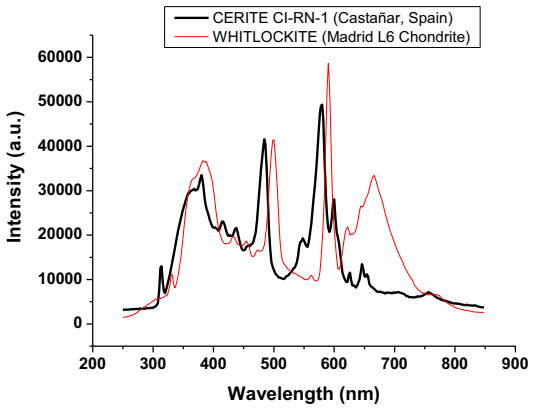

More surprisingly was to match very similar spectral CL curves recorded by ESEM/CL of a terrestrial silicate of REE (cerite) with the calcium phosphate whitlockite of the L6 Chondrite Madrid (Spain) (**Figure 2**). The strong similarity among both crystal lattices and both spectra CL suggest that the structural features provide a fruitful researching path to understand the whitlockite spectra cathodoluminescence.

References:

Moore, P.B. & Shen J. (1983) Cerite, RE_9 (Fe^{3+}, Mg) $(SiO_4)_6$ $(SiO_3$ OH) $(OH)_3$: its crystal structure and relation to whitlockite. *Am. Miner.* 68, 996-1003.

Hughes, J.M., Jolliff, B.L., Rakovan, J. (2008) The crystal chemistry of whitlockite and merrillite and the dehydrogenation of whitlockite to merrillite Am. Mineralo 93, 1300—1305

Götze J. (2009) Cathodoluminescence of lunar minerals and rocks. Proceedings of the CORALS-I Conference. Mainz. Germany.

NEW RAMAN SPECTROSCOPIC DATA OF ALMAHATA SITTA METEORITE

M. Kaliwoda[1,*], R. Hochleitner[1], V. H. Hoffmann[2], T. Mikouchi[3], A. M. Gigler[4], W. W.. Schmahl[1,4]
[1]Mineral State Collection Munich, Theresienstrasse 41, 80333 Munich (Germany) (Melanie.Kaliwoda@lrz.uni-muenchen.de), [2]Geophysics, LMU-München, Theresienstr. 41, 80333 Munich (Germany), [3]Earth and Planetary Science, Graduate School of Science, University of Tokyo, 7-3-1 Hongo, Bunkyo-ku, Tokyo 113-0033 (Japan), [4] CeNS and Section Crystallography, LMU-München, Theresienstr. 41, 80333 Munich (Germany)

Introduction: 2008 TC_3 was the first meteorite previously observed in space and discovered afterwards. 2008 TC_3 fall took place on 7 October 2008 in the Nubian Desert (Northern Sudan). Its mass was around 3.95 kg.
All specimen, belonging to this fall, were called Almahata Sitta (AS), and could be classified as a multicomponent breccia composing of different meteoritic lithologies like anomalous polymict ureilites and different chondrites [1-3]. Therefore, the meteorite revealed to be of a rare type of extraterrestrial material, with also large amounts of carbonaceous grains.

Raman research: The investigation of minerals by Raman spectroscopy is an suitable methode to typify minerals within these planetary material. Raman measurements could be used to classify the structure and composition of quartz, pyroxenes, olivines and other materials within meteorites. In combination with electron microprobe, Raman spectroscopy is an excellent tool to typify different polytypes and polymorphs. Therefore it is for example possible to distinguish between graphite, graphene and diamond within the investigated AS samples.
Furthermore we could map areas of 90 µm to 90 µm to determin mineral phases within rather inhomogenous clusters in AS. The following **minerals** could be classified within our AS samples due to Raman measurements:

Graphite (see Figure 1)
Diamond
Graphene
Suessite (see Figure 2)
Schreibersite
Cohenite
Kamacites
Troilite/Cr troilite
Pyroxene
Plagioklas

Results: By means of our Raman measurements it was possible to characterize graphite, graphene and also diamond. To some extend, these three minerals occur in clusters within one sample. Especially graphene and graphite change within diminutive areas.
Moreover it was possible to acquire the first suessite Raman data. Up to now no exact Raman spectra of suessite was existing.
In addition we mapped areas, i.e. clusters and mineral inclusions within AS, where the local chemical composition as well as the mineral content vary within short distance.

Conclusion: Micro-Raman spectroscopy proved to be a quick and valuable tool for investigation of extraterrestrial material. No special sample treatment is needed, with the exception of polished surface. Therefore it is a good methode to characterize different minerals and polytypes within one sample and to make preliminary work for later microprobe measurements.

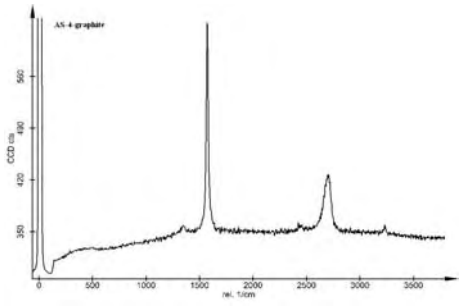

Figure 1: Graphite

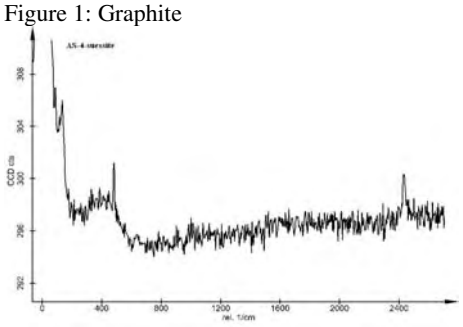

Figure 2: Suessite

References:

[1] Jenniskens P. et al. (2009), *Nature , 458:* 485-488. [2] Bischoff A. et al. (2010), *MAPS, in press.* [3] Hochleitner R. et al. (2004), *Journal of Raman spectroscopy, 35,* 515-518

Additional Information: This study was performed partly under the cooperative research program of the Center for Advanced Marine Core Research (CMCR), Kochi University, Japan (10B033).

THERMOLUMINESCENCE AS ONE OF THE METHODS FOR DETERMINATION OF THE CRYSTAL LATTICE STRUCTURE OF QUARTZ. L. L. Kashkarov, G. V. Kalinina , S. N. Shilobreeva. Vernadsky Institute of Geochemistry and Analytical Chemistry, Russian Academy of Sciences, 119991, Kosygin str. 19, Moscow, Russia , *leokash@mail.ru*

Introduction: Research of radiation-induced processes of structural and chemical reworking of the silicates, occurring under influence of an ionizing radiation, is now one of the important scientific problems. In a basis of these researches representation about radiation-induced structural changes of a crystal lattice of irradiated samples, formation in it of a different sort of micro-defects lays. As consequence, repeatedly accelerated diffusion leading redistribution of the elements concentration in the crystal volume, is observed [1, 2]. In the works of authors [3, 4] for the first time it has been shown radiation-stimulated redistribution of the implanted into quartz of the iron atoms that was caused by the subsequent irradiation of the accelerated protons. Thus, iron atoms or are undergoing diffusion in the crystal volume, or enter chemical interaction in a near-surface layer of quartz with formation of a chemically modified compound. Radiation-stimulated diffusion for greater depths can be treated as segregation of iron atoms on some centers such, for example, as oxygen vacancies of quartz. In view of these processes, it is important to perform an experimental definition of a degree of radiation-induced crystal lattice destruction. One of high-sensitivity methods of registration of structural changes of quartz is the method of thermoluminescence (TL) analysis. In work [5] at research of the TL- luminescence of quartz precise dependence of the TL-parameters on capacity of shock loading has been received. In the present work the results of TL-parameters measurement for the quartz of different crystal structure are presented. Enough high sensitivity to TL-storage, allowed to use this mineral for development of a TL-research technique of structural changes and destructions of the crystal lattice, occurred under action of nuclear irradiation, are discussed.

Samples and technique: TL-measurement was spent for a number of quartz samples: Qu-1 fusion, with amorphous structure and Qu-2 natural rock crystal. As have shown the optical analysis, the Qu-1 contained the microcrystallite inclusions, and Qu-2 were represented as the transparent, colorless monocrystals. Measurements were spent on the installation, allowing to register the very low levels of the TL-luminescence by a technique described in [6]. It was registered natural (TL_{NAT}) and artificially induced (TL_{IND}) when the samples were exposed to X-rays of energy E = 55 keV.

Results and discussion: From comparison of the TL glow curves for the studied quartz samples it is follows: 1) TL_{NAT} - intensity for both sample groups of quartz in the low (≤ 250 ^{o}C) temperature interval is approximately identical and lays at a level of 1×10^{-3} relative units, that corresponding to a background thermoluminescence (TL_{BAC}). However, at ~ 300 ^{o}C it is observed peak of the TL_{NAT} -luminescence, approximately on the order of magnitude exceeding a background luminescence in this temperature interval. This TL_{NAT}-luminescence is adequating to the trapped electrons, accumulated during all history of existence of the given samples. 2 TL_{BAC} was measured at repeated heating of the samples after measurement their TL_{NAT}, that specifies a minimum level of the TL-luminescence which can be registered on used installation. 3) TL_{IND} it is characterized by following features: For the samples of amorphous quartz Qu-1 on a glow curves it is observed, at least, five peaks in the low-temperature ~ (50-250) ^{o}C intervals and several peaks in the region of ~ (250-400) ^{o}C. Evaluation of the activation energies according for these peaks gives the values from ~ 1.1 eV up to ~ 1.8 eV. Single-peak in TL_{IND} glow curve for the samples of Qu-2 corresponds to the activation energy of ~ 1.2 eV.

Conclusion: Difference of the glow curves for TL_{IND} in Qu-1 and Qu-2 samples, and evaluation of the activation energy allow us to identify some crystal structural characteristics. It is apparently, that in fused quartz specific glow curves are caused by inclusions of microcrystals. Corresponding degrees in heterogeneity of structure in these samples as a whole can be estimated due of these data. Carrying out of the special calibration experiments on revealing of the activation energy levels at implantation of quartz by accelerated nuclei will enable for carrying out of a quantitative estimation of a degree of destruction the quartz crystal lattice, that arising under influence of nuclear particles of different charge and energy.

Study was supported by Russian Foundation for Basic Research, grant № 10-05-00253-a.

References: [1]. Wang K.-M. et al. (1990) *J. Appl. Phys., 68*, 3191-3193. [2]. Hosono H. (1995) *J. Non-Crystalline Solids, 187*, 457-472. [3]. Shilobreeva S.N. et al. (2006) *Nucl. Instr. & Meth., Phys. Res., 256*, 216-218. [4]. Shilobreeva S.N. et al. (2006) *Docl. Acad. Nauk (russian), 411*, 676-679. [5]. Ivliev A.I. et al. (1996) *Geochimiya,* 1011-1017. [6]. Ivliev A.I. et al. (1995) *Geochimiya,* 1368-1377.

Optical Absorption, Cathodo- And Radioluminescence In Diaspore. M.I.Katı[1], M.Türemis[1], I.C.Keskin[1], B.Tastekin[1], M.Hatipooglu[2], R.Kibar[1], A.Çetin[1] and N.Can[1], Celal Bayar University, Faculty of Arts and Sciences, Physics Department, 45140 Manisa-Turkey, email;miak_84@hotmail.com
[2]Dokuz Eylül University, İMYO, İzmir Multidisciplinary Vocational School, Gemmology and Jewelry Program, 35140 Buca-Izmir/Turkey.

Diaspore [α-AlO(OH)] is one of the bauxitic minerals in the Al_2O_3–H_2O system and is part of the gibbsite, bayerite, bohemite, diaspore, and corundum series. [1] The properties of diaspore (α-AlOOH) are of interest in different fields such as production of alpha-alumina, extraterrestrial water exploration and jewelry. Diaspore is the only oxo-hydroxide suitable as a direct precursor of α-Al_2O_3 when dehydration at 450–500 ^oC is reached. Diaspore in nature can be also considered as one of the precursors of natural crystalline alumina usually named corundum (α-Al_2O_3).[2]

In diaspore the oxygens are in a hexagonal close packed layer. Luminescence spectra of the naturel diaspore are typical of $^2E \rightarrow {}^4A_2$ transitions of Cr^{3+} luminescence centers (R-lines) substituting for Al^{3+} in six – fold coordination [3]. Gem quality diaspores are formed by four remobilization processes (extraction, mobilization, migration and re-crystallization) of the metabauxite components in an aqua-complex as open-space fillings. This formation and its rarest crystal are only found in the Ilbir mountains region of the Menderes crystalline massif (SW Turkey) around the world. Thus, the studies on gem quality diaspores have fairly limited [4]

Fig. 1 shows cathodoluminescence (CL) and radioluminescence (RL) spectra of diaspore at room temperature. As seen from the figure, diaspore exhibits luminescence maxima at 430, 488, 571, 697 and 712 nm at CL spectrum.

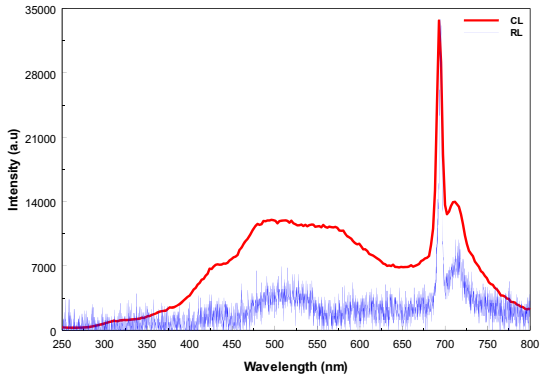

Fig.1 CL and RL spectra for diaspore at room temperature.

In the absorption spectrum of diaspore,there are a few peaks at 371 nm, 385 nm, 397 nm, 450 nm, 560 nm and 640-750 nm. These can be attributed to some impurity elements.

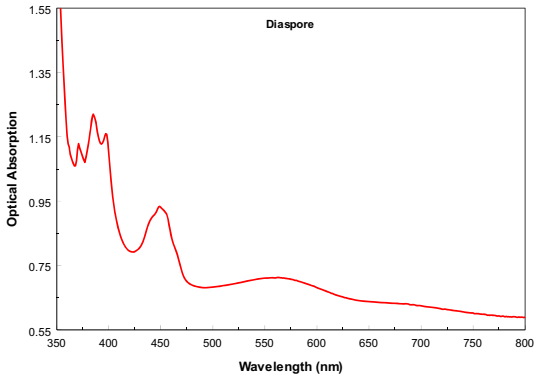

Fig.2 Optical absorption spectrum of diaspore in the range of 350-800 nm.

References: [1] J. Garcia-Guineaa; *et. al.* Radiation Measurements 33 (2001) 653– 658 [2] J. Garcia-Guinea et. al. Journal of Physics and Chemistry of Solids 66 (2005) 1220–1227 [3] S.Shoval et.al.Journal of Thermal Analysis and Calorimetry 71 (2003) 699-706 [4] M. Hatipoğlu et.al. Physica B 405(2010)1729–1736

"IN SITU" STUDY OF A COLLECTION OF 20 METEORITES USING RAMAN SPECTROSCOPY

Th. Katsaros[1] and Th. Ganetsos[1,2]
[1]Byzantine & Christiane Museum (Gr.) Laboratory of Gemstones (Vasilissis Sofias Ave. 22 Athens 10675 Greece tkatsaros@rhodes.aegean.gr),
[2]T.E.I. of Lamia, Department of Electronics (3rd Km O.N.R. Lamia-Athens, Lamia, 35100, Greece).

We investigate the ability to determine the mineralogical character of 20 samples of different meteorites from a private collection by the using of a portable Raman apparatus [6] not in the Laboratory.

We use the Rockhound Deltanu Raman spectrometer (Fig. 1a and b) (Laser: 120mW, 785nm, Resolution: 8 cm^{-1}). The samples which we studied are, Pallasites: 2 samples from Brahin (Russia), 3 samples from Brenham (USA), 1 from Thumrayt 001 (Sultanate of Oman), another group is the stony iron meteorites such as Drofar 020 and Chubara both from Sultanate of Oman. We investigated 2 samples of Moldavites from Czech Republic, one Tektite (Thailandite). The other meteorites which we made measurements are one sample from the following: Chondrite H5 from Chergach (Mali), Allende CV3 from Mexico, Octahedrite from Muonionalusta (Sweden), Octahedrite IA from Odessa Texas (USA), Octahedrite IIAB from Shikote-Alin Siberia (Russia), Ataxite from Santa Catherina (Brazil), Iron-IC meteorite from Bendego (Brazil), Ataxite from Dronino (Russia), Iron IIAB Campo del Cielo (Argentina), Medium Octahedrite from Nan-Tan (China), IAB-MG from Canyon Diablo, Arizona (USA), Gibeon (Namibia) and NWA-869 Stony Meteorite from Algeria (North Africa).

We well testified with Raman the characteristic presence of Olivine in the texture of Pallasites from Brahin and Brenham. [1-3] We observed a strong fluorescence in the sample from Allende CV3 which probably derived from its heating by the fall of it in the atmosphere. The characteristic Raman behavior of the glassy mass of Moldavites has well observed.

The Raman spectra of the olivine-group minerals have a characteristic set of two intense lines of the Si-O asymmetric stretching band (wavenumber κ1) and Si-O symmetric stretching band (κ2).[4-5] The κ1 and κ2 values of the Mg_2SiO_4-$Ca(Mg, Fe)SiO_4$ series, in which the M2 site is occupied by nontransition elements, vary from 847 cm^{-1} to 857 cm^{-1} and from 815 cm^{-1} to 825 cm^{-1}, respectively [6] Fig. 2 represents the experimental results in very good agreemtn with bibliography. We testified the presence of the mineral phase of Troilite in the case of the meteorite sample from Campo del Cielo and on the surface of the sample from Muonionalusta. We observed also the characteristic Raman spectrum of Nickel in the samples of Iron-Nickel meteorites such as Canyon Diablo, Gibeon, Sikhote Alin. Last but not least we propose the application of the portable Rockhound Deltanu Raman spectrometer on the primary investigation of the samples In Situ of its plase of finding. It is very important for a field researcher scientist to understand the identification of an unknown material as a first approach using a non-destructive technique.

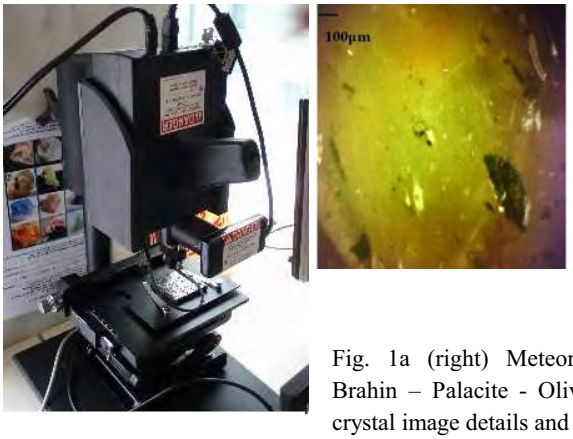

Fig. 1a (right) Meteorite Brahin – Palacite - Olivin crystal image details and b (left) Rockhound Deltanu Raman Spectrometer

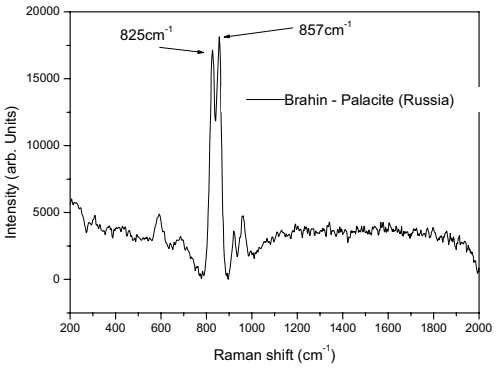

Fig. 2 Raman spectrum of the meteorite Brahin (Russia)

References

[1] Kolesov B A, Geiger C A (2004), *Physics and Chemistry of Minerals*, *31*, 142-154.
[2] Mouri T, Enami M (2008), *Journal of Mineralogical and Petrol. Sci.*, *103*, 100-104.
[3] Katsaros Th. et al. (2007), *GSA, Ann. Meet*., *6*, 574.
[4] Kolesov B. A., Tanskaya J. V. (1996), *M.R.B*., *31*, 1035-1044.
[5] Mikouchi T., Miyamoto M. (2000) *Meteoritics & Planet. Sci.* , *35, 1*, 155–159
[6] Mouri T. and Enami M. (2008) *J.Min. and Petr. Sci*., *103*, *2* , 100-104.

CLARIFICATION OF SHOCK-INDUCED EFFECT ON CATHODOLUMINESCENCE OF ALKALI FELDSPAR. M. Kayama[1], H. Nishido[1], T. Sekine[2], T. Nakazato[1], A. Gucsik[3,4] and K. Ninagawa[5], [1]Research Institute of Natural Sciences, Okayama University of Science, 1-1 Ridaicho, Kita-ku, Okayama 700-0005, Japan (E-mail: kayama@rins.ous.ac.jp); [2]Department of Earth and Planetary Systems Science, Graduate School of Science, Hiroshima University, Kagami-yama 1-3-1, Higashi-Hiroshima, Hiroshima 739-8526, Japan; [3]Department of Earth and Planetary Materials Science, Graduate School of Science, Tohoku University, Aoba 6-3, Aramaki, Aoba-ku, Sendai, 980-8578, Japan; [4]Konkoly Observatory of the Hungarian Academy of Sciences, H-1121, Budapest, Konkoly Thege Miklós út 15-17., Hungary; [5]Department of Applied Physics, Okayama University of Science, 1-1 Ridaicho, Kita-ku, Okayama 700-0005, Japan;

Introduction: Materials subjected to shockwaves display characteristic and irreversible structural changes on both macroscopic and microscopic scales, depending on the applied shock strength. The shock pressure at the time of impacting, therefore, is the most important parameter that needs to clarify the collisional history of asteroid and meteorite impacts. Shock metamorphic process caused by hypervelocity meteorite impacts, however, has not been fully understood yet. Cathodoluminescence (CL) spectroscopy and microscopy provide useful information on the existence and distribution of defects and trace elements in materials with high spatial resolution. This technique is expected to be applied to clarify shock pressure effect on the minerals in meteorites and impactites. In this study, CL analysis of experimentally shocked alkali feldspar has been conducted to evaluate shock-induced effect on CL of feldspar.

Samples and methods: Single crystals of sanidine ($Or_{87}Ab_{13}An_0$) from Eifel, Germany, and microcline ($Or_{63}Ab_{37}An_0$) from Marumori, Japan were selected as starting material for shock recovery experiments. The shock pressure was induced on sanidine at 10.0, 20.0, 31.7 and 40.1 GPa using a propellant gun. CL images and spectra were obtained by an SEM-CL system.

Results and discussion: Color CL images of unshocked (Sa00) and experimentally shocked sanidine at 10 GPa (Sa10) indicate a red–violet emission. Sanidine at 20 GPa (Sa20) displays a blue emission with vein-shaped textures and a red–violet luminescent background. A blue emission is also distinguished in the color CL images of shocked samples at 31.7 GPa (Sa30) and 40.1 GPa (Sa40). Color CL images of unshocked (Mi00) and shocked microcline at 10.0, 20.0, 31.7 and 40.1 GPa (Mi10, Mi20, Mi30 and Mi40, respectively) exhibit blue CL emissions, where the intensity increases with an increase in shock pressure. Raman spectra of unshocked and shocked sanidine as well as microcline at 10 GPa consist of pronounced peaks at 180, 290, 485 and 510 cm^{-1}, which are assigned to T–O–T stretching vibration. Shocked sanidine and microcline above 20 GPa present rather weak peaks at 510 and 600 cm^{-1}. Shock metamorphism breaks a linkage of the T–O–T bond in the framework structure of sanidine, resulting in the transition of sanidine and microcline into diaplectic glass. Blue CL areas in shocked sanidine are identified to diaplectic glass, but red-violet areas to diaplectic or unshocked sanidine.

CL spectra of Sa00 and Mi00 show a blue emission band at 420 nm and a red-IR one at 730 nm. Shocked sanidine and microcline above 20 GPa have UV-blue CL emissions at 380 and 330 nm of which intensities increase with an increase in shock pressure. Spectral deconvolution of CL spectra from shocked sanidine and microcline provides Gaussian components at 2.948, 3.261 and 3.881 eV. The components at 3.261 and 3.881 eV are recognized in diaplectic glass, but not in diaplectic or unshocked sanidine and microcline. It indicates that these components are characteristic of CL signals derived from diaplectic glass. Shock metamorphism destroys a linkage of T–O–T bond in the framework structure of sanidine and microcline, but resulting in formation of shock-induced defect center related to the components at 3.261 and 3.881 eV. Their component intensities increase with an increase in shock pressure, where the increasing rates are different between sanidine and microcline. It is noteworthy that the intensity depends on not only shock pressure, but also phase composition and structural order-disorder which are closely related to transition shock pressure from feldspar into diaplectic glass. The component at 2.948 eV was detected in both diaplectic feldspar and glass, suggesting that the shock-induced defect center is almost independent of the breaking of the linkage of the T–O–T bond caused by shock metamorphism. The intensity correlates linearly with peak shock pressure induced on sanidine and microcline, with little dependence on composition or structure. The correlation can provide quantitative values of the shock pressures experienced on the feldspar at the time of impacting, which can estimate shock pressures of meteorites and impact crater impactite with higher precision than conventional method. This shock barometry should be extensively used in the clarification of meteoritic or planetesimal collision history and the interpretation of the ejection process on Mars and Moon.

CHARACTERIZATION OF RADIATION EFFECTS IN ALBITE BY CATHODOLUMINESCENCE. M. Kayama[1], H. Nishido[1], S. Toyoda[2], K. Komuro[3] and K. Ninagawa[2], [1]Research Institute of Natural Sciences, Okayama University of Science, 1-1 Ridaicho, Kita-ku, Okayama 700-0005, Japan (E-mail: kayama@rins.ous.ac.jp); [2] Department of Applied Physics, Okayama University of Science, 1-1 Ridaicho, Kita-ku, Okayama 700-0005, Japan.; [3]Earth Evolution Sciences, University of Tsukuba, Ten-nodai, Ibaraki, 305-8571, Japan;

Introduction: Cathodoluminescence (CL) microscopy and spectroscopy provide useful information about the existence and distribution of lattice defects and trace elements in materials with high-spatial resolution of a few micron meters. The CL spectral features are closely related to radiation dose of alpha- or gamma-particles, suggesting geoscientific applications for geodosimeter using CL of minerals such as quartz and zircon. No CL investigations on radiation effects in feldspar which is a most important rock-forming mineral on earth's crust have been conducted to date, although the visible halos caused by alpha-particle can be easily found in the feldspar directly attached to radioactive minerals. In this study, He^+ ion implantation at 4 MeV, corresponding to the energy of alpha-particle from ^{238}U, has been conducted to characterize radiation effect of alpha-particle by CL in albite.

Samples and methods: Single crystals of albite from Minas Gerais, Brazil, from Itoigawa Japan, and from Tanogami, Japan were used in the present study. He^+ ion implantation (dose density: 2.18×10^{-6} to 6.33×10^{-4} C/cm^2) on the samples was performed using a 3M-tandem ion accelerator at 4 MeV corresponding to the energy of alpha-particles from ^{238}U. A scanning electron microscopy-cathodoluminescence (SEM-CL) was used to obtain CL spectra of these albite samples. Operating conditions were set at 15 kV (accelerating voltage) and 1.0 nA (beam current).

Results and discussion: CL images of He^+ ion implanted albite from Minas Gerais, Brazil, from Itoigawa Japan, and from Tanogami Japan show a bright luminescent band of ~14 μm width from the implanted surface, which is identified as a CL halo. The width of the halo is consistent with the theoretical range of He^+ ion implantation at 4 MeV. CL line analysis revealed that an increase in the CL intensity along depth direction substantially corresponds to the Bragg's curve, indicating an energy loss process of specific ionization along the track of a changed particle.

CL spectra of unimplanted albite from Minas Gerais, Brazil, from Itoigawa Japan, and from Tanogami Japan have emission peaks at 350, 400, 570 and 740 nm which are assigned to Ce^{3+} impurity, Ti^{4+} impurity or Al-O^--Al center defect, Mn^{2+} impurity and Fe^{3+} impurity centers, respectively. Similar emission peaks were recognized in CL spectra of the implanted albite. The intensities of all of these CL emissions decrease with an increase in radiation dose of He^+ implantation. Raman spectroscopy on these albite indicates that Raman peak at 505 cm^{-1} shows a decrease in the intensity and an increase in the full width at half maximum (FWHM) with increasing the He^+ dose. These observations suggest that He^+ implantation breaks a linkage of T-O-T bonds in the framework of albite, resulting in a reduction of CL emissions due to impurity centers.

CL spectra of all implanted albite have a red emission at 700 nm, of which the intensities increase with an increase in the radiation dose. Deconvolution of CL spectra from the unimplanted and implanted albite can successfully provides six Gaussian components at 3.05, 2.82, 2.10, 1.86, 1.67, and 1.56 eV, where the component at 1.86 eV is observed only in the implanted albite samples. Integral intensity of the component at 1.86 eV linearly correlates with the radiation dose. These results suggest that the component at 1.86 eV is assigned to radiation-induced defect center formed by He^+ ion implantation. The component intensity at 1.861 eV correlates with the radiation dose as a function of radiation sensitivity, but does not depend on the density and distribution of other emission centers, degree of Si-Al ordering, the presence of microstructures or texture, nor the provenance, i.e., Minas Gerais, Brazil, from Itoigawa Japan or Tanogami Japan.

CL microscopy, therefore, was found to be useful to visualize radiation halo, and CL spectral deconvolution can quantitatively evaluate radiation dose of alpha particles from natural radionuclides on albite, which could be a geodosimeter.

Thermoluminescence Of The Blue And White Chalcedony From Turkey. I.C.Keskin, M.I.Katı, M.Turemis, B.Tastekin, R.Kibar, A.Çetin and N.Can, Celal Bayar University, Faculty of Arts and Sciences, Physics Department, 45140 Manisa-Turkey, email; ilkercetinkeskin@hotmail.com

Chalcedony is a cryptocrystalline form of silica, composed of very fine intergrowths of the minerals quartz and moganite. These are both silica minerals, but they differ in that quartz has a trigonal crystal structure, whilst moganite is monoclinic. Chalcedony's standard chemical structure (based on the chemical structure of quartz) is SiO_2 (silicon dioxide). Chalcedony includes carnelian, sard, plasma, prase, bloodstone, onyx, sardonyx, chrysoprase, thundereggs, agate, flint, chert, jasper, petrified wood, and petrified dinosaur bone just to name a few of the better known varieties. The name is an old name, and almost all mineral reference guides and collectors distinguish chalcedony separately from quartz. Natural chalcedony crystals are found in nature with white, blue, red, green, yellow, orange, brown, pink, purple, gray, black, colorless, and multicolored. In the gem trade, the name chalcedony usually describes only white or blue chalcedony, to distinguish it from the multicolored banded variety agate and other unique varieties of this mineral. Impurities are frequently present in chalcedony. They may form a moss like growth in the mineral, forming what is known as moss agate. Another example is dendritic agate, a variety of Chalcedony containing manganese oxide impurities that form fabrications resembling trees.

In this study, we compared with blue and white chalcedony. For this purpose, thermoluminescence (TL) glow curves in the temperature range between 50-400 ^{o}C were recorded from these minerals after exposed to X-ray. As seen form figure 1, the glow curve pattern shows TL peaks at 110 ^{o}C, 150 ^{o}C, 310 ^{o}C, 355 ^{o}C for white chalcedony while one main peak is observed at 110 °C for blue chalcedony. Figure 2 shows the TL glow curves of white chalcedony after exposure to X-ray in the dose range from 300 to 900 Gy. As can be seen from the figure, up to the maxima dose investigated no saturation was observed in the behaviours of the TL curves but their intensities increased with larger doses. The samples was also studied by using optical absorption spectroscopy.

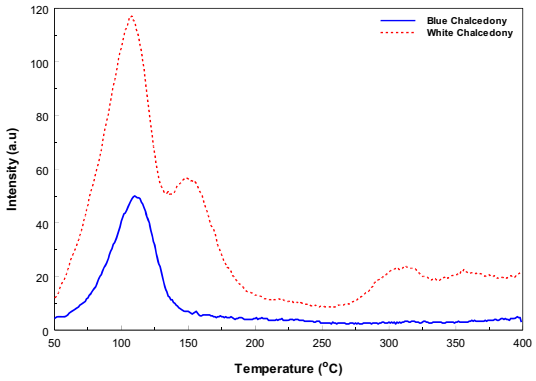

Fig.1 TL glow curves of blue and white chalcedony from Turkey after exposed to X-ray for 10 minutes.

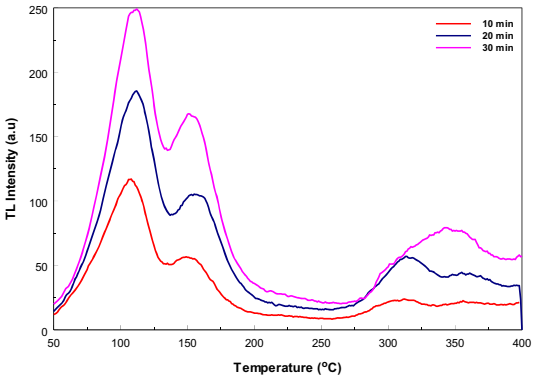

Fig.2 TL spectra of white chacedony after exposure to X ray in different doses.

.

References: [1] M. Hatipoğlu et.al. Physica B 405 (2010) Issue 22, 4627–4633. [2] M. Hatipoğlu et.al. Physica B: Condensed Matter, 405 Issue 7, (2010), 1729-1736.

STRUCTURE AND LUMINESCENCE CHARACTERISTICS OF AQUAMARINE FROM TURKEY.
R. Kibar[1], M.I. Kati[1], A. Çetin[1], M. Türemis[1], I.Ç. Keskin[1], B. Tastekin[1], M. Hatipoglu[2] and N.Can[1], [1]Celal Bayar University, Faculty of Arts and Sciences, Physics Department, 45140 Manisa-Turkey, email;rkibar@yahoo.com
[2] Dokuz Eylül University, İMYO, İzmir Multidisciplinary Vocational School, Gemmology and Jewelry Program, 35140 Buca-İzmir / Turkey.

The beryl crystal has the chemical formula $Be_3Al_2Si_6O_{18}$ and is composed of hexagonal rings.The each ring is formed of six SiO_4 tetrahedrons. Pure beryl is colorless and transparent. However, beryl crystals may show various color tones if they contain transition metal ions as an impurity localized in crystalline sites. The beryl crystal can accommodate several kinds of impurities, either as interstitials or in the channel, substituting ions on the wall. Natural beryl crystals are found in nature with green (emerald), blue (aquamarine), yellow (golden beryl), pink (morganite) colors. Colorless minerals (goshenite) are also found. The color and other physical properties of beryl are sensitive to the presence of impurities [1-3]

Aquamarine (blue beryl) from TURKEY was investigated in this work. The ICP-AES and ICP-MS techniques were used to find composition of the mineral. Large variation was found, generally with little bearing on the properties of aqumarine investigated, this being essentially 0.13% MgO, 0.03% MnO, 3.08% Fe_2O_3 and of course, SiO_2, Al_2O_3 and BeO. The crystal structure of the sample was analysed by using X-ray diffraction (XRD).

Thermoluminescence (TL) is a sensitive technique for recording the presence of defects and for monitoring the changes in defect concentrations in insulators. Naturally occurring crystals of minerals are usually insulators so that TL is useful in characterizing minerals. The aquamarine sample displays spectral luminescence emissions of thermoluminescence (TL) and cathodoluminescence (CL). As seen from the figure 1, aquamarine has a broad peak at 105 ^oC in TL glow curve when it was exposed to X-ray. CL data of aquamarine at 300 K (Figure 2) show two peaks at 450 nm and 580 nm for different modulation frequencies.

The sample was also studied with SEM and optical absorption.

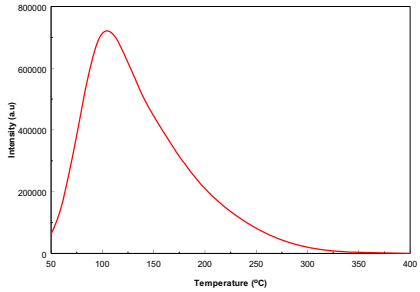

Fig.1 TL spectrum of diaspore after exposure to X ray.

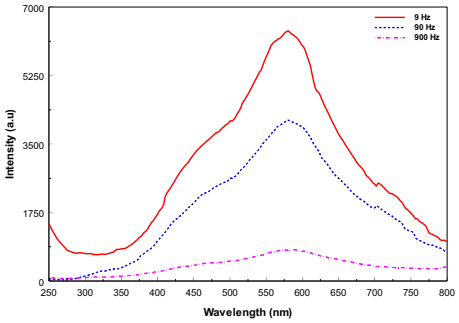

Fig.2 The AC CL spectra of aquamarine crystal 300 K

References: [1] R.I. Khaibullin et.al. Nuclear Instruments and Methods in Physics Research B 206 (2003) 277–281 [2] Tae HoYeom and Ae Ran Lim, Journal of Physics and Chemistry of Solids 72 (2011) 56–59 [3] J.C.R. Mittani et.al. Surface and Coatings Technology 158 –159 (2002) 708–711 [4]Petit P.E. et al. (2001) *J. Synch. Rad., 8,* 952-954.

COMPOSITIONAL ANALYSES OF F, Cl AND OH BY RAMAN SPECTROSCOPY IN APATITE FROM MAFIC-ULTRAMAFIC PIPES OF THE IVREA VERBANO ZONE (NW ITALY). P. Kollegger[1], F. Zaccarini[1], R. J. Bakker[1], G. Garuti[1] and O.A.R. Thalhammer[1], [1]Department of Applied Geosciences and Geophysics, University of Leoben, Peter Tunner Str.5, Leoben, Austria (peter.kollegger@unileoben.ac.at).

In this contribution we present the Raman spectra obtained from selected apatites occurring in mafic-ultramafic pipes of the Ivrea Verbano zone (WN Italy). These pipes, hosting Ni–Cu–Platinum group elements (PGE) sulphide deposits, have an alkaline signature and are enriched in volatiles and fluids that encouraged the formation of hydromagmatic phases like apatite, phlogopite and amphibole [2]. Based on accurate electron microprobe analyses, the apatites of our study are characterized by a wide spectrum of substitution of F, Cl and OH and therefore all the three end-members (flour-, hydroxyl- and chlorapatite) have to be taken in consideration for the Raman study.

Electron microprobe quantitative analysis is one of the most used techniques to analyse apatites and to discriminate the three endmembers. However, the analysis of light elements (Z<9) such as O and F, by electron microprobe, presents numerous problems and H cannot be detected. As a consequence, OH can be only calculated and reliable analyses of F can be obtained only with very modern electron microprobe, equipped with appropriate diffracting crystals. Furthermore, apatite is generally unstable under the high-voltage electron beam that produces relatively large craters on the crystals. Therefore, the size of apatite should be at least bigger than 50 microns. Thus, to analyse precisely apatite using electron microprobe is not always an easy target.

In the last 20 years, Raman spectroscopy was successfully applied to determine the compositional variation in apatite, involving great application areas such as biological research (dental and bone investigation), palaeontology (fossilized teeth) and medicine (cancer research) ([1],[4],[3]). These previous studies indicate that Raman spectroscopy can provide, in principle, relatively simple and fast semi-quantitative analyses of the anion composition also on very small apatite crystals.

The structure of apatite, (Ideal: $Ca_5(PO_4)_3(F,Cl,OH)$), is influenced by the different size and structural position of the monovalent anions (F, Cl and OH), shifting the cell parameters. A free phosphate group (PO_4^{3-}) possesses four Raman-active modes ν_1 (980 cm^{-1}), ν_2 (363 cm^{-1}), ν_3 (1082 cm^{-1}) and ν_4 (514 cm^{-1}). In our samples we could observe that each of the modes is shifted to lower levels and that the FWHM of the single peaks are widened by the incorporation of other species than F. Because our samples do not possess apatites with an end-member composition we included other studies ([1],[5],[4],[6]) for correlation with our data.

The results of this study demonstrated, for the first time, that there is a linear correlation between the Raman shift and the FWHM of the peaks, with the composition of the apatites not only between two end-members, but between the end-member fluorapatite on the on the one hand and the end-members hydroxyapatite plus chlorapatite on the other hand (Fig.1). We showed that the influence of Cl and OH on the Raman active modes of the apatite´s phosphate group is nearly the same. Therefore Raman investigations provide an instrument for the quantification of F contents in comparison with the sum of Cl plus OH.

Knowledge of the presence of F, Cl of OH in apatite provides information about fluid phase properties at formation conditions in geological environments.

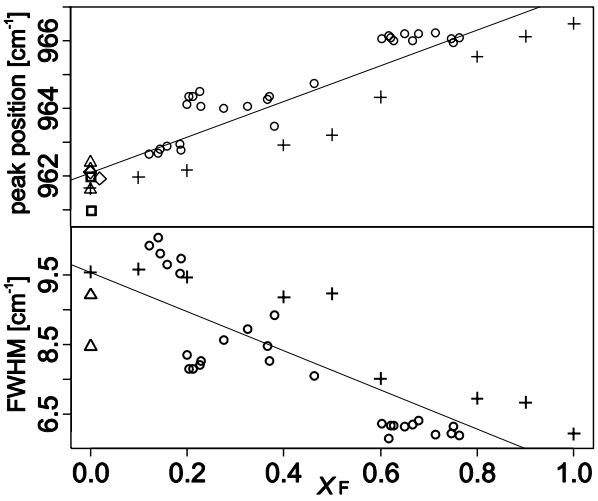

Fig. 1: a) peak position, and b) FWHM of the ν_1 PO_4^{3-} band in correlation to X_F = F/(F+Cl+OH) [apfu.]. Open circles: this study; Crosses: F-Cl apatites; Triangles: OH apatites; Rectangle: $(OH)_{0.29}Cl_{0.69}F_{0.02}$ apatite. [1],[4],[5],[6]

References: [1] DeMul F.F.M. et al. (1986) *Journal of Dental Research, 65(3)*, 437–440 [2] Garuti G. et al. (2001) *Journal of Petrology, 42(2)*, 433–457 [3] Haka A.S. et al. (2002) *Cancer Research, 62(18)*, 5375–5380 [4] Pasteris J.D. et al. (2004) *Biomaterials, 25(2),* 229 – 238 [5] Tsuda H. and Arends J. (1993) *Journal of Dental Research, 72(12),* 1609–1613 [6] Yu H. et al. (2007) *Journal of Physics and Chemistry of Solids, 68(10),* 1863 – 1871

MANGANESE-ACTIVATED CATHODOLUMINESCENCE OF SELECTED CARBONATE MINERALS.

C. Lenz[1] and J. Götze[2], [1]Institut für Mineralogie & Kristallographie, Universität Wien, Althanstr. 14, A–1090 Wien (christoph.lenz@univie.ac.at); [2]Institut für Mineralogie, TU Bergakademie Freiberg, Brennhausgasse 14, D–09599 Freiberg (goetze@mineral.tu-freiberg.de).

Cathodoluminescence (CL) microscopy is a routine tool in the investigation of geological materials. This technique is particularly sensitive to minute amounts of trace elements and other defects. In trigonal calcite-group ($R\bar{3}c$) and orthorhombic aragonite-group (*Pmcn*) minerals, Mn^{2+} and/or Rare Earth Elements (REE) are generally referred to as activators, aside from crystal-lattice defects, whereas Fe^{2+} is considered as a main quencher element of the CL in carbonates.

One major advantage of cathodoluminescence imaging lies in the visualization of internal textures, e.g., complex zonations displaying the growth history of carbonate crystals in cements and fossils. The interpretation of cement generations and the stratigraphic correlation are based mainly on the Mn^{2+} luminescence of their carbonate constituents [1–4]. Recently published results on the Mn^{2+} luminescence of various calcite- and aragonite-group carbonates [5,6], however, are controversial; perhaps due to misassignment of narrow-band REE as complex Mn emission.

We have studied a broad range of naturally grown trigonal and orthorhombic carbonates using CL spectroscopy and imaging. Calcite-group minerals are commonly characterized by an intense Mn^{2+} luminescence band, which occurs as broad-band emission in the orange to red range (Fig. 2). The broadness of the emission is explained by strong interaction of *3d* ions with the surrounding crystal field, which is strongly affected by lattice and atomistic vibrations of the ligands. By contrast, Mn^{2+} luminescence is rarely observed in aragonite-type carbonates (due to generally low Mn concentrations in these minerals); it is only common in biogenic aragonite [7]. We found, however, characteristic REE luminescence emissions in several of the aragonite and strontianite samples studied. These emissions are similar to those observed by by [5,6]. Synthetic REE-free, Mn-doped aragonite was found to show one single, broad Mn^{2+} band near 560–565 nm wavelength.

References: [1] Meyers W. J. (1974) *J. Sediment. Res.*, *44* (3), 837–861. [2] Bruckschen P. et al. (1992) *Sediment. Geol., 81*, 195–214. [3] Habermann D. et al. (1998) *Sediment. Geol., 116*, 13–24. [4] Richter D. et al. (2003) *Miner. Petrol.*, *79*, 127–166. [5] Calderon T. et al. (1996) *Radiat. Meas.*, *26*, 719–731. [6] Del Castillo H. C. et al. (2006) *Nucl. Instr. Meth. B*, *249*, 217–220. [7] Götte T. and Richter D. (2009) *Sedimentology*, *56*, 483–492.

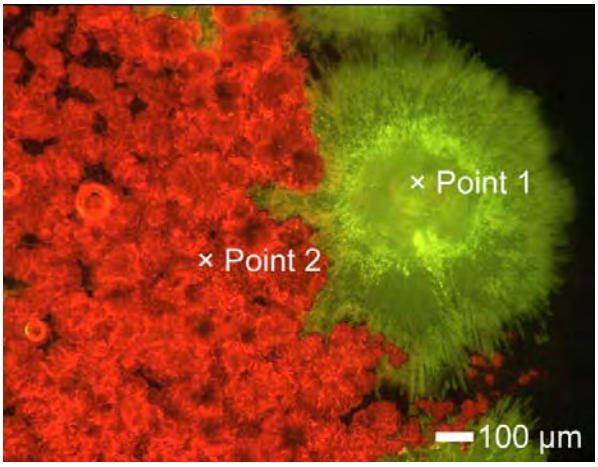

Fig. 1: *Cathodoluminescence image (OM–CL) of synthetic Mn-doped aragonite (0.004 apfu Mn) overgrowing Mg-calcite (0.066 apfu Mn; 0.134 apfu Mg). The Mn^{2+} causes green CL in aragonite whereas the Mg-calcite shows bright red Mn^{2+} luminescence.*

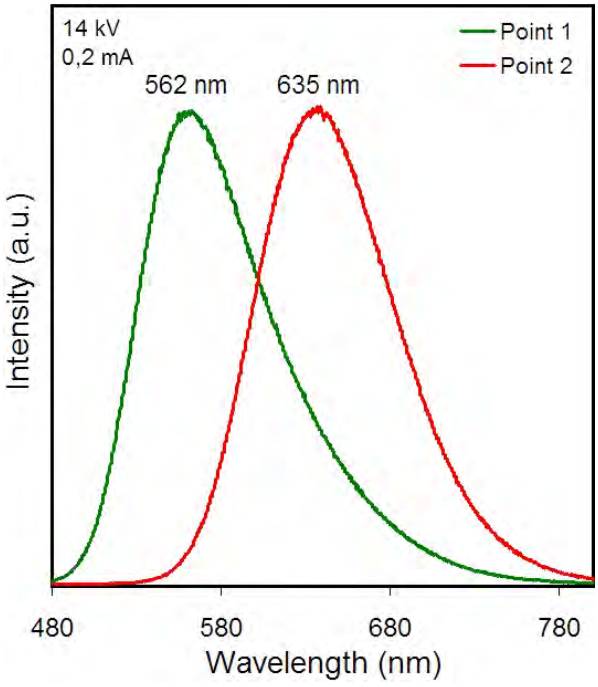

Fig. 2: *Cathodoluminescence spectra of synthetic Mn-doped aragonite and Mn-doped magnesian-calcite (analysis points refer to Fig. 1). Both minerals show a broad luminescence band caused by Mn^{2+}.*

EVALUATION OF PORTABLE RAMAN FOR THE CHARACTERIZATION OF SALT EFFLORESCENCES AT PETRA, JORDAN. P. López-Arce[1], A. Zornoza-Indart[1], C. Vázquez-Calvo[1], M. Gomez-Heras [1,2], M. Álvarez de Buergo[1] and R. Fort[1]. Instituto de Geología Económica/Instituto de Geociencias (CSIC-UCM), C/ Jose Antonio Nováis 2, Madrid 28040, Spain (plopezar@geo.ucm.es), [2]Departamento de Petrología y Geoquímica, Universidad Complutense de Madrid. C/ Jose Antonio Nováis 2, Madrid 28040, Spain

Abstract: The advantages of using a portable Raman equipment are contrasted with some of its shortfalls, that make other analytical techniques necessary to characterize salt efflorescences on historic buildings. In-situ analyses were carried out at some monuments of Petra (Jordan). Samples were also taken to the laboratory and analyzed with this and other techniques. This research shows the pros and cons of these analytical techniques - and how they complement each other- to identify the presence of soluble salts, which are deeply damaging these rock-cut monuments by salt crystallization processes.

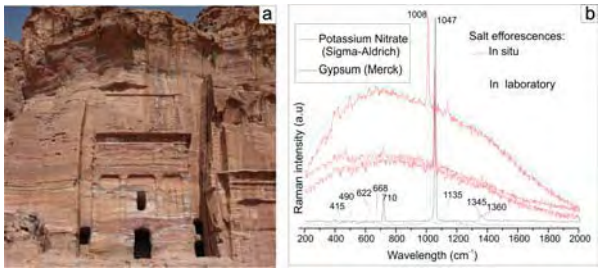

Fig.1. 'Silk Tomb', Petra (Jordan) and Raman analyses of salt efflorescence sample from this monument.

Materials and Methods: Twenty two samples of salt efflorescences were collected from the so-called 'Silk Tomb' (Fig.1a) and the 'Monastery' at the Archaeological Park of the Nabatean City of Petra (Jordan) in a first field trip to the site. All the samples were analyzed in the laboratory through X-ray diffraction (XRD). The salt efflorescences samples were also tested in the laboratory with a portable Raman equipment (Inspector Raman Delta Nu with a 785 nm diode laser for excitation) together with pure commercial salts, in order to create a database and to set a methodology, testing the most accurate analyses conditions for making easier the in-situ monitoring in a second field trip to the site. Approximately 100 measurements were made in the field, with the portable Raman equipment, from those areas previously sampled and their surroundings. Samples containing all type of salts were also analyzed with Environmental Scanning Microscopy with Energy-Dispersive X-ray Spectroscopy and Cathodoluminiscence detectors (ESEM-EDS-CL).

Results and discussion: Salt efflorescences of gypsum ($CaSO_4 \cdot 2H_2O$) and niter (KNO_3) were quickly and easily identified with Raman spectroscopy (Fig. 1b) in most of the samples analyzed in the buildings. The in-situ monitoring of these salts in cleaning and consolidation treatments of artworks helps restorers to decide when the treatment is concluded [1]. Assessment of stone deterioration by salt crystallization can also be carried out with portable Raman [2].

Laboratory and in-situ Raman analyses. A higher number and better quality spectra, with less fluorescence, of salt efflorescences were obtained in the field compared to the lab (Fig.1b). In-situ-monitoring avoids also sampling and environmental changes that affect phase transitions of hygroscopic salts (gypsum) during transportation to be analysed in the lab.

XRD, ESEM-EDS-CL analyses. Some of the most common salts sampled from the buildings and analyzed in the laboratory with XRD (Fig.2a), contained halite (NaCl) and sylvite (KCl), which are not sensible to Raman vibrations due to their strong ionic bond.

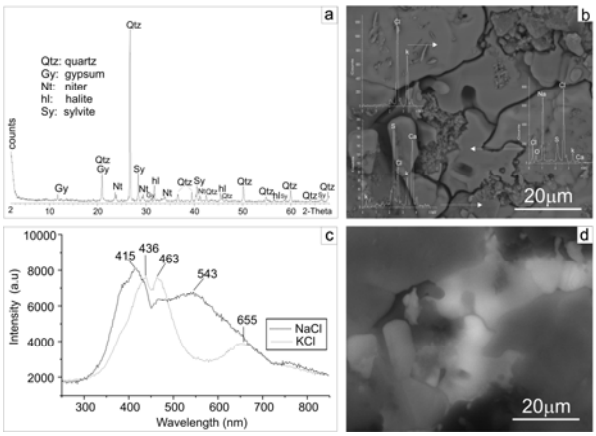

Fig.2. a) XRD of the sample shown in Fig 1b; b) ESEM-EDS of same sample; c) CL spectra of Na and K chlorides; d) Pancromatic map showing CL of these salts.

Nevertheless, these chlorides show strong luminescence, and can be easily identified by means of ESEM-EDS-CL (Fig.2b-d). Their CL signals allow distinguishing the stronger luminescence of halite that could be related to the presence of Mn^{2+} in its crystal lattice [3]. Other salt efflorescences, easily identified with Raman do not show luminescence, as gypsum, or are not detected with ESEM-EDS, as N in Niter.

References: [1] Martínez-Azcarazo I. et al. (2010) *Anal Bioanal Chem*, *397*, 2717–2725 [2] Kramar S. et al. (2010) *J Raman Spectrosc 41(11), 1441-1448* [3] Gorobets V. S. and Rogojine A. A. (2002) *Luminiscent Spectra of Minerals, 300pp*.

LASER INDUCED ARTIFICIAL FULGURITES FORMATION: PRELIMINARY RESULTS.

S. Martinez-Ramirez[1], J.J. Camacho[2] and L.Diaz[1]
[1]Instituto de Estructura de la Materia (CSIC). C/Serrano 121. 28006 Madrid, Spain, sagrario@iem.cfmac.csic.es; luisol@cfmac.csic.es, [2] Departamento de Química-Física Aplicada, Facultad de Ciencias, Universidad Autónoma de Madrid, Cantoblanco, 28049 Madrid, Spain, j.j.camacho@uam.es

Introduction: Fulgurites are glassy irregular tubes produced by the fusion of soil, which has been struck by lightning. The formation of a fulgurite occurs during the rapid transfer of lightning energy to a narrow channel in the ground [1, 2].

Artificial building materials are made from siliceous sand, calcite and ferrous materials from the same origin that the soil where fulgurites are formed.

IR lasers are an adequate tool to supply onto a limited area of a surface controlled thermal energy. The interaction of CO_2 lasers pulses with the surface material induces ablation and under specific conditions it could produce also structural transformations and crystallization on the surface material [3].

Raman spectroscopy is a non-destructive analytical technique that has been used to study a wide range of glassy silicate materials. Those materials are characterized by a number of broad bands that reflect the framework of the silicate structures [4, 5].

Aim: The main objective of this work is to study the formation of fulgurites in artificial building materials irradiated with CO_2 laser radiation

Methodology: Samples of 1x1x6 cm of the mortar were exposed to CW CO_2 (Synrad Firestar t80) laser radiation at different powers (8W and 40W) and different times (5 and 30 seconds).

Optical Emission Spectroscopy (OES) was used to analize the composition of the plasma plume.

After the exposure time, samples were studied by Raman spectroscopy. Raman spectra were recorded with a confocal Raman microscope (Renishaw RM2000) equipped with a 514-nm laser, a Leica microscope, and a thermoelectrically cooled CCD camera. The spectra shown were obtained with a 50× objective lens. The laser output was 100 mW, and the exposure time 10s. The area where vibration modes are found, i.e. 4000–100 cm−1, was the spectral region scanned.

Results: Figure 1 shows the aspect of the sample under CO_2 laser radiation showing the glassy fulgurite formed after irradiation. The size of the spot is bigger when higher power radiation. For the same power radiation longer time exposure produce bigger spot.

Raman spectra of the artificial fulgurite is showed in Figure 2. The presence of crystalline quartz (464; 355 and 210 cm^{-1} band) as well as several small broad bands from different Si-O bonds can be observed. When 50% of the laser power irradiated the sample, no quartz was observed; however a small band at 965 cm^{-1} indicate the presence of Si_2O_7 groups. The surface temperature reached at different conditions of irradiation were measured from emission spectra and it range from 4000 K to 5000 K.

Conclusions: For the first time fulgurites formation from an artificial building materials from CO_2 laser radiation has been studied.

Figure 1. Image of artificial fulgurite; left: irradiated 5s at 8W; middle: irradiated 30s at 8W and right: irradiated 5s at 40W

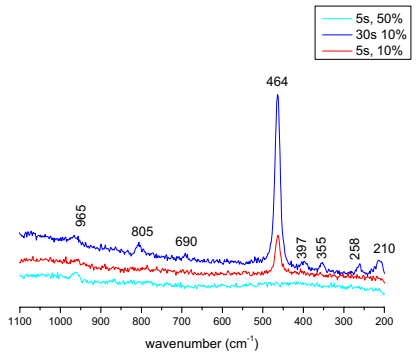

Figure 2. Raman Spectra of artificial fulgurite

References: [1] Garcia-Guinea J. et al. (2009) *Micro-Raman Spectroscopy and Luminescence Studies in the Earth and Planetary Sciences 128-134*.

[2] Carter E.A. et al. (2010) *Phil. Trans. R. Soc. A. 368*, 3087–3097.

[3] Díaz L., et al. (2006) *Appl. Phys.A* 85, 33-37

[4] Colomban P (2006) *J. Am. Ceram. Soc. 88*, 390-395.

[5] Martinez-Ramirez S (2006) *J. Raman Spectrosc 37*, 555-561.

Acknowledgments: This research was supported by the MICINN (Ministerio de Ciencia e Innovación) (BIA00767-2008, CTQ2008-05393/BQ and CTQ2010-15680) and Ministerio de Fomento (C31/2006).

RAMAN SPECTROSCOPIC STUDY OF ALLENDE (CV3) AND SARATOV (L4) CHEMICAL RESIDUES AND ITS IMPLICATION TO PHASE Q. J. Matsuda[1], K. Morishita[1], M. Nara[2] and S. Amari[3], [1] Department of Earth and Planetary Science, Graduate School of Science, Osaka University, Toyonaka 1-1, Osaka 560-0043, Japan (e-mail: matsuda@ess.sci.osaka-u.ac.jp), [2]Laboratory of Chemistry, College of Liberal Arts and Science, Tokyo Medical and Dental University, Chiba 272-0827, Japan, [3]Laboratory for Space Sciences and the Physics Department, Washington University, St. Louis, MO 63130-4899, USA.

Introduction: The noble gases have played important roles to study various events during the evolution of our solar system. The planetary noble gases in meteorite are highly enriched in heavy noble gases. They are carried by so-called "phase Q" . Phase Q is in a HF/HCl resistant residue (about 0.5% of the bulk meteorite) of the meteorite, but is destroyed by oxidants such as HNO_3, $Na_2Cr_2O_7$ etc. Phase Q is now identified as carbonaceous material [1], but its precise chemical state is not yet known. In this study, we compared the Raman spectroscopic data of the original HF/HCl residues (Q-rich) and their etched residues (Q-poor) for Allende (CV3) and Saratov (L4), in order to examine the carbon feature of the phase Q. Both phase Q and presolar diamond are preserved in the Allende meteorite, but presolar diamonds are not detected in ordinary chondrites of petrologic type >3.8 [2]. Thus we hoped to be able to determine the phase Q in Saratov without the disturbance of presolar diamond.

Sample and Experimental: We prepared the original HF-HCl residues using a chemical procedure commonly used to concentrate Q. The etched residues were prepared with an oxidant from the original residues. We also prepared a colloidal fraction for the Allende original residue. The noble gas measurements were carried out using the VG5400 noble gas mass spectrometer in Osaka University. The Raman spectroscopy was carried out using a Raman microscope (Kaiser Hololab 5000, Kaiser Optical Systems, Inc.) with a 532nm YAG laser.

Results and Discussion: The noble gas and Raman data of the Allende chemical residues are given in Matsuda et al. [3]. As for Saratov, only the noble gas data of the HF-HCl residue and a bulk sample are given in Matsuda et al. [4]. We confirmed that the heavy noble gases were surely enriched in the original residues (Q-rich) but depleted in the etched residue (Q-poor) in both chondrites.

Noble gas concentrations in the colloidal fraction of Allende original residue are a factor of 2-4 higher than those in the non-colloidal fraction [3]. The Raman spectroscopic parameters show that the colloidal fraction of the original residue is more amorphous compared to the non-colloidal fraction in Allende [3]. The ion irradiation evolves the carbon into more amorphous [5], indicating that the "plasma model" [6] is a plausible one as the origin of phase Q [3]. As for Saratov, the original residue contains only a portion of the trapped heavy noble gases, but they are largely removed in the etched residue, suggesting that phase Q is surely present in Saratov but is damaged by thermal metamorphism [4].

The Raman spectroscopic parameters such as peak positions and intensity ratios of the original residues are very much different for Allende and Saratov. The Raman spectroscopic parameters of the original residues have changed discretely after the oxidation in both meteorites. This suggests that the oxidization not only dissolves out the oxidizable carbon but also changes the whole carbon structure. After the oxidation, the D band positions at about 1350 cm^{-1} increased in both meteorites, but the intensity ratio of D and G bands (I_D/I_G) decreased in Allende but increased in Saratov. The different change of I_D/I_G ratios may be due to the difference stage of graphitic carbon for Allende and Saratov. Allende carbon is in the stage of nanocrystalline graphite to amorphous carbon (Stage 2 in Ferrari and Robertson [7]) where the decrease of I_D/I_G ratio indicates the evolution to amorphous state. Meanwhile, Saratov carbon is in the stage of graphite to nanocrystalline graphite (Stage 1 in Ferrari and Robertson [7]) where the increase of I_D/I_G ratio indicates the evolution to amorphous state. Thus our Raman data indicate that the oxidation changes the carbon structure to more amorphous (disordered) state in both meteorites.

Our results indicates that release of Q-gases is simply due to the disordered rearrangement of carbon structure by oxidation [1,8], although there still is a possibility that phase Q consists of very fine grains of a discrete phase and it is always covered by the major disordered carbon under the Raman spectroscopic observation [3].

References: [1] Ott U. et al. (1981) *Geochim. Cosmochim. Acta,* 45,1751-1788. [2] Alexander C. M. O' D. et al. (1990) *Earth Planet. Sci. Lett.*, 99, 220-229. [3] Matsuda J. et al. (2010) *Geochim. Cosmochim. Acta,* 74, 5398-5409. [4] Matsuda J. et al. (2010) *Meteorit. Planet. Sci.,* 45, 361-372. [5] Brunetto R. et al. (2009) *Icarus,* 200, 323-337. [6] Matsuda J. and Yoshida T. (2001) *Meteorit. Planet. Sci.,* 36, A127. [7] Ferrari A. C. and Fobertson J. (2000) *Phys. Rev.*, B61, 14095-14107. [8] Ott U. (2002) *Rev. Mineral. Geochem.,* 47, 71-100.

OPTICALLY STIMULATED LUMINESCENCE RESPONSE OF MODERN FLASH-FLOOD DEPOSITS IN SMALL MOUNTAIN CATCHMENTS. A. Medialdea[1], N. Porat[2], G. Benito[1] [1]Museo Nacional Ciencias Naturales-CSIC, Serrano 115-bis, 28006 Madrid, Spain, [2] Geological Survey of Israel, Jerusalem, Israel.
Correspondence author: amedialdea@ccma.csic.es

Introduction: OSL is increasingly being used as an accurate tool in dating recent flood deposits for improved flood hazards assessment. This work presents a study on the OSL response of sediments from recent (last 200 years) flash-flood deposits in the Guadalentín River (SE Spain). Two problems can be anticipated in the luminescence response for dating such recent deposits. Firslty, poor bleaching due to short duration of flood-flash flows and limited transport distance at the catchement headwater. Secondly, geological setting dominated by carbonate bedrock [1]. This study aims to provide preliminary diagnostic analysis with those parameters which might show an irregular OSL behaviour on these young samples [2]. The samples showed a positive behaviour despite their young age, namely a high signal-to-noise ratio making possible to measure the response at low doses, and lack of thermal transfer after preheating treatment. Furthermore, tests on the recuperation and recycling ratio were carried out showing a reproducible response. Possible feldspard contamination was checked by using IRSL. Equivalent Dose (D_e) values were determined for 24 aliquots. The results show a high scatter which could be caused by a insufficient bleaching prior to deposition. This effect typically results in an overstimation of the age.

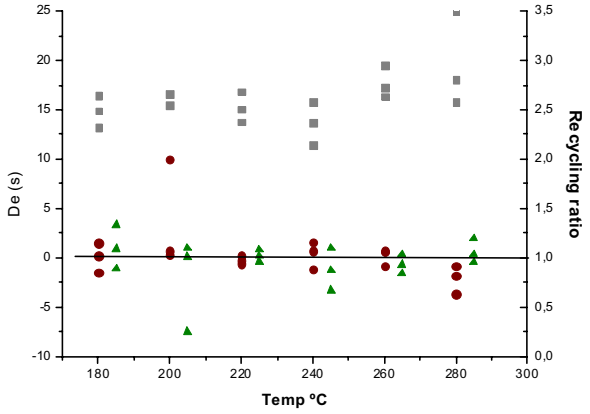

Figure 1- Measuring cycle effect on the recycling ratio (circles); IR stimulation effect on recycling ratio (triangle); D_e values (squares).

These preliminary OSL tests point out that single grain analysis may provide more accurate D_e values thus being the appropiated procedure for dating these flash flood deposits.

References:

[1] Benito, G., Rico, M., Sánchez-Moya, Y., Sopeña, A., Thorndycraft, V.R., Barriendos, M. (2010) The impact of late holocene climatic variability and land use change on the flood hydrology of the Guadalentin River, Southeast Spain. *Global and Planetary Change*, vol. 70, Issues 1-4, 53-63.

[2] Madsen, A.T., Murray, A.S. (2009) Optically stimulated luminescence dating of young sediments: A review. *Geomorphology*, 109, 3-16.

CHARACTERIZATION OF THE DIFFERENTIATION PROCESS BY CLATHRATION IN EUROPA SATELLITE USING RAMAN SPECTROSCOPY.

M. V. Muñoz-Iglesias[1], L. J. Bonales[1, 2] and O. Prieto-Ballesteros[1] . [1]Centro de Astrobiología. INTA-CSIC. Torrejón de Ardoz, 28850 Madrid. Spain (mugnoziv@inta.es), [2]Departamento de Química Física I, Facultad de Química, Universidad Complutense, 28040 Madrid, Spain.

Introduction: Clathrate hydrates are solid crystal structures of water, with cavities inside containing gas molecules, which form at low temperature and high pressure. In icy satellites of the outer solar system, such as Europa, have been detected the clathate-forming compounds and also exist the conditions required for their formation. Based on this, we can assume that gas clathrates may be present in those satellites, although they have not been detected yet.

In the present work, we crystallize and dissociate CO_2-clathrates from an aqueous solution of $MgSO_4$ and CO_2. We assume that the aqueous magmas from the Europa interior are salt-rich. This assumption is based on the NIR Galileo observations of dark terrains, which seems to be endogeneous and composed by salt hydrates [1]. Our results confirms the theoretical models which predict that clathrates are stable from the icy crust to the potential salty ocean that may exist below the icy crust [2, 3].

Experimental apparatus and procedure: Experiments were carried out in the High Pressure Planetary Environment Chamber (HPPEC), a simulation chamber facility of Centro de Astrobiología, Madrid, Spain. Runs were done at several pressures to obtain the phase diagram of the system H_2O-CO_2-$MgSO_4$. We have analyzed the clathrate kinetic formation with the iH550 Spectrometer (Horiba Jobin Ybon,), by using a 1200/1800/2400 grooves/mm diffraction grating and a solid state laser Nd:YAG 532 nm.

Results: In Figure 1 we compare the two Fermi dyad peaks (≈1280 and 1380 cm^{-1}) of CO_2 molecule in different states: gas, dissolved and enclathrated, respectively. We observe that it is possible to differentiate between each state of the molecules by Raman spectroscopy, despite the Raman shift difference is very small (≈1 cm^{-1}) between the dissolved and the clathrated CO_2 . It should be note that the peak area around 980 cm^{-1} corresponding to the $MgSO_4$ decreases after the crystallization (see the lowest spectra in Fig. 1). This could be due to the fact that sulfate (and all salts) is expelled from the clathrates structure, increasing the concentration in the remaining aqueous solution. If the eutectic composition is exceeded, precipitation takes place, seeing a decrease of the sulfate peak about 980 cm^{-1}.

Conclusions: These results are of a deep planetologic importance because it can explain satellite internal differentiation and cryovolcanism processes which may occur in the satellite. Features explained previously in the Fig. 1 can be associated to different stages of the differentiation process (Fig. 2). Figure 2 shows schematically the evolution of a cryomagma trough the time: (Fig. 2.A) Cryomagmatic chamber with H_2O, salts y volatiles, (Fig. 2.B) Clathrate formation and concentration of the salt in the remaining solution (with or without precipitation), (Fig. 2.C) Differentiated chamber by clathration and (Fig. 2.D) Cryomagma ascent after depressurization and clathrate destabilization, which produce the positive buoyancy of the liquid respect to the icy crust. Hydrated salts observed by Galileo's probe on the surface support this theory because it appear as extrusions from the inner in the geologic accidents mentioned [1].

Similar experiments will be performed in the future with other salts (Na_2SO_4 and mixtures) and volatiles (SO_2, H_2S) also detected in Europa. From the obtained data, we will propose a compositional model for Europe to support Raman spectroscopy as a potential instrument for the next missions to the satellite.

Acknowledgements: We thank MALTA (CSD2007-00045) and QUIMAPRESS (S2009/PPQ-1551) Projects for the support.

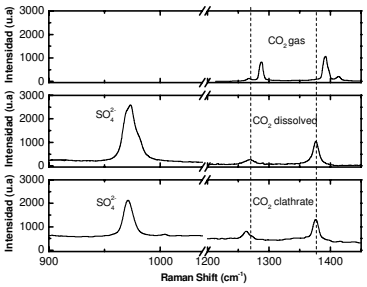

Figure 1. Spectra of the CO_2 gas, CO_2 dissolved in an aquous solution of $MgSO_4$ and spectra of the same compounds after clathration.

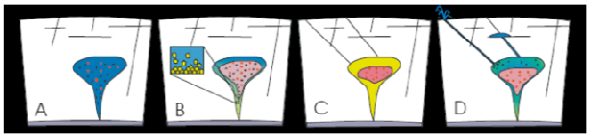

Figure 2. Magmatic differenciation by clathration and subsequent cryovolcanism process

References: [1] Dalton J. B. et al. (2005) *Icarus, 177*, 472-490. [2] Prieto-Ballesteros O. et al. (2005) *Icarus, 177*, 491-505. [3] Kivelson M. G. et al. (2000) *Science, 289*, 1340-1343.

EVENTS IN THE LIFE OF THE OLDEST ZIRCON ON THE MOON: A COMBINED SIMS, CL, EBSD AND RAMAN STUDY. R. T. Pidgeon[1a], A. A. Nemchin[1], M. Grange[1], N.Timms[1], [1]Department of Applied Geology, Curtin University, Kent Street, Bentley, WA 6102, Australia ([a] r.pidgeon @curtin.edu.au)

Introduction: Zircon has been identified in a number of KREEP-rich breccias in lunar samples. Precise U-Pb isotopic analyses of these grains began in the 1980's, with the development of the SHRIMP ion microprobe [1,2] and zircon U-Pb geochronological research since this time has revealed a complex history of lunar magmatism beginning at c 4.42 Ga, the age of the oldest zircon on the moon [3] and ending at c. 3.9 Ga, the age of the later heavy bombardment [4]. An important question that needs to be resolved is whether magmatic events dated by zircon are impact related or represent endogenic lunar igneous activity. In most cases information is not available to resolve this issue but where SHRIMP U-Pb measurements are made on skeletal zircons that crystallized in cooling impact induced melt the zircon age clearly dates an impact event. A second possibility for dating an impact is by investigating the U-Pb age pattern in a zircon that has been disturbed by one or more impacts. This is less straightforward and to unravel the history of such grains it is necessary to apply a combination of optical and cathodoluminescence (CL) imagery, electron backscattered diffraction (EBSD) and Raman spectroscopy besides SIMS U-Pb measurements. In this contribution we describe results using these techniques on the oldest lunar zircon found so far [3]. This c. 4.42 Ga grain from the matrix of Apollo 17 breccia sample 72215,195 contains evidence of its igneous origin and also of one or more later impact events.

The c. 4.42 Ga lunar zircon: The location of this zircon in the breccia matrix is shown in the following CL image. The grain is a broken fragment , about

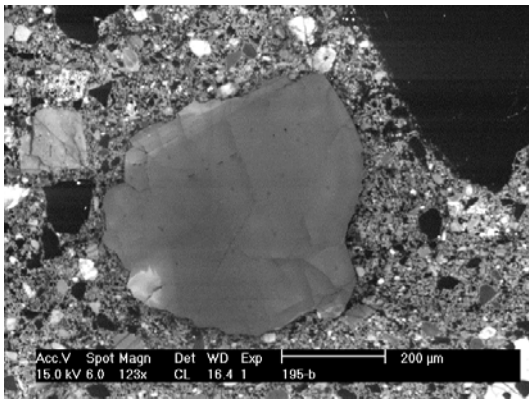

500μm in diameter, with an equidimensional, rounded form suggesting mechanical abrasion during transport. The main body of the grain has a uniformly low CL intensity and grey-pink birefringence indicating extreme radiation damage. Exceptions are a small bright (CL) patch on the left side of the grain and a bright linear sliver along the top. The grain does not have PDFs or other structures indicative of severe impact.

SHRIMP U-Pb measurements: A total of 41 SHRIMP U-Pb isotopic measurements were made on this grain. The $^{207}Pb/^{206}Pb$ ages vary within the grain from 4.42 Ga in two areas in the centre to 4.35 Ga in areas of bright CL. The inhomogeneous age distribution is attributed to an impact event at c. 4.35 Ga. The reduction in $^{207}Pb/^{206}Pb$ age is due to the progressive and incomplete removal of radiogenic Pb from the zircon, despite the grain having little radiation damage. Whereas it would appear at first sight that only Pb has been lost from the grain it can be demonstrated from a plot of $^{207}Pb/^{206}Pb$ age versus U and Th that some loss of these elements has also occurred in areas of bright CL.

EBSD and Raman measurements: EBSD, optical birefringence and Raman intensity maps and the distribution of U and Th, show an identical pattern delineating the distribution of radiation damage in the grain. A comparison of this pattern with the Pb-Pb age distribution shows that these are not the same indicating that Pb loss occurred independently of the distribution of U and Th and the radiation damage at c. 4.35 Ga. The Raman width data confirm the highly radiation damaged structure of the zircon. By comparison with Raman data from unannealed zircon grains it is evident that radiation damage in the c. 4.42 Ga grain has been annealed by a later event.

History of the c. 4.42 Ga zircon: A combined SIMS, CL, EBSD, Raman and optical investigation has revealed a complex history for the grain from initial crystallization at c. 4.42 Ga, severe chemical disturbance at c. 4.35Ga and a number of impact and transport events culminating in final deposition and annealing at c. 3.8 Ga.

References: [1] Compston W. et al. (1984) *JGR*, 89, B525-B534. [2] Pidgeon R.T. et al. (2010) *Precam. Res*., 44-49. [3] Nemchin A.A. et al. (2009) *Nature Geosc.,*2, 133-136. [4] Nemchin A.A. et al. (2008) *Geochim. Cosmochim. Acta*. 72, 668-689.

SPECTRA LUMINESCENCE OF URANYL GROUPS ASSOCIATED TO SILICA PHASES IN HYDROTHERMAL AND SEDIMENTARY OPALS FROM MADRID (SPAIN). Pozo, M.[1], Garcia-Guinea, J[2], Furio, M[2]., Fernandez-Cortés, A.[2], Correcher, V.[3] [1]Departamento de Geología y Geoquímica. Universidad Autónoma de Madrid. 28049 Spain. [2]Museo Nacional Ciencias Naturales. CSIC. 28006 Madrid. Spain. [3]CIEMAT. Av. Complutense 22. Madrid 28040, Spain.
Correspondence author: manuel.pozo@uam.es

HYDROTHERMAL OPAL.- The late hydrothermal activity occured in the La Cabrera (Madrid) granitic pluton along with miarolitic cavities and pegmatite bodies produced different mineral parageneses linked to the temperature decreasing. The maximun hydrothermal activity ocurred at 250ºC ± 50ºC decreasing up to circa 140ºC. Accordingly, the pegmatitic cavities of the Cabrera granite are zoned from the inner to the outer as follows: (i) calcite with gypsum, opal, uranospinite and johnbaumite in the core, (ii) prehnite, laumontite, heulandite-Ca, stilbite-Ca, chabazite, fluorapophyllite, datolite and bavenite, (iii) epidote, (iv) quartz–feldspar pegmatite being the outer layer of the cavity, and (v) granite as the host rock.

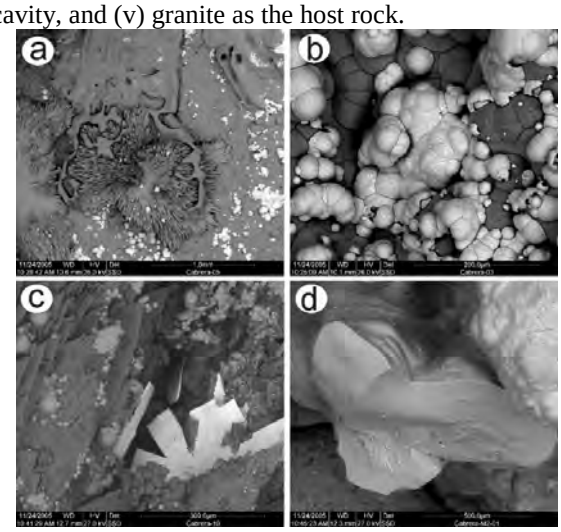

Figure.1.- ESEM pictures of the hydrothermal opal parageneses of La Cabrera (Madrid): (a) Grey background is opal, white sphaeres are johnbaumite, grey needles are calcite and grey masses resembling liquid are gypsum. (b) Black background is opal, white sphaeres are johnbaumite coating opal (c) Uranospinite plates on the former parageneses (d) Broken opal with cavities and aggregate of johnbaumite on the upper right (white).

SEDIMENTARY OPAL.- They are are thin siliceous layers and infills of translucent white colour up to 2 cm thick. The silica phases sporadically occur associated to chert nodules in the sepiolite deposit from the Batallones Butte (Neogene Madrid Basin, Spain). These layers are commonly filling or coating brown silicified sepiolite, being interpreted as a late stage of silicification (Figure 2). XRD analysis indicates opal CT and quartz as main composition with traces of sepiolite. Under the petrographic microscope microcrystalline quarz clusters and cements affecting an opal groundmass have been observed.

Figure 2. Hand sample and texture in thin section (N//).

The ICP-MS chemical analysis displays high silica content (93.44 wt %), moderate LOI (5.10 wt %) and around 1.5 wt% of other major and trace elements. Among trace elements is noteworthy the U content (69.1 µg/g) higher almost five times its abundance in silicified sepiolite. Other trace elements include V, Cr, Ni, Zn, Rb, Sr, Sb and Ba. Under the ESEM-CL microscope we record a mixed spectra (Figure 3).

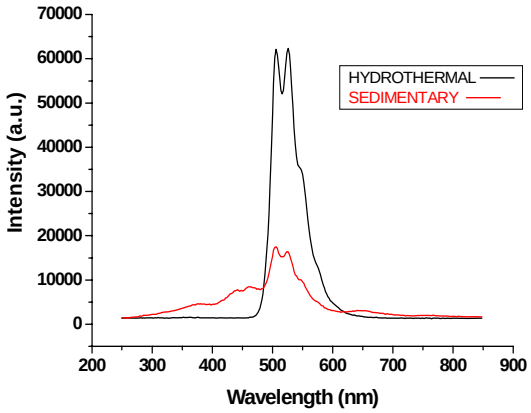

Both spectra CL recorded on opal areas clearly depicts close uranyl groups. Moreover, it is important to note that intensities and minor peaks are different. Explanation: in the case of the hydrothermal opal specimen we collected light emission coming from micro-uranospinite crystals hidden in the small vugs, while in the sedimentary case we recorded the characteristic peaks of the quartz and less significant uranyl peaks association which could be attached uranyl groups sited in hydrous cluster of the same opal.

ANALYSIS OF THE RESIDUALS IN GRAVE GOODS FROM THE VACCAEA ERA AT THE NECROPOLIS OF 'LAS RUEDAS' IN PINTIA.

A.C. Prieto[1], M. Avella[1,2], M.A. González[1], J. Jiménez[1], F. Romero[3], R. De Pablo[3], C. Górriz[3] and C. Sanz[3],
[1]GdS Optronlab, [2]Unidad de Microscopía Avanzada. Parque Científico UVa, Edificio de I+D, Campus "Miguel Delibes", Paseo de Belén, 11, E-47011 Valladolid, Spain. (prieto@fmc.uva.es), [3]Dpto. Prehistoria, Arqueología, Antropología Social y Ciencias y Técnicas Historiográficas. Universidad de Valladolid, Plaza del Campus, E-47011 Valladolid, Spain.

Introduction:

The archaeological site of Pintia (Padilla de Duero/Peñafiel, Valladolid), located at the oriental side of the vaccaea region, was occupied for more than thousand years, between IV century B.C and VII century A.C, by different cultures: Vaccaean, Roman and Visigothic. The Vaccaea era has yielded the more interesting archaeological records regarding the different functional areas that involve the oppidum: the fortified village of 'Las Quintanas' – surrounded by a wall and a moat-, the artisan neighbourhood of 'Carralaceña', the necropolis of Las Ruedas, etc.

Pottery, metal and bone/skeletal remains are the more common objects recovered. The pottery remains are very well preserved, so they are optimal for analysing and the subsequent study of the food contained, such as milk-based products, animal fats, beer, wine, etc.

The vessels from the funerary area of 'Las Ruedas' are specially interesting. They contained the food for the afterlife and therefore have a great symbolic value. The wealth of the grave, the absence or presence of objects or contents contributes significantly on the assessment of the deceased's profile (age, sex, social status, etc). Therefore, the analysis of the residuals found in the vessels becomes highly significant.

The use of three complementary instrumental techniques has been assessed as an analytical methodology. Light microscopy (visible and ultra-violet light), Environmental Scanning Electron Microscopy equipped with an Energy Dispersive X-ray Analysis system (ESEM-EDX) and micro-Raman spectroscopy (μ-RS) have been used in this work. Samples were set up on a common holder for all the techniques

Experiment: The specimens studied in this work were extracted from a crateriform vessel which belongs to the grave goods of the grave #154. The grave corresponds to a tall individual, probably female, buried in the II century BC.

Light microscopy analysis were carried out with a petrographic microscope Leica DMLP with both transmitted and epi-illumination. The environmental electron scanning microscopy was carried out with FEI-Quanta 200F equipped with a Genesis XM2i from EDAX. Micro-Rama spectra were acquired with a high resolution Raman spectrometer LABRAM HR 800UV from Horiba-Jobin & Yvon Spex, equipped with an Olympus BX41 microscope and a XYZ-axis motorized stage. A x100 objective and backscattering configuration were used for Raman spectra acquisition. A 632.8 nm HeNe laser were used as excitation probe. The nominal laser power on the samples was 1mW and the irradiance was about 100 $kWcm^{-2}$. The spectral window was [200-3800] cm^{-1}, the integration time was [5-60] s and 2 accumulations were used as acquisition parameters. All this results in an spectral resolution less than 1 cm^{-1}.

Results and Discussion: The results show the presence of phytoliths, vegetal fibres and stems with parenchymal structures at different alteration degree. Low crystallization structures, with elemental composition of C, O and Ca were detected. They are probably related to oxalates that can come from milk-based derivatives or vegetal residuals.

Degradation and age of organic natural fibres can be assessed by the relative intensity relationship between the $\nu_{as}(COC)$, $\nu_{s}(COC)$ glycoxilic and $\nu_{as}(CH_2)$ bands at 1098, 1124 and 2917 cm^{-1} respectively. We have obtained for I_{1124}/I_{1098} and I_{1098}/I_{2917} values of 0.9 and 0.6 respectively which are characteristic of old and degraded fibres.

The presence of organic materials with low crystallinity and order can be assessed by the study of the 1595 cm^{-1} and 1386 cm^{-1} bands, related to C-C bonds vibrations, and their relative intensities.

Raman bands assigned to compounds related to agricultural processes can be identified and therefore can be distinguished from the residuals of interest.

Conclusions: We have stated herein that the use of the Raman spectroscopy together with complementary high resolution analytical techniques becomes a powerful tool for the study about the contents and use of ceramic vessels from archaeological heritage.

Acknowledgments: This work was funded by Spanish Government through Ministerio de Ciencia e Innovación, MCINN.

Project HAR2010-21745-C03-01.

RAMAN SPECTROSCOPY ANALYSIS OF A PLAYING CARD FROM THE XVIII CENTURY. A. C. Prieto[1], M. Avella[1,2], O. Martínez[1], J. Jiménez[1], J.L. Alonso[3], I. Sánchez[4], R. Martín[4] and M. Barrera[4], [1]GdS Optronlab, Parque Científico UVa, Edificio de I+D, Campus "Miguel Delibes", Paseo de Belén, 11, E-47011 Valladolid, Spain (prieto@fmc.uva.es). [2]Unidad de Microscopía Avanzada. Parque Científico UVa, Edificio de I+D, Campus "Miguel Delibes", Paseo de Belén, 11, E-47011 Valladolid, Spain. [3]Servicio de Restauración de la Diputación Foral de Alava, Urartea 4, E-01010 Vitoria-Gasteiz, Spain. [4]Centro de Conservación y Restauración de Bienes Culturales. Junta de Castilla y León. Carretera 2. E- 47130 Simancas, Valladolid, Spain.

Introduction: We present herein the characterization, by means of three complementary experimental techniques (light microscopy-LM, scaning electron microscopy equiped with energy dispersive X-Ray spectroscopy–SEM-EDX and micro-Raman spectroscopy– μRaman), of a card belonging to a deck of the Spanish pattern, made in Perú at the time of *Virreinato de Peru* (XVIII century): The objective is to obtain detailed information of the pictoric palette used for the decoration of the cards, where two basic colors, red and green, are seen. Small samples from both colored regions have been analysed.

Experiment: The material selected for the study is a piece of civil goldsmiths, a card (number five, swords) of a traditional deck which has been restored in the Servicio de Restauración de la Diputación Foral de Alava and analysed in the Centro de Conservación y Restauración de Bienes Culturales de la Junta de Castilla y León. In particular, the study concerns to a piece made of Silver alloyed with a small amount of Copper, whose typology corresponds to the colonial culture of that period (XVIII century).

A first inspection of the samples (stratigraphies) was performed by LM, using a petrographic microscope LEICA DMLP, with transmited and epi-illumination. Elemental analysis was performed by using an environmental SEM (ESEM), model FEI Quanta 200FEG, equiped with EDX, Genesis XM2i from EDAX. μRaman analysis was performed using a LABRAN HR 800 UV (Horiba Jobin-Yvon). The Raman spectra were collected in backscattering configuration, using a x100 magnification objective and a HeNe laser (λ=632.8 nm) for excitation. The nominal power onto the sample was 100 $kWcm^{-2}$. The spectral resolution is better than 1 cm^{-1} using a difraction grating of 1200 lines/mm.

Results and Discussion: The analysis of the samples using LM –white light ilumination – shows three pictoric layers in a stratigraphic disposition, for both samples from red and green regions. That from the green area shows a non homogeneous distribution of micro-crystals in the three stratigraphic layers. The EDX analysis of the green samples show the presence of Cu salts as the main pigment. An EDX profile along the three layers, with a step size of 0.08 μm, shows the presence of Cu in the two lower layers. The upper layer shows high Fe/low Cu concentrations. The EDX analysis of the samples from red areas show the presence of cinnabar (HgS) as the main pigment. The lower (glue) layer present high contents on Si, O, Al, C and K, with Mg and Fe traces. (The composition of the glue layer of both green and red areas is similar). The upper layer, which is a re-painting layer, has high contents of C, Al, Si, O and Fe, with some traces of K, Ca, S and Hg, coming from the intermediate layer (first painting layer). Such composition suggests the presence of silicoaluminates of clay type used as dispersion vehicles, and crystals containing some Fe pigment as a cromophore.

The Raman spectra for the green areas show, for the upper layer, broad and not well defined bands, together with a sharp peak at 2154 cm^{-1} – with a shoulder at 2128 cm^{-1} – , as well as a band with intermediate intensity at 2092 cm^{-1}, ascribable to the Fe^{+3}-C≡N-Fe^{+3} bonding. Intense bands are also observed at 271 and 527 cm^{-1}, ascribables to the Prussian blue pigment, $Fe_4[Fe(CN)_6]_3$, as well as two intense bands at 1368 and 1399 cm^{-1}, due the Cr^{3+} fluorescence; Cr^{3+} appears as an impurity associated to the Al_2O_3 used during the polishing of the sample. The two lower layers in the green areas show bands associated to the verdigris pigment, corresponding to the copper acetate with different hydration levels. The Raman spectra for the red areas show peaks at 254 and 344 cm^{-1} – with a shoulder at 354 cm^{-1} –, together with a small band at 285 cm^{-1}, ascribable to the A_1 , E_{LO} and E_{TO} modes of HgS (Vermilion), respectively. The upper layer shows the intense bands of the Vermilion and Prussian blue pigments. The lower layer shows a fluorescence band centered at ~682 nm. Broad and not well defined bands superpossed to this band could be ascribable to colophony (rosin) used as a glue.

Conclusions: The complementary use of Raman spectroscopy togheter with high resolution analytical techniques allows to reveal the pigments used for the decoration and the further manipulation history of cards belonging to the historic and archeological heritage.

DETECTION OF CARBONACEOUS MATERIAL IN FOSSIL MARINE MICROBIALITES BY RAMAN SPECTROSCOPY (LÁNCARA FORMATION, LOWER CAMBRIAN, CANTABRIAN MOUNTAINS, SPAIN). A.C. Prieto[1], M.P. Avella[1,2], O. Martínez[1], E. Moreno-Eiris[3], S. Menéndez[4], M. Rodríguez-Martínez[5], A. Perejón[6]. [1]GdS Optronlab, [2]Unidad de Microscopía Avanzada. Parque Científico UVa, Edificio de I+D, Campus "Miguel Delibes", Paseo de Belén, 11, 47011 Valladolid, Spain. prieto@fmc.uva.es, [3]Universidad Complutense, Dpto. Paleontología, 28040 Madrid, Spain, [4]Museo Geominero (IGME), 28003 Madrid, Spain, [5]Universidad de Alcalá, Dpto. Geología, 28871, Alcalá de Henares, Spain, [6]Instituto Geología Económica, 28040 Madrid, Spain.

Introduction: Marine carbonate lithofacies formed 512 My ago (lower Cambrian, Stage 4) in tidal plains in a mixed carbonate platform – where sedimentation was strongly influenced by tides and storms – have been analyzed. The carbonate sedimentation was produced by enzymatically controlled mineralization [1] through the epibenthonic fauna such poriferans (Archaeocyaths –extinct taxa), echinoderms and molluscs, as well as by induced biomineralization by benthonic microbial communities (BMC). The lithofacies correspond to high energy deposits like bioclastic pelletoidal limestones and oncolitic facies and low energy deposits like fenestral limestones and microbialites. Microbia-lites are mineral deposits formed through trapping and binding of detrital sediment as well as the locus of the mineral precipitation of BMC [2]. Microbial activity favoured characteristic macrostructures like digitate thrombolites [3] and spongiostromata oncolites (related with cyanobacteria coatings) and microstructures like microbial peloids, crusts and clotted microfabrics [4].

Raman spectroscopy has been used to differentiate the main carbonate minerals and to detect the presence of carbonaceous material in enzymatically controlled minerals (skeletal elements), microbially induced biominerals and abiotically precipated cements. Different macro and microestructures (thrombolites, oncolites, fenestral bindstones, microbial crusts and microbial peloids) have been analyzed in the microbialites.

On studing carbonaceous material it is known that the two crystalline forms of carbon, diamon and graphite, are characteried by two Raman bands at 1386 (D band) and 1595 cm^{-1} (G band), respectively. The Raman parameters of these bands are very sensitive to structural disturbances by electronic configuration sp^2-sp^3 changes in the carbon bands (C-C) and consequently their presence are use to estimate the structural properties of the carbonaceous material. In particular, the intensity ratio between the G and D bands has been shown to be indicative of the crystallinity degree of the material. This can provide intersesting information about the thermodicamical processes of crystallization.

Materials and methods: The Raman experiments were performed on thin sections using a high resolution Raman spectrometer LABRAM HR 800UV from Horiba-Jobin & Yvon Spex, equipped with an Olympus BX41 microscope and a XYZ-axis motorized stage. A x100 objective and backscattering configuration were used for Raman spectra acquisition. A 632.8 nm HeNe laser were used as excitation probe. The nominal laser power on the samples was 1mW and the irradiance was about 100 $kWcm^{-2}$. The spectral window was [200-3800] cm^{-1}, the integration time was [5-60] s and 2 accumulations were used as acquisition parameters. All this results in an spectral resolution higher than 1 cm^{-1}.

Results and discussion: Skeletal remains (Archaeocyaths and hyolithids) are composed of $CaCO_3$ and show weak bands of disorganized carbonaceous material. Microbial macro- and microstructures show important changes in compositon. A Raman profile along a columar thrombolite shows compositional variations between microsparitic calcite ($CaCO_3$) and dolomicrospar $(CaMgCO_3)_2$ and presence of carbonaceous material. Intercolumn space is filled by microbial peloids ($CaCO_3$) with low intensity vibrational bands characteristic of the disorganized carbonaceous materials. However, thrombolites, fenestral bindstones and microbial microsparitic crusts in close localities are solely composed of calcite and carbonaceous material displaying well differentiated D and G bands. The Spongiostromata oncolites related with cyanobacteria do not show rests of carbonaceous material. Microbial peloids are dolomitized and preserve low cristalinity carbonaceous material. The precipitation sequence of calcite cements in cavities shows two distinct phases: an early marine cementantion phase with signatures of disorganized carbonaceous material and a later burial cementation phase abiotically precipitated.

Conclusions: Raman spectroscopy is shown to be a powerfull technique to analyze the presence of carbonaceous material in fossil marine microbialities as well as to give insight into the thermodinamical crystallization processes occurring in the Cambrian samples.

References: [1] Mann S. (2001) *Biomineralization -principles and concepts in bioinorganic materials chemistry*, Oxford University Press, 210 pp. [2] Burne R. V. and Moore L. S. (1987) *Palaios*, 2, 241-254. [3] Aitken J. D. (1967) *J. Sed. Petrol*., 37, 1163-1178. [4] Flügel E. (2004) *Microfacies of carbonate rocks*, Springer, 976 pp.

QUANTITATIVE DETERMINATION OF GASEOUS PHASES IN FLUID INCLUSIONS BY RAMAN MICROSCOPY. A. C. Prieto[1], A. Guedes[2], A. Dória[2], F. Noronha[2] and J. Jiménez[1], [1]GdS Optronlab, Parque Científico UVa, Edificio de I+D, P. de Belén, 1, E-47011 Valladolid, Spain (prieto@fmc.uva.es), [2]Centro de Geologia/ DGAOT, Faculdade de Ciências, Universidade do Porto, P-4169-007 Porto, Portugal.

Due to its non-invasive nature, together with its high lateral resolution, micro-Raman spectroscopy reveals itself as a powerful technique to perform qualitative analysis and to determine the relative molar fractions of the gaseous species present in minerals fluid inclusions. However, the integrated Raman intensity depends, among others, of the concentration of the analyte and of the Raman cross-sections, and these depend on the state variables of the system, therefore, the concentrations of the molecular species present in the gas phase of fluid inclusions determined from Raman spectra are relative quantitative values. From the calculation of the molar concentrations of the gases in the fluid inclusion, and once all phases characterized, it is possible to determine the system state variables (P-V-T-X) in solid-liquid-gas equilibrium.

There are numerous publications concerning the application of micro-Raman spectroscopy to the determination of the composition of fluid and solid inclusions in minerals and processes to obtain molar fractions in COHNS multi-component systems have been also been described [1-5]. Micro-Raman qualitative analysis requires the identification of the various constituents of a mixture though the position (ϖ, cm^{-1}) and the intensities of the fundamental vibration modes of the ionic or molecular group in the Raman spectrum. A collection of the species contained on fluid inclusions and their characteristic vibrational modes are described on Burke [6] and for the relative quantification of gaseous phase of the ionic or molecular species *i* present in a fluid inclusion, using the theory of Placzek [7] improved by Dhamelincourt et al.[8], the integrated Raman intensity is $I_i=I_0\sigma_i N_i \xi_i$, where I_0 is the intensity of incident radiation on the sample, σ_i, the Raman scattering cross-section, N_i, the number of molecules of the species *i*, ξ_i, the spectral efficiency factor, dependent on the spectrometer, optical instruments and CCD detector. Therefore, the Raman integrated intensity gives information on the number of molecules of a species per unit of volume. The molar fraction X_i of the species *i* is $Xi=[(I_i/\sigma_i\xi_i)]/\Sigma[(I_i/\sigma_i\xi_i)]$.

The present work addresses the determination of the molar fractions percentage on a multi-component system, calculated from the integrated Raman intensity of the bands characteristic of each molecular group. The experimental study has focused on the analyses of CH_4-CO_2-N_2 fluid inclusions in cassiterites from the Panasqueira mine (Portugal), previously studied by microthermometric analyses, and were performed using a microRaman Dilor spectrometers interfaced to an Olympus microscope with 100x objective lens and excitation wavelengths of 488.0 and 514.5 from Ar+ lasers (Valladolid University) and 632.8 nm from a HeNe laser (Porto University). Spectral decomposition of bands were performed using the program of Dilor LabSpec-Jobin Yvon-Spex, and Raman parameters obtained. Although calibration procedures were already described in the literature, an important controversy is presented to define whether one or both bands of the Fermi resonance (FR) of CO_2, which should contribute to the calculation of the integrated intensity of CO_2. Dubessy et al.[3] suggest that the sum of both intensities [$I(\nu_1)$+$I(2\nu_2)$] is constant, although the relative ratio of their areas [$I(\nu_1)$:$I(2\nu_2)$] varies with the density and internal pressure. Its pressure dependence and detection limits are reflected in the study of Rosso and Bodnar [9]. Raman intensity studies [10-11] and of the roto-vibrational spectrum [12] of the doublet of the FR of CO_2, show that, on the equilibrium, the population of states of both vibrational quantum levels [$CO_2(10^00)\leftrightarrow CO_2(02^00)\pm102$ cm^{-1}].

The present work describes the methodology used for the quantification of the different species in the fluid inclusions paying attention to the calibration of measurement spectrometers and to the Fermi resonance of CO_2 vibrations (ν_1-$2\nu_2$; 1285 -1388 cm^{-1}).

References: [1] van der Kerkhof A.M. (1988) *Bull. Mineral, 111,* 257-266. [2] van der Kerkhof A.M. (1990) *Geochimica et Cosmochimica Acta, 54,* 621-629. [3] Dubessy J. Poty B and Ramboz C. (1989) *Europeam J. Mineral, 1,* 517-534. [4] Thiery R. van der Kerkhof A.M. and Dubessy J. (1994) *Europeam J. Mineral, 6,* 753-771. [5] Bakker R.J. (2003) *Chemical Geology, 14101,* 1-21. [6] Burke E. A. J. (2001) *Lithos, 55,* 139-158. [7] Placzek G. (1934) *Handbuch der Radiologie. H. Marx Akad. Verlag. Leipzig, 6, 2,* 209-375. [8] Dhamelincourt P. Beny J.M. Dubessy J. and Poty B. (1979) *Bull. Soc. Fr. Min. Cris., 102,* 600-610. [9] Rosso K.M. and Bodnar R.J. (1995) *Geochimica et Cosmochimica Acta, 59,* 3961-3975. [10] Fernández-Bertran J. (1983) *Spectrochimica Acta, Part.A. 39-2,* 119-121. [11] Howard-Lock H.E. and Stoicheff B.P. (1971) *J. of Molecular Spectroscopy, 37,* 321-326. [12] Millot G. and Roche C. (1998) *J. Raman Spectroscopy, 29,* 313-320.

CROSS-SECTION ANALYSIS TO ESTABLISH THE PENETRATION LEVEL OF ATMPOSPHERIC POLLUTION IN MORTARS. N. Prieto-Taboada[1], O. Gómez-Laserna, I. Ibarrondo, I. Martinez-Arkarazo, M. A. Olazabal and J. M. Madariaga, University of the Basque Country (UPV/EHU), Department of Analytical Chemistry, Barrio Sarriena s/n, 48080, Bilbao, Spain. Tel.: +34 946018294. Email[1]: nagore_prieto@ehu.es.

Introduction: The impact of the acid gases in buildings has been widely studied because of their notable and visible consequences in building materials [1-4]. Buildings are known to be pollutant repositories [5], but not always the penetration level of the pollutant is studied although it is an important factor to evaluate the real conservation state of building materials. Surface analysis do not allow to detect internal decaying processes that are the precursors of crackings and even material loss when soluble salts are formed. Cross-section analyses, however, are suitable to determine the depth reached by pollutants and thus, to determine the conservation state of the materials in order to preserve the integrity of the building. With this purpose, Raman spectroscopy was used in this work to analyse rendering mortars of a building located in an industrialized neighbourhood of metropolitan Bilbao.

Experimental: Two types of rendering mortars were analysed. Although they were collected from the same facade, the first (MF) belonged to the first floor of the building and was completely covered by a black crust, while the second one (MG, from the stone pillar of the groundfloor) showed almost the original appearance. The samples were analysed by two different Raman spectrometers: (i) an InnoRam® (B&WTEK$_{INC}$) ultramobile spectrometer, equipped with 20x and 50x focusing lens and a 785 nm laser with a Peltier cooled CCD detector and (ii) an InVia Raman spectrometer (Renishaw), coupled to a Leica DMLM microscope provided with a 514 nm wavelength excitation source and CCD detector.

Results: The analysis of the internal part of the MF mortar revealed that it was a mixture including beach sand (bioclastic signatures), hematite and diverse silicates. The surface showed the typical composition of a black crust: carbon, gypsum ($CaSO_4 \cdot 2H_2O$) and occasionaly anhydrite ($CaSO_4$). However, coquimbite ($Fe_2SO_4 \cdot 9H_2O$) was also detected as a result of a degradation process described elsewhere [5]. Moreover, the analysis of the cross section revealed subefflorescences composed of calcite ($CaCO_3$) at 3mm from the surface.

The second type of mortar, which was not black crusted, was indeed composed mainly by quartz and traces of anatase (TiO_2), silicates, hematite and calcite in the surface (till 1mm depth). This layer suggested a high deterioration of the material by solubilisation of the cement and giving quartz as the final remaining compound. Besides, the analysis of the cross section of the mortar sample revealed the widespread presence of nitrocalcite ($Ca(NO_3)_2 \cdot 4H_2O$) at 4mm-11mm depth. The figure below shows the degradation products formed by the combined attact of SOx and NOx gases against calcite, giving gypsum and coquimbite, and nitrocalcite respectively.

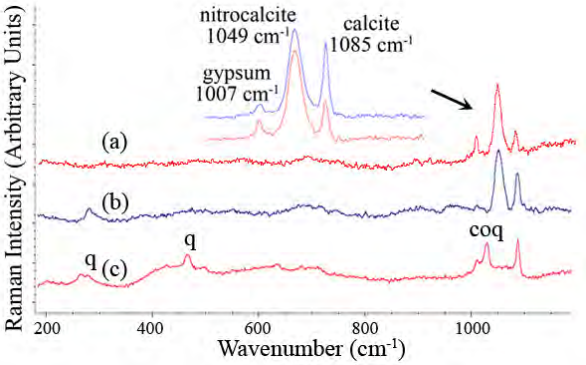

Figure: Raman spectra of MG mortar. (a) and (b) gypsum, nitrocalcite and calcite at different proportions at 11mm depth (c) quartz, q, belonging to the original composition together with gypsum, coquimbite, coq, and calcite at 2mm depth.

The nitrate band is quite broad to be related to a unique compound and thus the presence of other nitrates should not be ruled out. In the same way, the main Raman band of gypsum (1007cm^{-1}) appeared also sometimes with a shoulder, shifted to higher wavenumbers corresponding to anhydrite (1017cm^{-1}). Even more, coquimbite was also identified in this sample at 2mm depth joint to gypsum and calcite.

References: [1] Martínez-Arkarazo I., Angulo M., Bartolomé L. et al (2007) *Anal Chim Acta, 584,* 350-359. [2] Massey SW (1999) *Sci Total Environ, 227,* 109-121. [3] Sarmiento A., Maguregui M., Martínez-Arkarazo I. et al (2008) *J Raman Spectrosc, 39,* 1042-1049. [4] Sabbioni C., Zappia G., Ghedini N. et al (1998) *Atmos Environ, 32,* 215-223. [5] Prieto-Taboada N., Maguregui M., Martinez-Arkarazo I. et al (2010) *Analytical and Bioanalytical Chemistry,* 1-11.

Acknowledgements: This work was financially supported by the Spanish Government (MICINN) through IMDICOGU project (ref. BIA2008-06592). N. Prieto-Taboada acknowledges her grant from the Spanish MICINN. Technical support provided by the Raman-LASPEA laboratory of the SGIker (UPV/EHU, MICINN, GV/EJ, ERDF and ESF) is gratefully acknowledged.

BSE, CL AND RAMAN SPECTROSCOPY STUDY OF PHOSPATES AND MASKELENYTE IN THE H6 CANGAS DE ONIS REGOLITH BRECCIA. A. Rubio-Ordóñez[1] , V. Cárdenes[1], L. Rodríguez-Terente[2], L. Tormo[3], J. García-Guinea[3]. [1]Dpto de Geología, Univ. de Oviedo (arubio@geol.uniovi.es). [2]Museo de Geología, Univ. de Oviedo. [3]Museo Nacional de Ciencias Naturales, Madrid.

Historical settings of the Cangas de Onís meteorite: Fall of Cangas de Onís chondrite was held in the morning of December 6th of 1866. Several fragments of a flying body fell around the town of Cangas de Onís, in Asturias, NW Spain. The fall was seen by numerous locals, which collected over 22 kg of material. Most of the recovered meteorite was brought to the Oviedo University, where it was studied for the first time [1]. Fragments of the meteorite were sent to other reseach centers and museums [2, 3] for their study and classification. Throughout time, meteorite category changed according with the historical classifications in effect at the moment.

The H6 Cangas de Onis regolith breccia: According to previous works [4], it is formed by 60 ± 5% volume of H6 clasts with some H5 fragments, and 40 ± 5% of clastic matrix. Studied sample is composed by two main clasts and a clastic mesostasis with felspar-rich melts ($An_{13}Ab_{80}Or_6$) included, less recrystallized than the main clasts. All components are affected by an intense fracturation, filled by taenite-kamacite and troilite. Also, there are evidences of melting processes and reabsorption of the olivine, plagioclase and pyroxene by the Fe-Ni melts. These data agree with [4, 5], which assume at list two fracturation and gravitational accretion processes of the parental body. Differences in characteristics and cooling ratios are also agree with the primary structure (onion-shell) of the fragmented parental body [6-8].

Results: *Maskelenite*: A plagioclase representing one of the main components of the silicate melt formed during the shock metamorphism [9]. Punctual chemical analyses showed a slight range of variation for the Ab-An-Or proportions, with abundances of MgO up to 2,8 % for the more anortitic melts. CL specters from these silicate glasses showed small differences in the intensity of 430 and 460 peaks. Results obtained by EMP and CL suggest the occurrence of two melts of similar composition. These melts may be related with processes of secondary accretion.

Phosphates: Occurrence of phosphates in ordinary chondrites is quite common. In this chondrite, existence of anhedral crystals of calcium phosphates is documented in the clastic matrix. Chemical analyses are clearly different for these two minerals, with a relative higher content of REE+Y in the whitlockite than the chlorapatite. CL spectra showed this difference between the Cl-apatite and the whitlockite (Fig. 1). The whitlockite had several peaks of variable intensity related with the REE abundance. Raman spectroscopy also showed substantial differences for the obtained spectra. Both spectra showed a common shape, with their distinctive peaks for the PO_4 in the interval 460 – 520 cm^{-1}, maximum intensity peak at 1450 cm^{-1} and a secondary intensity peak at 1900 cm^{-1}. Whitlockite spectrum is quite complex, probably due to the presence of REE in its structure, and partially coincident with the spectral bands for the monazite [10] (e.g. RUFF ID:R060925). O-H peaks were not observed, pointing out to the anhydrous character of both phosphates.

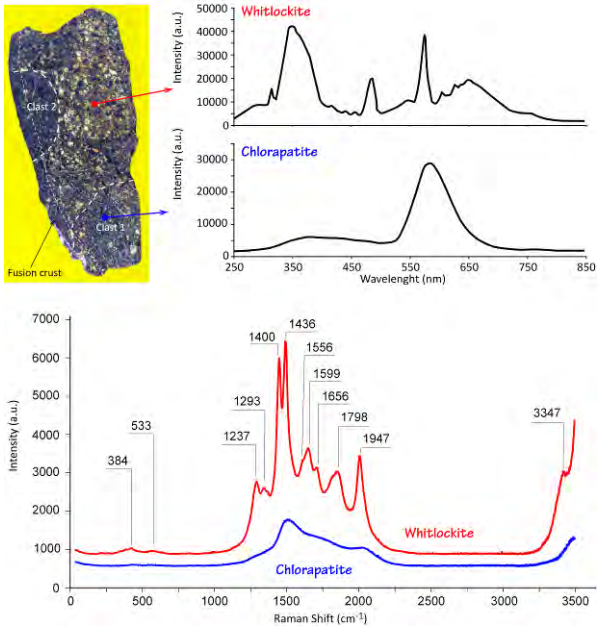

Figure 1: *CL and Raman spectra of withlockite (red) and clorapatite (blue).*

Acknowledgements: This work was financed by Ministerio de Ciencia y Tecnología, Proyecto Paleoandes II – Uniovi (CGL2009-13706-C03-02).

References:

[1] Luanco J. R. (1874). Anales de la Sociedad Española de Historia Natural, 3, 69-95. [2] Ordaz J., et al. (1999). Boletín de Ciencias de la Naturaleza, 45, 21-34. [3] Martín Escorza C., et al. (1999). Tierra y Tecnología, 19, 38-44. [4] Williams C. V., et al. (1985). Meteoritics, 20, 331-345. [5] Williams C. V., et al. (2000). Chemie der Erde, 60, 269-278. [6] Harrison Keith P. and Grimm Robert E. (2010). Geochimica et Cosmochimica Acta, 74, 5410-5423. [7] Trieloff Mario, et al. (2003). Nature, 422, 502-506. [8] Wood John A. (2003). Nature, 422, 479-481. [9] Schaal Rand B., et al. (1979). 2547-2571. [10] Podor R. (1995). European Journal of Mineralogy, 7, 1353-1360.

Uranyl Groups coupled to Evansite Granite Vein Infills in the Porto Undergrounds (Nw Portugal).

Sanchez-Moral, S[1], Fernandez-Cortes, A.[1], Cuezva, S.[2], Cañaveras, J.C. [2], Correcher, V.[3], Miller A.Z.[4] , Dionisio A.[4], Marques J.M.[4], Saiz-Jimenez C.[5], Afonso M.J.[6], Chamine H.I.[6], Furio, M[1]., Garcia-Guinea, J[1].

[1] Departamento de Geologia. Museo Nacional Ciencias Naturales. CSIC. 28006 Madrid. Spain. [2]Laboratorio de Petrología Aplicada, Unidad Asociada Universidad de Alicante-CSIC, 08040-Alicante, Spain [3]CIEMAT. Av. Complutense 22. Madrid 28040, Spain. [4] Centro de Petrologia e Geoquímica, Instituto Superior Técnico, Lisboa, Portugal [5]Instituto de Recursos Naturales y Agrobiología. CSIC Sevilla, Spain. [6]Laboratório de Cartografia e Geologia Aplicada (DEG), Instituto Superior de Engenharia do Porto; e Centro GeoBioTec|UA, Portugal. Correspondence author: ssmilk@mncn.csic.es

Introduction.- The Evansite mineralization associated to Porto granite vein infill's was firstly described by Rosas da Silva (1935) as layers up to 2 cm of amorphous $Al_2(PO_4)_{3\text{-}5}.nH_2O$ precipitated from recent hydrothermal fluids. This author analyzed the Porto Evansite screening a chemical composition of P_2O_5 % 12,20; Al_2O_3 % 40.62; H_2O % 40.03 which is roughly correct. In those years, Iglesias (1927) also found Evansite in several Spanish outcrops. Concurrently, it was described an amorphous hydrated phosphate from Campo Lameiro also in Galicia as pale greenish yellow fracture-fillings up to 1 cm thick in granite, so-called amorphous Bolivarite specimen with formula $Al_2(PO_4)_3.5H_2O$. Van-Wambeke (1971) studied a new uranium-Bolivarite from Kobokobo (Congo) and later, co-author Garcia-Guinea et al., (1995) demonstrated as the Bolivarite-type (Campo Lameiro, Spain) and the Evansite-type (Mt. Zeleznik, Slovakia) are the same mineral phase, and accordingly, the International Mineralogical Association (IMA) discarded the Bolivarite name. Sometime later, Van-Wambeke wrote us supporting the Bolivarite mineral denomination on the basis of that the Kobokobo Bolivarite has circa 0.3% uranium at the same time as we wait for further analytical opportunities to check the uranium content of all possible classic Evansite specimens from Porto, Zeleznik, Kobokobo, Galicia outcrops, etc. In July 2010 Evansite samples were taken in the underground galleries excavated in granite in Porto urban. The non-destructive current techniques (ESEM-CL) together with the strong CL-spectral visibility of the uranyl-water group placed in "white insulators" such as the hydrous $AlPO_4$ compounds offer an excellent system to analyze uranium to broad knowledge on the Evansite phase **(**Fig. 1**).**

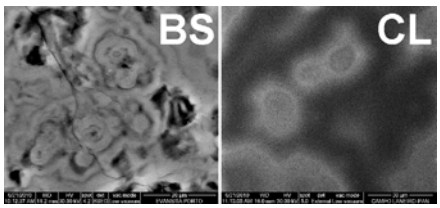

Fig.1: Porto Evansite: BS.- Backscattering ESEM image and CL.- Panchromatic CL image showing the physical positions of the uranyl groups.

A practical result of the analyses of uranium in the Porto evansites case me be useful to explain the high levels of radon gas (from 6000 to 7000 Bq/m^3) detected in summer 2010 in the Porto undergrounds coming from the Evansite infill veins throughout the well-know sequence U—Th—Rn. In addition, the radon gas ranges between 2 to 800 Bq/L in groundwater (Afonso et al., 2010).

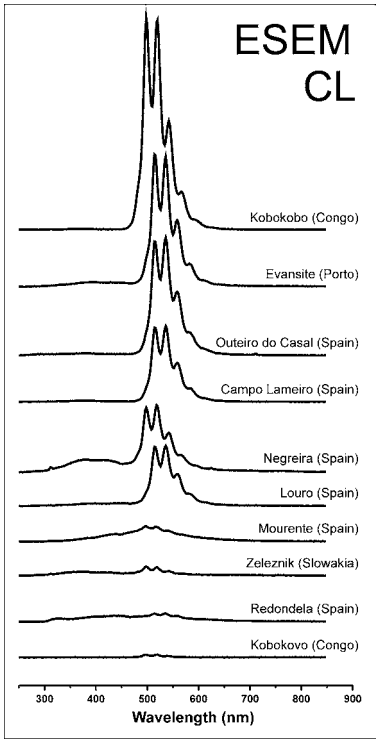

References.-

Rosas da Silva D.J. (1935) Depósitos de evansite nos granitos do Porto (Portugal). *An. Fac. Ciên. Pôrto* 19, 1-8.

Van Wambeke L. (1971) The uranium-bearing mineral Bolivarite: new data and a second occurrence. *Min. Mag*. 38, 418-423.

Garcia-Guinea et al (1995) A re-investigation of Bolivarite and Evansite. *Can. Miner*. 33, 59-65.

Afonso et al (2010) Using GIS mapping to assess groundwater studies in urban areas (Porto, NW Portugal): combined potential contamination sources and radon susceptibility. *Abstract 38th IAH Congress*, Krakow, 1, 80-82.

RAMAN STUDY OF SYNTHETIC $BaCO_3$ - $SrCO_3$ SOLID SOLUTIONS. N. Sánchez-Pastor[1], A. M. Gigler[2], and L. Fernández-Díaz[1]. [1]Departamento de Cristalografía y Mineralogía. Universidad Complutense de Madrid. 28040, Madrid (Spain), [2]CeNS and Department for Earth and Environmental Sciences, Ludwig-Maximilians-Universität. 80333, Munich (Germany).

The characteristics of the $Sr_xBa_{1-x}CO_3$ solid solution have been subject to controversy because of the important implications that the Sr/Ba ratio of naturally occurring members of this series have for the geochemistry of carbonates. The fact that intermediate compositions of the $Sr_xBa_{1-x}CO_3$ solid solution are scarse in nature, together with the remarkable difference between the ionic radii of 10.88% between Sr^{2+} (1.31 Å) and Ba^{2+} (1.47 Å), support the picture that there is a miscibility gap at low temperatures [1]. Nevertheless, experimental studies of its thermodynamic characteristics concluded that this solid solution is ideal and, consequently, complete [2].

Previous works showed that a variety of zoned $Ba_xSr_{1-x}SO_4$ crystals can be experimentally produced by counter-diffusion within a column of porous silica gel at room temperature [3]. Similar crystal growth gel experiments conducted using mixed SO_4^{2-}/CO_3^{2-} solutions as the anionic reactant, allowed us to observe not only the formation of zoned $Ba_xSr_{1-x}SO_4$ crystals but also their subsequent replacement by the $Ba_xSr_{1-x}CO_3$ solid solution. The experimental arrangement consist of a U-tube where a column of silica hydrogel occupies the horizontal branch, while the vertical branches A and B correspond to the reservoirs of the parent solutions. Here, A and B were filled with $BaCl_2$ (0.9 M) + $SrCl_2$ (0.1 M) and Na_2CO_3 (0.5 M) + Na_2SO_4 (0.3 M), respectively [4]. One month after starting counter-diffusion, crystals of the $Ba_xSr_{1-x}SO_4$ solid solution were formed within the gel. These crystals show progressive as well as sector zonings, with an increase in the Ba/Sr ratio from core to rim. Moreover, an oscillatory zoning is often superimposed. These characteristics have been observed by both electron microprobe and Raman analysis.

The $Ba_xSr_{1-x}SO_4$ crystals recovered from the gel after one year showed identical size and external morphology, as well as the same type of chemical zonation patterns. However, microprobe analyses indicated that these crystals contain no S, but are completely replaced by the $Ba_xSr_{1-x}CO_3$ solid solution: these crystals are now $Ba_xSr_{1-x}CO_3$ pseudomorphs after the original $Ba_xSr_{1-x}SO_4$ crystals (Fig. 1). In order to further characterize the replaced crystals, a Raman spectroscopy study has been carried out.

In spite of the importance of the witherite-strontianite solid solution, very few authors report spectroscopic measurements on the intermediate compositions [5, 6]. In the present work, synthetic samples obtained by co-precipitation were studied. The wide thermodynamic, kinetic, and vibrational spectroscopic database of the end members of the solid solution constitutes an excellent starting point for this investigation.

All spectra of the end members and the intermediate compositions of the solid solution showed the fundamental internal modes and the lattice modes. The $\nu1$, $\nu2$, $\nu3$ and $\nu4$ internal modes arise from the symmetric stretching, the out-of-plane bending, the asymmetric stretching and the in-plane bending mode of the carbonate ion group, respectively. The variation of wavenumbers of internal and lattice modes as a function of the chemical composition was studied. The results show that progressive substitution of strontium ions by barium ions produces bandshifts towards higher wavenumbers. This is due to the fact that a molecular vibration with a stronger bonding energy has a higher vibration frequency. As the Ba cation has a larger radius (1.6 Å) than that of the Sr cation (1.44 Å), the shorter bonding length and consequently the stronger bonding strength of Sr-O compared to that of Ba-O can explain bandshifts toward higher wavenumbers [7].

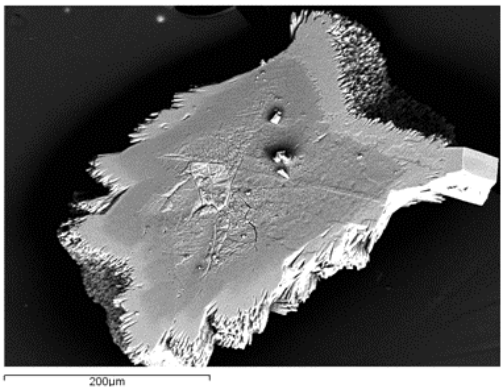

Figure 1. SEM image of $Ba_xSr_{1-x}CO_3$ pseudomorphs after C/S-replacement in the original $Ba_xSr_{1-x}SO_4$ crystals

References:

[1] Baldasari, A. and Speer, J.A. (1979) *Am. Min*. 64, 742-747. [2] Chang, L.L.Y. (1971) *Am. Min*. 56, 1660-1973. [3] Prieto, M. et al. (1997) *Geochimi. Cosmochimi. Acta*. 61, 3383-3397. [4] Henisch, H.K. and García-Ruíz, J.M. (1986) *J. Cryst. Growth*. 75, 195-202. [5] White, W.B. (1974) *Min. Soc. Monogr*. 4, 227-284. [6] Böttcher, M.E. et al. (1997) *Eur. J. Mineral*. 9, 519-528. [7] Chen, Y-H. et al. (2010) *Physica B*. 405, 4386-4388.

LUMINESCENCE DATING OF MORTARS FROM ANCIENT ARCHITECTURAL ELEMENTS. J. Sanjurjo-Sánchez[1] and Rebeca Blanco Rotea[2], [1]University Institute of Geology "Isidro Parga Pondal", University of A Coruña, Campus de Elviña, 15071 A Coruña, Spain, jsanjurjo@udc.es, [2]Laboratorio de Patrimonio (LaPa) - CSIC c/ San Roque,2. 15704, Santiago de Compostela, Spain, rebeca.blanco-rotea@iegps.csic.es).

Introduction: Lime mortars are one of the most used building materials from prehistoric times. They are composed of a lime binder and an aggregate, usually sand. Historic buildings have commonly been constructed and modified in several periods of their history, or their construction date is unknown. Some of the building materials used in the construction and reconstructions (bricks or ashlars) could been reused and thus could not provide information on the constructive stages. However, mortars cannot be reused. Therefore, they are interesting targets to date buildings. Attempts to date lime mortars by ^{14}C and geochemical dating have been unsuccessful or have shown limited succes [1], [2]. Optically Stimulated Luminescence (OSL) has also been scarcely tested to date lime mortars by OSL with promising results. Boetter-Jensen et *al*. [3] reported that manufacturing procedures for mortars erase the geological paleodose of quartz grains of the aggregate sand enough to be used as a dosimeter. Reports of luminescence dating of mortars have been carried out [4], opening a new way to date buildings constructed using not typically datable materials such as rock ashlars. Goedicke [5] established a bleaching model assuming the bleaching of some grains due to the manual transport and manufacturing of mortars and the bleaching of quartz grains in deeper layers due to the transparency of sand layers in gravel pits.

Mortar dating by OSL involves technical and architectural considerations regarding both the paleodose and the annual dose. Considering the beta annual dose, microdosimetry can be important if heterogeneous mortars are dated. It must be considered that, in some cases, buildings were reconstructed or modified in past times, causing variation of the gamma dose.

Aim of the study: The Luminescence Laboratory of the University Institute of Geology (University A Coruña, Spain) has reconstructed the history of ancient buildings and historic walls of the NW of Spain by dating lime mortars by OSL. Mortars and bricks from the cupola and a wall of a Romanesque Basilica of San Martiño de Foz and restoration lime mortars from ancient city walls of Santiago de Compostela (Galicia, NW Spain) have been taken and dated by OSL. The mortars of the former building are lime mortars made of lime and aggregate sand. The mortars of the latter are made of lime, and sand-gravel aggregate.

Results: The paleodose calculation showed problems related to the quartz content in the mortars made with sand-gravel aggregate. Also, a sample aggregate of the Basilica of San Martiño de Foz had quartz-poor sand and a feldspar contaminated quartz aliquots have been measured by a Post-IR OSL procedure [6]. Results showed ages in agreement with the archaeological and architectural hypoteses. In the case of the Romanesque Basilica of San Martiño de Foz the mortars allowed to date the cupola in the 10-11th Centuries, while the bricks dated are older, and they have been probably reused. The mortars of the ancient city walls of Santiago de Compostela correspond to the 17-18th centuries, and they match the archaeological hypothesis, as they are restoration mortars. Thus, carefully sampling, handling and measurement of OSL provide reliable ages for lime mortars, even when the aggregate is not quartz-rich sand.

References:

[1] Heinemeier J, Jungner H, Lindroos A, Ringbom A, von Konow T, Rud N (1997) Nuclear Instruments and Methods in Physics Research B 123:487-495

[2] Vendrell-Saz M, Alarcon S, Molera J, García-Vallés M (1996) Archaeometry 38:143-149

[3] Zacharias N, Mauz B, Michael CT (2002) Radiation Protection Dosimetry 101:379-382

[4] Boetter-Jensen L, Solongo S, Murray AS, Banerjee D, Jungner H (2000) Radiat Meas 32:841–845

[5] Goedicke C (2003) Radiation Measurements 37:409-415.

[6] Roberts HM, Wintle A (2001) Quaternary Science Reviews 20: 859-863

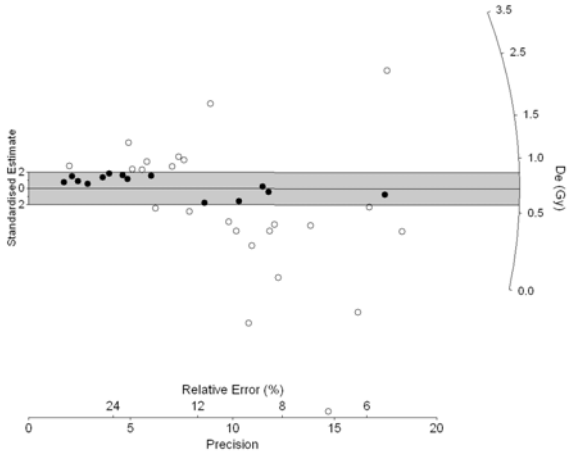

Figure 1. Radial plot of a lime mortar sample from San Martinho de Foz.

LUMINESCENCE DATING OF PSEUDOKARST SPELEOTHEMS: A FIRST APPROACH. J . Sanjurjo-Sánchez[1] and J. R. Vidal Romaní[2], [1]University Institute of Geology "Isidro Parga Pondal", University of A Coruña, Campus de Elviña, 15071 A Coruña, Spain, jsanjurjo@udc.es, [2]University Institute of Geology "Isidro Parga Pondal", University of A Coruña, Campus de Elviña, 15071 A Coruña, Spain, xemoncho@udc.es.

Introduction: Speleothems are secondary mineral deposits formed in limestone or dolostone solutional caves. In granitic massifs, water trickling through the rock discontinuities causes a slow chemical and physical weathering of the rock related to biological activity [1]. The weathered materials are first eroded and later deposited in either fissures or the water output of fissures. The formed speleothems are comparable to their congeners in karstic (limestone) systems although always smaller in size and volume. Geochemical studies of such deposits have reported three different types of speleothems regarding the mineral composition: pigotite, evansite-bolivarite, opal-A.

Pigotite speleothems are composed of alumina and organic acids. They grow by rhythmic accretion of concentric layers as it occurs in calcite speleothems. The different layers alternatively show cream light (Al prevails) and reddish dark colours (Fe prevails) that seem to correspond to seasonal stages (winter-summer) similar to the varves of lake deposits. They have been studied and dated by ^{14}C, as they contain abundant organic mater [2]. The only absolute ages know for this kind of speleothems in NW Spain indicate their formation during the late Holocene.

Opal-A speleothems are the most common speleothems in acid rocks and they are episodically formed by accretion of new layers of precipitated opal-A. They show two main morphological types: cylindrical (stalactites, anti-stalactites and stalagmites) and in crusts or sheets (flowstone and microgours). Opal-A speleothems are a suitable microenvironment for the settlement and development of microorganisms as bacteria, fungi, algae, diatoms, polychetes, mites, etc., and different spores and pollen grains are frequently found trapped in the opal layers or on the speleothem surface [2], [3]. Thus, they can be interesting paleoclimatic records if they were dated. However, organic carbon is not abundant or absent, and other methods than ^{14}C must be tested.

Evansite-bolivarite are yellowish to brown-reddish speleothems frequently found in well diaclased rocky massifs with development of sheet structure [2]. They show a layered structure (flowstone) and they are some centimetres thick, covering surfaces of various square metres. Evansite is amorphous and massive and forms botryoidal or reniform coatings. Chemical analyses indicated that there are composed of hydrous aluminium phosphates. Some authors [4], [5] believe that under the name of evansite-bolivarite there may be represented transition terms between alumina silicates and alumina phosphates where the phosphorous that appears in them increases progressively as Si diminishes till substituting it completely. They also contain some detritic quartz and feldspar grains transported from the weathered rock.

Aim of the work: In this work, the luminescence characteristics of opal-A and evansite-bolivarite speleothems, and of other minerals contained in their layered structures, are investigated to apply a dating procedure for this kind of deposits. As they are very frequent in NW Spain (but also in other parts of the World such as Venezuela, Australia, Argentina or Slovakia), an opal-A flowstone sample from Monte Louro and an evansite-bolivarite flowtone from Monte Costa Grande (Muros, A Coruña, NW Spain) have been taken and studied to test for luminescence dating. As scarce detritic quartz content have been found, polymineral aliquots have been studied and dated.

Results: First tests, showed luminescence characteristics typical of high feldspar content and both thermoluminescence (TL) and post-IR OSL (Infra-Red Optically Stimulated Luminescence) [6] have been used to obtain a reliable ages. Results indicated an Holocene age for the opal-A speleothem sample. The Evansite-Bolivarite sample correspond to the Upper Pleistocene. Thus, they can be used as paleoclimatic records in areas of acid rocks.

References:

[1] Vidal Romaní J. R., Bourne J. A., Twidale C. R., Campbell E. M. (2003) - Siliceous cylindrical speleothems in granitoids in warm semiarid and humid climates. Zeitschrift für Geomorphologie, 47(4): 417-437.

[2] Vidal Romaní J.R., Sanjurjo-Sánchez J., Vaqueiro Rodríguez M., Fernández MosqueraD. (2010) Speleothem development and biological activity in granite cavities. Géomorphologie (in press).

[3] Twidale C. R., Vidal Romaní J. R. (2005) Landforms and geology of granite terrains. Balkema, London, 351 pp.

[4] Martín Cardoso G., Parga Pondal I. (1935) - Hallazgo de la eosforita en el Son (Coruña). Las Ciencias, t.II, 849-850.

[5] García-Guinea J., Millán Chagoyen A., Nickel, E.H. (1995) - A re-investigation of bolivarite and evansite. The Canadian Mineralogist, 33, 59-65.

[6] Roberts HM, Wintle A (2001) Quaternary Science Reviews 2: 859-863.

Raman spectra on Fluid Inclusions in Glauberite from Miocene saline lakes of the Madrid Basin: evidence for microbial activity.

M.E. Sanz-Montero[1], L. González-Acebrón[2]; J.P. Rodríguez-Aranda[1] & C.P. Marshall[3]

1 Dpto. Petrología y Geoquímica. Fac. CC. Geológicas (UCM). IGE-CSIC. C/ José Antonio Novais, 2. 28040 Madrid, Spain.
2 Dpto. Estratigrafía. Fac. CC. Geológicas (UCM). IGE-CSIC. C/ José Antonio Novais, 2. 28040 Madrid, Spain.
3 Department of Geology, University of Kansas, Lawrence, KS 66045-7613, USA

Glauberite ($Na_2Ca(SO_4)_2$) layers occur interbedded with magnesitic marlstone and evaporites (mostly halite and anhydrite) in the Madrid Basin, Central Spain. These rocks were deposited in a saline lake-mudflat sedimentary system during the Lower Miocene. The Ca-Na sulfate generally occurs as intrasedimentary crystals, although contorted or nodular beds are also observed. Glauberite consists of euhedral to subhedral hemipyramidal crystals which in some beds are tightly cemented by cubic halite precipitates. Glauberite crystals show both fluid and fluorescent solid inclusions of the host magnesitic marls. Magnesite precipitation has been interpreted to be mediated by microbial activity. Although glauberite is a common sulfate in inland evaporitic basins, its origin continues to be a matter of debate. Primary fluid inclusions in glauberite are analysed in this study in order to get more information in the formation of the mineral and to elucidate the possible role of microorganisms in the precipitation processes. Primary fluid inclusions (related to growth zones) have been recognized in this glauberite in oil-prepared thin sections from a core. Fluid inclusion assemblages (2 and 40 μm) are formed by very variable liquid: vapour ratio fluid inclusions (10/90 to 60/40), including all-liquid and all-gas fluid inclusions, which is characteristic of a low-temperature heterogeneous entrapment. An attempt to measure the final melting of ice temperature (in order to obtain the salinity conditions of formation) has been done in a Linkam stage, but no results have been obtained because the sample degrades upon freezing. To our knowledge, no salinity data from glauberite inclusions has been collected, probably due to the delicate nature of this mineral. Thus, Raman microprobe provided an adequate alternative to obtain the main components present in the fluid inclusion assemblages. Raman analysis of the samples was performed on a XRD confocal Raman Thermo Fischer Microscope in the MNCN, Madrid. Excitation was provided by the 532 nm line of a diode laser. Zones of primary fluid inclusions have been studied preferentially; nevertheless, spectral signatures of the glauberite host mineral have been examined as well. Glauberite presents its characteristic spectral features with mean bands at 1150, 998, 648, 470, 449 cm^{-1} and the presence of broad features attributed to hydrocarbons, between 1615 and 1440 cm^{-1}. These features assigned to hydrocarbons became more important in the fluid inclusions, in which the glauberite signature is weaker. In fluid inclusions, complex Raman spectra in the C-Hx stretching modes (2700-3000cm^{-1}) are observed which can be attributed to diversity of CH, CH_2 and CH_3 groups. A 1440 cm^{-1} band is assigned to bending CH_2 modes. Bands from 3000-3100 cm^{-1} are aromatic C-H stretching modes. A mode at 1610 cm^{-1} is an aromatic C=C stretching mode. The spectral signatures of the fluid inclusions reveal also the presence of N_2 (2320 cm^{-1}), O_2 (1550 cm^{-1}), CO_2 (1370 and 1290cm^{-1}), SO_2 (1150 cm^{-1}) and COS (842 cm^{-1}). The inclusion of liquid hydrocarbons and organic-rich compounds in fluids would be indicative of microbial communities in the matrix embedding the sulfate crystals. Therefore, the microorganisms and the organic compounds may have favoured the precipitation of glauberite.

Additional work is being undertaken to determine the type of organic matter included in the minerals by resonance Raman spectroscopy.

Acknowledgment: Financial support of Projects CGL2008-01648 and UCM-BSCH GR58/08 (grupo 910404) is acknowledged. We thank Marta Furió for her technical support.

IRON OXIDES ON AG(111) - REVERSIBLE SWITCHING BETWEEN HEMATITE AND MAGNETITE.

C. Schlueter[1,2], A. M. Gigler[2,3], and W. Moritz[2], [1]ESRF European Synchotron Radiation Facility. 38043 Grenoble (France), [2]Department of Earth and Environmental Sciences. Ludwig-Maximilians-Universität. 80333 Munich (Germany), [3]Center for Nanoscience (CeNS). Ludwig-Maximilians-Universität. 80799 Munich(Germany).

Iron oxides are of growing interest in environmental remediation [1], catalysis [2], magnetic data storage technologies [3, 4, 5] and most recently, spintronics applications [6]. So far, most thin films of iron oxides were grown on oxidic substrates like α-Al_2O_3 (corundum) [7, 8] or MgO (manganese oxide) [9]. However, iron oxide films on insulating substrates are subject to charging effects in electron spectroscopies. As metal substrates only Pt(111) has been used successfully for both hematite and magnetite [10]. The low lattice mismatch to the iron oxides makes Ag(111) a promising candidate for epitaxial growth and an alternative to Pt(111). In the literature, only one report of magnetite thin films on Ag(111) was found [11]. Our results show that depending on the oxygen pressure and film thickness all the three phases of iron oxides, wuestite (FeO), magnetite (Fe_3O_4) and hematite (Fe_2O_3) can be obtained.

Our iron oxide films were grown on Ag(111) surfaces by multiple cycles of iron deposition (EFM3 Omicron) between room temperature and 150° C followed by oxidation in 2×10^{-6} mbar O_2 at temperatures up to 400° C. Hence, the films were characterized in-situ with Low Energy Electron Diffraction (LEED), X-ray diffraction (XRD), and ex-situ by Confocal Raman microscopy. Thus, the three different phases wuestite, magnetite and hematite can be distinguished from their diffraction patterns as well as their characteristic Raman spectra. The confocal Raman microscope was also used in order to spatially characterize our films.

Wuestite films were formed for films below 10 Å thickness. This result was confirmed by both Raman spectroscopy and XRD. Films of more than 10 Å showed the magnetite structure. The symmetry of LEED and XRD results indicate the formation of an epitaxial magnetite film in two domains.

Oxidation of magnetite films by a flash to 450° C in 9×10^{-6} mbar molecular oxygen leads to the formation of hematite. LEED images indicate a complete transformation to hematite whereas XRD measurements show small quantities of a remaining magnetite structure in the films. Islands of magnetite were found within a matrix of hematite by spatially resolved Raman spectroscopy. Figure 1a shows an intensity map of the second order scattering peak at ~1300 cm^{-1} only present for hematite. The dark regions enclosed in this homogeneous hematite film could be clearly identified as magnetite (Figure 1b), while the remaining parts correspond to hematite (Figure 1c).

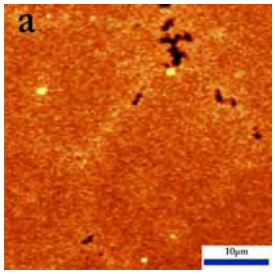

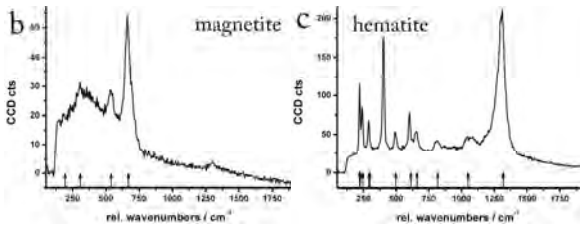

Figure 1: (a) Intensity map of the most prominent hematite feature at ~1300 cm^{-1}. (b) Spectra of the darker region reveal magnetite. (c) The residual area of the film shows the characteristic hematite spectrum.

Moreover, the possibility of reversible switching between hematite and magnetite was observed. It has been shown that the hematite can be reduced back to magnetite by annealing at 350° C in ultra high vacuum (UHV) conditions. SXRD results and the LEED patterns document the maintained epitaxy during these transformations.

The interplay of diffraction techniques and confocal Raman spectroscopy facilitates the surface phase analysis providing both structural analysis and spatial surface characterization.

References: [1] Cornell, R.M. & Schwertmann, U., (2003) *VCH Weinheim*, New York. [2] Zscherpel, D. et al. (1998) *J. Chem. Phys.*, 108, 9506-9515. [3] Morrish, A.H. (1995) *World Scientific*, Singapore.[4] Prinz, G.A. (1995) *Phys. Today*,48, 58-63. [5] Auciello, O. et al. (1998) *Phys. Today*, 51, 22-27. [6] van der Zaag, P.J. et al. (2000) *J. Magn. Magn. Mater.* 211, 301-308. [7] Yi, S.I. et al. (1999) *Surf. Sci.*, 443, 212-220. [8] Chambers, S.A. & Joyce, S.A. (1999) *Surf. Sci.*, 420, 111-122. [9] Kim, Y.J. et al. (1997) *Surf. Sci.*, 371, 358-370. [10] Ketteler, G. et al. (2001) *Surf. Rev. Lett.*, 8, 661-683. [11] Waddill, G.D. & Ozturk, O. (2005) *Surf. Sci.* 575, 35-50.

RAMAN AND LUMINESCENCE SPECTROSCOPY OF METEORITIC NANODIAMONDS.
A. A. Shiryaev[1], A. V. Fisenko[2], I. I. Vlasov[3], L. F. Semjonova[2], [1]Institute of Physical Chemistry and Electrochemistry RAS, Moscow, Russia (shiryaev@phyche.ac.ru) for first author, [2]Vernadsky Institute of Geochemistry and Analytical Chemistry RAS, Moscow, Russia, [3]General Physics Institute, Moscow, Russia.

Introduction: Meteoritic nanodiamonds (MND) are the most abundant protoplanetary Solar System relic phases in comparison with other compounds. We discuss results of extensive spectroscopic comparative investigation of meteoritic nanodiamonds from several chondrites with synthetic nanodiamonds produced by different methods: CVD and detonation (DND). The samples were analysed using luminescence and Raman spectroscopies, EELS and NEXAFS, X-ray diffraction and scattering [1].

Results

Raman spectroscopy: Use of the UV laser allows detection of even small amounts of sp^3-carbon [2]. The analysed samples were embedded in copper to minimize laser heating. The UV Raman spectra of samples of Efremovka nanodiamonds are shown on Fig. 1 (left). Broad, asymmetric downshifted diamond peak is clearly observed along with broad bands due to graphite-like carbon and C=O bonds. The presence of the C=O bonds is due to oxygen, most likely chemisorbed on the nanodiamond grains during chemical oxidation. Such spectra are typical for DND.

At least two different phenomena which may act simultaneously could be responsible for the observed downshift of the Raman peak to 1326-1327 cm^{-1}: 1) phonon confinement [3], and 2) presence of hexagonal diamond polytypes (hex-Dia).

The phonon confinement model gives the average size of the Efremovka nanodiamond grains of 4-6 nm. These values are higher than the median size of the nanodiamonds as determined from TEM and XRD (2.6-3 nm). The discrepancy might be explained by uncertainties due to selected phonon dispersion curves, but it is also possible that the Raman and X-ray scattering are dominated by the larger grains.

Though the fraction of purely hex-Dia particles is not very high, the MND grains often contain stacking faults and other similar imperfections [4]. From crystallographic point of view many types of stacking faults in cubic diamond lattice may be regarded as hexagonal polytypes. The Raman peaks of 2H and 6H diamond polytypes are observed between 1319 and 1327 cm^{-1} [5]. At least partially the observed downshift may be due to such extended defects.

Photoluminescence: The photoluminescence spectra of the MND samples studied at room- and liquid helium temperatures are broadly similar indicating inhomogeneous, i.e. strain-related, line broadening as is expected for nanoparticles. The spectra are dominated by a broad band with a maximum around 560 nm (red emission) with shoulders around 530 and 610 nm and are similar to recorded for DND (fig. 1, right). The broad band represents overlapping signals from non-diamond carbon and from defects on the surfaces of diamond grains.

The spectra were recorded in a broad wavelength range which allowed observation of a remarkable feature at 737 nm (1.681 eV) with a weak shoulder at 750 nm. This feature is an unambiguous manifestation of well-known "silicon" defect, most probably consisting of silicon ion in the divacancy (commonly called a silicon-vacancy complex or Si-V [6]). The observed band is broad and the fine structure is not observed due to size/stress effects. We emphasize that the observed signature of the "silicon" defect should not be confused with SiC or Si in amorphous carbon.

A defect present in all types of irradiated diamonds – the GR1, is absent in spectra of the studied samples.

Conclusions: We show that the phase compositions of the meteoritic and the synthetic detonation nanodiamonds are similar, suggesting that both types of nanodiamonds consist of a diamond core surrounded by (semi)amorphous and graphite-like carbon.

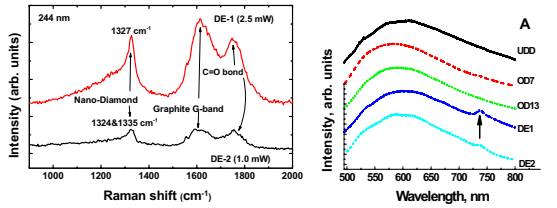

Fig. 1. Left – Raman spectra of meteoritic nanodiamonds; Right – photoluminescence. Arrow shows the Si-V defect.

For the first time the silicon-vacancy complex has been observed in meteoritic nanodiamond by photoluminescence. This is the first observation of this defect in dispersed nanodiamonds of any origin.

References: [1] Shiryaev et al. (2011) http://arxiv.org/abs/1102.0880; [2] Ferrari A.C. and Robertson J. (2004) *Phil.Trans.R.Soc. Lond* A362, 2477, [3] Lipp M. et al., (1997) *Phys.Rev.* B56, 5978, [4] Daulton T.L. et al., (1996) *GCA*, 60, 4853, [5] Knight D. and White W. (1989) *J. Mater. Res.* 4, 385, [6] Zaitsev A., (2001) Optical properties of diamond, Springer.

DIFFERENTIATION OF NATURAL AND IRRADIATED BLUE TOPAZ BY CATHODOLUMINESCENCE(CL) PROPERTIES

Ying Song[1] and Ying Qi[2]

[1]Earth Science Department, China University of Petroleum (East China), No.66 Changjiang Road, Huangdao District, Qingdao, Shandong Province, China, 266555, Email: yingsong@upc.edu.cn, [2]School of Economics & Management, China University of Petroleum (East China), No.66 Changjiang Road, Huangdao District, Qingdao, Shandong Province, China, 266555, Email: bonnie_qy@hotmail.com

Introduction: Blue topaz is presently one of the gem industry's most commercialized gemstones. Being quite rare in nature, most commercially available blue topazes have been generated during the past thirty years by laboratory treatment with gamma radiation, neutrons or electrons, or with combinations of them. The origin of the blue color in topaz is not well understood, and a method to nondestructively distinguish natural blue topaz from its irradiated counterpart has been widely sought. This investigation showed that natural blue and artificially irradiated blue topaz could be distinguished by their different cathodoluminescence responses.

Digital Formats:

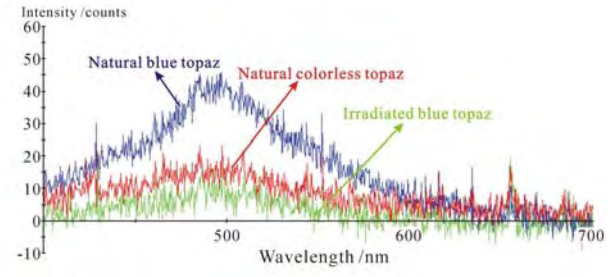

Fig1. CL spectra characteristics of natural blue, natural

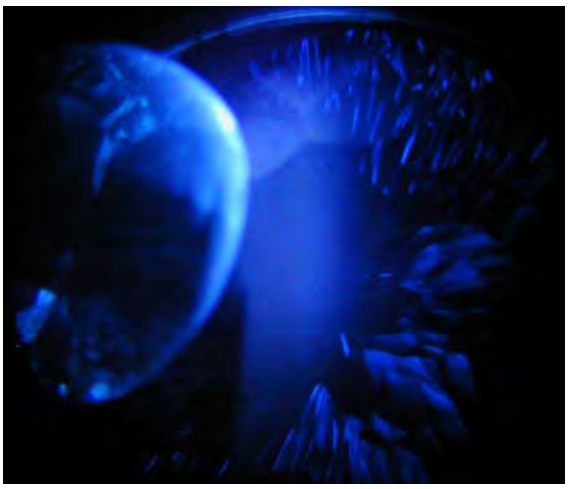

colourless and irradiated topaz

Fig2.CL brightness comparison of natural (L)and irradiated blue topaz(R)

References:

[1] Yukihara E.G., Piters T.M., Okuno E. (1999). On the thermoluminescent properties and behaviour of Brazilian topaz. *Nuclear Technology Publishing,* 84: 265-268.

[2] Gatta G. D., Nestola F., Bromiley G. D., Loose A.(2006). New insight into crystal chemistry of topaz: A multi-methodological study. *American Mineralogist,* 91: 1839-1846.

[3] Leala A.S., Krambrockb K, Ribeiro L.G.M., Menezes A.B.C, Vermaercke P, Sneyers L. (2007). Study of neutron irradiation-induced colors in Brazilian topaz. *Nuclear Instruments and Methods in Physics Research*, 58:423–426.

Effects of Thermal Annealing on The Thermoluminescence Properties of Ion-Implanted $SrTiO_3$ B.Tastekin, M.Turemis, M.I.Katı, I.C.Keskin, R.Kibar, A.Çetin and N.Can, Celal Bayar University, Faculty of Arts and Sciences, Physics Department, 45140 Manisa-Turkey, umbra@ymail.com

The wavelength, intensity and temperature dependence of luminescence signals are widely used to provide highly sensitive monitors of imperfections in insulating crystals since variations in local lattice site configurations are reflected by variations of the luminescence. The thermoluminescence is excited by X-ray irradiation of an entire sample. Room temperature ion-implantation into the surface layer changes the TL signals both in terms of their relative intensities and peak temperatures, as well as modifying the emission spectra. Such an intense perturbation of the bulk signals resulting from surface ion beam implantation is extremely unusual. The ion-implantation damage in the surface is thought to act as a trap. There are consequent changes in the thermoluminescence in terms of defect stability and glow peak temperature [1].

In the present work, we present new data from investigations of the TL glow peaks of pure and Cu implanted $SrTiO_3$ (STO). Single crystal of STO has been implanted at room temperature with 200 keV Cu ions 1.10^{16} ions/cm^2 . Thermoluminescence spectra were taken following furnace annealing at different temperatures for 1 h in air. After implantation and after post-irradiation annealing there are changes in the TL glow curves. Figure 1 shows the TL glow curves of pure STO after exposure to X-ray in the dose range from 300 to 1800 Gy. As seen from figure, the glow curve pattern shows TL peaks at 88 ^{o}C, 141 ^{o}C, 185 ^{o}C and 258 ^{o}C, after annealed at 400 ^{o}C while it is not observed any TL peaks for unannealed sample.

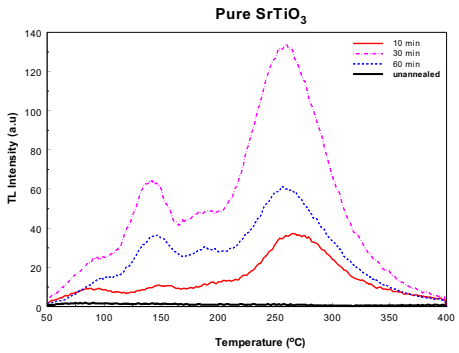

Figure 1. TL response of pure $SrTiO_3$ as a function of X-ray irradiation time after annealed at 400 ^{o}C.

Figure 2 shows TL response of Cu implanted STO after annealed for different temperatures.

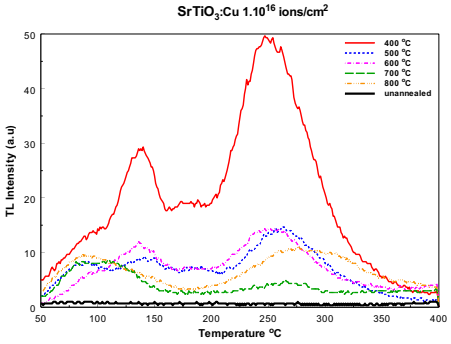

Figure 2. TL glow curves of Cu implanted STO as a function of annealing temperatures. The samples exposed to X-ray for 30 min.

Figure 3 shows the experimental optical absorption spectra of the STO samples implanted with Cu^{+} ions to different ion doses. For the sample implanted with copper to a lower dose, the spectrum is similar to that of unimplanted STO, except for a slight increased absorption in the short-wavelength region. Note also that at high implant doses, and strain induced by nanoparticles, implanted layer may no longer be fully crystalline which will increase the band edge absorption. We may conclude that for the lower implant concentration there is no clear indication of the presence of Cu nanoparticles, but the Cu surface plasmon resonance is seen for the higher dose giving a wide absorption band with a maximum near 600 nm, as is typical for copper.

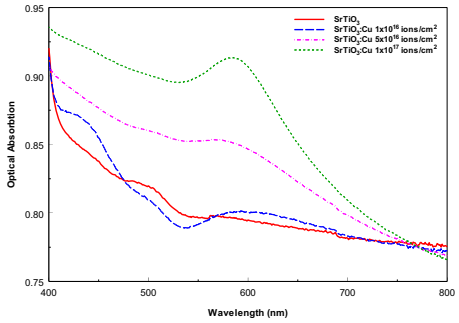

Figure 3. The experimental optical absorption spectra of the $SrTiO_3$ samples implanted with Cu ions to different ion doses.

References: [1] B.Yang et.al. (2004) Nuclear Instruments and Methods in Physics Research Section B: Beam Interactions with Materials and Atoms 226 549-555. [2] R. Kibar et.al. (2010) Physica B 405 888–890.

LUMINESCENCE AND RAMAN SCATTERING OF STABILIZED ZIRCONIA CRYSTALS. D. I. Torres[1] and J. Llopis[2], [1]Department of Natural Science, Inter American University of Puerto Rico, Bayamon Campus, Puerto Rico 00957, [2]Departamento de Física de Materiales, F. CC Físicas, Universidad Complutense, Madrid 28040, Spain.

Introduction: Zirconium dioxide (ZrO_2) has monoclinic form at room temperature, but can be stabilized in cubic phase by partial substitution of Zr^{4+} with metal cations like Ca^{2+} or Y^{3+}[1]. This cation substitution causes the creation of oxygen vacancies in order to preserve electrical neutrality. This base defect structure of stabilized zirconia (SZ) has a significant influence on their optical properties, and can be modified by exposing the samples to reducing conditions. As a result of thermal reduction, which generate new oxygen vacancies, the SZ become coloured modifying their main characteristic [2],[3]. The changes in coloration can be related to a broad absorption band centred at 365 nm [4],[5], associated with defects formed with oxygen vacancies. However, the detailed structure of such defects is yet uncertain. Temperature dependent Photoluminescence (PL) and Raman spectra have been used to study the defect structure of untreated and thermochemically reduced Y-stabilized cubic zirconia (YSZ). The method of moments has been applied to the emission (EM) bands in order to obtain more information of the defects generated in the stabilization process, and in the reduction process.

Experiment setup: PL spectra were determined with a Perkin-Elmer LS-5 fluorescence spectrometer. Raman spectra were excited using 514.53 nm radiation line from a Coherent Innova99 Ar-ion laser. Spectra were measured in the backscattering geometry using a Raman microprobe (Olympus) attached to a triple spectrometer configured in the subtracting mode (Jobin Yvon T64000) and a multichannel detector charged coupled device (CCD). For the temperature dependence studies, we measured the EM in the range of 110-300 K, and the Raman spectra from 70-580 K. The YSZ single crystals used, purchased from Ceres Corp., contained 9.5 mol% Y_2O_3 with (100) orientation. For the thermochemical reduction, the samples were placed in a graphite box inside a furnace with a flowing inert atmosphere and then quenched in liquid nitrogen.

Results: *PL spectra.* Over the whole temperature range the EM spectrum of the untreated crystals can be decomposed into three broad bands, a red component peaked at 2,0 eV, a yellow-orange component peaked at 2,2 eV and a blue component peaked at 2,6 eV. The behavior of these bands with temperature and the parameters obtained from the moments theory (Huang-Rhys parameter S and phonon mean energy $\hbar\omega$) confirms that they can be associated with three different defects, F_{AA}-center for the red component, F_A-center for the yellow-orange component, and F-center for the blue component [6],[7]. As a result of thermochemical reduction, the crystals became colored with tonalities ranging from pale-yellow to dark-brown, and there appeared a broad absorption band centered at ~365 nm similar to that previously reported [4],[5]. The rate of the luminescence decay with thermoreduction of each EM spectrum component was different, consistent with previous assumption of three different complexes. Results from moments theory applied to the EM bands in colored samples points out to T-centers [8],[9] as the main defect generated in the reduction process.

Raman spectra. The Raman spectra of the as-received crystals showed the characteristic broad T_{2g} band centered at ~600 cm^{-1}. The Raman spectrum of the most reduced sample exhibited a decrease in intensity at frequencies below 300 cm^{-1}. This region mostly contains contributions from the acoustic modes, which arise from the in-phase motion between the oxygen and the cation sublattice, with the cations as the major contributors of the vibration [10]. This observation is indicative of improved order since the acoustic modes are activated by disorder. This improvement of the lattice arrangement can be understood as indicating that the concentration of vacancies is not randomly distributed, but that they are arranged in periodic sequences. This is in agreement with our PL measurements and moments theory which associated a specific mean phonon frequency to each band component. The decrease in intensity at 300 cm^{-1} can be associated with the decay of PL intensity of the blue band and the formation of T-centers.

References: [1] J. G. Cai, C. Raptis, Y. S. Raptis, E. Anastassakis, Phys. Rev. B 51 (1995) 201. [2] R. Ben-Michael, D. S. Tannhauser, J. Genossar, Phys. Rev. B 43 (1991) 7395. [3] V. R. PaiVerneker, A. N. Petelin, F. J. Crowne, D. C. Nagle, Phys. Rev. B 50 (1989) 8555. [4] D. I. Torres, S. E. Paje, J. Llopis, G. Morell, R. S. Katiyar, J. Lumines. 72-74 (1997) 724. [5] G. Morell, R. S. Katiyar, D. Torres, S. E. Paje, J. Llopis, J. Appl. Phys. 81 (6) (1997) 2830. [6] P. Li, I.-W. Chen, J. E. Pender-Hann, Phys. Rev. B 48 (1993) 10063. [7] N. G. Petrick, D. P. Taylor, T. M. Orlando, J. Appl. Phys. 85 (1999) 6770. [8] C. B. Azzoni, A. Paleari, Phys. Rev B 40 (1989) 9333. [9] V. M. Orera, R. I. Merino, Y. Chen, R. Cases, P. J. Alonso, Phys. Rev B 42 (1990) 9782. [10] D.W. Liu, C. H. Perry, A. A. Feinberg, R. Currat, Phys. Rev. B 36 (1987) 9212.

The Influence of Annealing on Thermoluminescence Behaviour in ZnO, M.Turemis, B.Tastekin, M.I.Katı, I.C.Keskin, R.Kibar, A.Çetin and N.Can, Celal Bayar University, Faculty of Arts and Sciences, Physics Department, 45140 Manisa-Turkey, muratturemis@hotmail.com

Zinc oxide is a very perspective material for applications in optoelectronics. The wide direct gap of 3.37 eV and the large exciton binding energy of 60 meV suggest the use of ZnO in short-wavelength emitting devices.

In this study, effect of annealing on thermoluminescence characteristics of annealed and unannealed pure ZnO, implanted ZnO samples have been studied that were x-ray irradiated at different dose levels. Surface implants with Tb strongly modified the room temperature bulk thermoluminescence properties generated by X-ray irradiation. The TL spectra were measured by RA 94 reader analyser.The structural properties of Tb on ZnO crystaline were investigated by atomic force microscopy (AFM).

As seen from figure 1, the glow curve pattern shows TL peaks at 83 ^{o}C and 255 ^{o}C for pure ZnO. After annealed at 1000 ^{o}C for 1 hour, it has been observe that there are four peaks at 103 ^{o}C, 200 ^{o}C, 262 ^{o}C and 289 ^{o}C. Figure 2 shows TL glow curves of pure and Tb implanted ZnO single crystals with ions with a dose of $1x10^{16}$ ions/cm^2 . The Optical Absorption spectra were measured using a Perkin-Elmer Lambda 950 spectrophotometer in the wavelength range of 200–800 nm. The optical absorption spectrum of Tb implanted ZnO showed absorption bands centered at approximately 458 nm and 510 nm (Fig. 3).

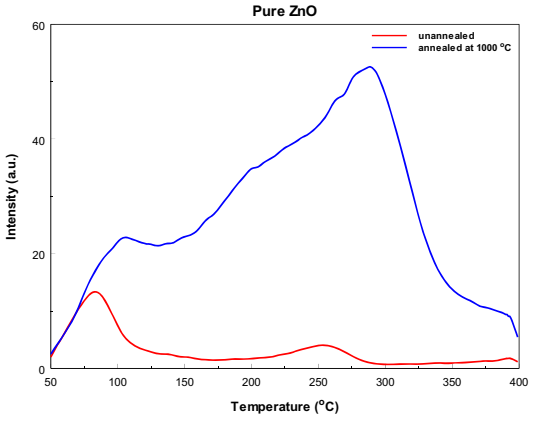

Figure 1. TL spectra for unannealed and annealed at 1000 ^{o}C of pure ZnO ranging from 50 to 400 ^{o}C after exposure to X ray.

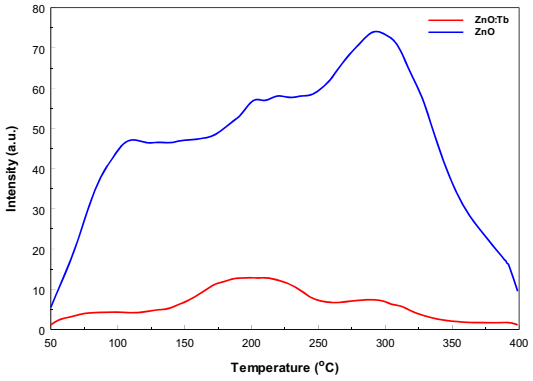

Figure 2. The TL glow curves of pure and Tb implanted ZnO single crystals with ions with a dose of $1x10^{16}$ ions/cm^2. Note that the sample was annealed at 1000 °C for 1 hour in tube furnace

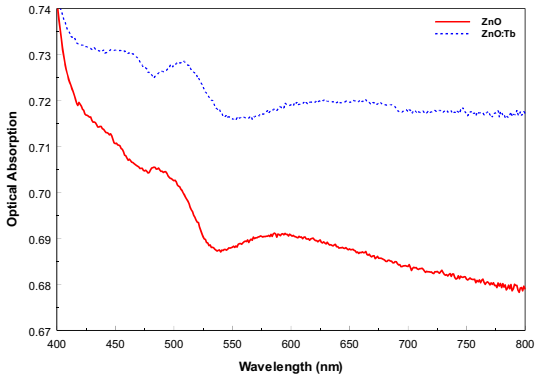

Figure 3. Optical absorption spectra of the 400-800 nm region of pure and Tb implanted (2.10^{16} ions/cm^2) ZnO at annealed 1000 ^{o}C.

References: [1]Lakshman S.V.J. et al. (1973*) Physica*, *66(3),* 601-610. [2]Mills S.J. et al. (2005) *Spectrochimica Acta Part A, 62,* 171-175. [3]Farquhar M.L. et al. (2003) *Min. Mag., 67(6),* 1205-1219. [4]Petit P.E. et al. (2001) *J. Synch. Rad., 8,* 952-954.

Spectral Decomposition Methods for Coherent Raman Spectroscopy

L. Ujj[1], R. Hemasinha[2], C. Prayaga[1],
[1]Department of Physics, University of West Florida, Pensacola, Florida 32514, email: LUJJ@uwf.edu,
[2]The Department of Mathematics and Statistics, University of West Florida, Pensacola, Florida 32514

Spectral fidelity of any coherent Raman spectra is a major concern of building and/or using an instrument in "real-time" applications such as e.g. chemical component monitoring in a reaction chamber, or mapping the distribution of certain chemicals in a solid sample matrix. Mainly, three methods are used to recover the vibrational information from the measured spectra: 1. Nonlinear fitting based upon the Levenberg-Marquardt algorithm[1], 2. Maximum Entropy Method[2], and 3. Direct phase retrieval procedure based upon the assumption that the third order susceptibility is an analytic function[3].

Corrections for instrumental response and the problem of finite sampling with appropriate "windowing" are also necessary to recover the vibrational bands needed to identify or characterize the samples.

These mathematical methods will be explained and a computer program written in LabView will be presented. Spectra taken by a nanosecond (at UWF)[4] and a picosecond (at UofA)[5] CARS spectrometer will be presented and analyzed by all three methods, vice infra. It is concluded that the third method is the most appropriate one for "real-time" data processing.

References:

[1] W. H. Press, S. A. Teukosky, W. T. Wetterling, B. P. Flannery (1992), Numerical Recipes in C, Second Ed., Section 15.5, Cambridge University Press.

[2] E. M. Vartiainen, H. A. Rinia, M. Müller, M. Bonn (2006), Optics Express 14, 8, 3622-3630.

[3] Y. Liu, Y. J. Lee, M. T. Cicerone(2009), Optics Letters, 34, 9, 1363-1365.

[4] L. Ujj, F.Bartha, Z. Chen, C. Prayaga, T. Royappa, C. Amos, M. Tsukuda (2010), XXII International Conference on Raman Spectroscopy (ICORS 2010), Boston.

[5] L. Ujj, C. G. Coates, J. M. Kelly, P. E. Kruger, J. J. McGarvey, G. H. Atkinson (2002), *J. Phys. Chem. B*,106, 4854-4862.

Preliminary Studies tor the Use of Portable Raman in the Identification of Conservation Treatments Applied in the Architectural Heritage.

C. Vazquez-Calvo[1*], S. Martinez-Ramirez[2*], Alvarez de Buergo[1] and Fort R[1]
[1] Instituto de Geología Económica / Instituto de Geociencias. (CSIC-UCM). Facultad de Ciencias Geológicas. c/ José Antonio Nováis 2. 28040 Madrid, Spain, carmenvazquez@geo.ucm.es
[2]Instituto de Estructura de la Materia (CSIC). C/Serrano 121. 28006 Madrid, Spain, sagrario@iem.cfmac.csic.es

Introduction: During the last decades the use of consolidants and waterrepellents as a remedial and conservation technique for stopping or slowing down the deterioration of stone used in the construction of buildings and monuments has been very common and widespread. The application of these type of products is and has been, in most of the cases, not documented, or if documented, not annotated which specific product was used. Sometimes these treatments need to be removed or even a re-application; or the building stone that was treated has developed stains and decay forms linked to these products. Regarding the instrumental technique, Raman-Spectroscopy has shown to be a useful technique in this field of scientific conservation research [1-4]. In general, laboratory equipment performs better than portable Raman, however, for Cultural Heritage it is very important to study the artefacts with a non destructive technique as well as the ability of *in situ* studies.

Aim: The aim of this work is to validate the use of the portable and non destructive Raman equipment "Inspector Raman Delta Nu" for the recognition of conservation treatments in the architectural heritage, avoiding in this way intensive sample collection which is not recommended at all when working with cultural heritage.

Methodology: Several products were analysed, but, for the purpose of this work, only two of them, consolidants, were selected: FTB SH75 (ethyl orthosilicate, 75%) and PARALOID™ B-72 (ethyl methacrylate co-polymer). A limestone was employed as substrate for the treatmens (Colmenar stone). Small specimens (3x3x1cm) were impregnated with both conservation products. This stone has been characterised by different authors [5,6], and has been used in buildings from architectural heritage for centuries [7]; mineralogically it is mainly composed by calcite ($CaCO_3$). Analyses were performed, first on the untreated fresh limestone, to consider any possible spectra influence; and secondly, on the impregnated specimens. The product was also analysed in its original liquid form in order to compare spectra. This portable Raman is equipped with a 785 nm diode laser for excitation, which has a maximum output power of 120mW at the source and a thermoelectrically cooled charge-coupled device detector, with a range of 200–2000 cm^{-1}.

The spectra were recorded with integration time 5s. The resolution is 8 cm^{-1}.

Results: In the case of the Raman technique, stone fluorescence represented a problem. However it has been posible to acquire spectra that may help in the in situ identification of conservation products. The results show that the application of the product over calcite allows identification of the support with 1085 cm^{-1} band observation. Adittionally the intensity of several bands from the product increases indicating some interactions between product and support (figure 1).

Conclusions: The technique is non-destructive, there is no need of sample preparation, and the equipment is portable. The portable raman is able to identify the support stone, conservation product, and the interactions between the product and the calcite.

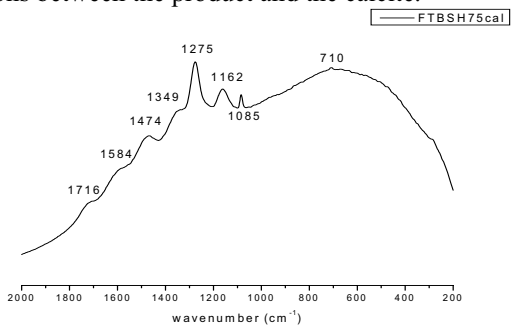

Figure 1. Spectra of FTHSB75 conservation product applied over calcite.

Acknowledgments: The authors thank you the national project CONSOLIDER-INGENIO 2007 (CSD2007-0058) y and the Madrid Regional Goverment project GEOMATERIALES (S2009/MAT-1629). And to the research UCM group: *"Alteración y Conservación de los Materiales Pétreos del Patrimonio"*.

References:

[1] Martinez-Ramirez et al. (2003) *Cement Concrete Res, 33*, 2063–2068, [2] Domingo et al. (2008) *Prog. Org. Coat.* 63 (2008) 5–12, [3] Edwards H.G.M. and Munshi E.T (2005). *Anal. Bioanal. Chem.* 382, 1398–1406, [4] Vandenabeele et al (2007) *Anal. Chem Acta.* 588, 108-116, [5]Dapena, E. R. at al. (1989). *Ingeniería Civil* 71, 67-77, [6]Bustillo, A. (1980) *Boletín Geológico y Minero*. T XCI-III: 503-514, [7] Fort et al (1996) *Geogaceta*, 20, 1236-1239.

RAMAN SPECTROSCOPY STUDY OF TEKTITES. M. V. Volovetsky[1], A. A. Averin[2], A. A. Shiryaev[2]
[1]Vernadsky Institute of Geochemistry and Analytical Chemistry RAS, 19, Kosygin Str, 119991 Moscow, Russia, volovetsky@gmail.com; [2]Frumkin Institute of Physical Chemistry and Electrochemistry, 31, Leninsky Prosp., 119991 Moscow, Russia, shiryaev@phyche.ac.ru.

Introduction. Tektites are iron containing natural silicate glasses of impact origin. They formed during a meteorite or comet impact events as a result of partial melting and evaporation of the target rocks. So tektites are important geochemical indicators of substance differentiation which is caused by impact events during formation of planets. High temperature processes in silicate melts are accompanied with redox reactions involving multi-valent elements and in the first place Fe. An analysis of the iron oxidation state in tektites is important for understanding of the conditions which take place during the impact events.

Experiment and results. Tektites form different strewn fields were investigated using complementary techniques such as Mossbauer and Raman spectroscopies, X-ray Absorption Spectroscopy and magnetic methods. Raman spectra were acquired for collection including various moldavites, philippinites, indochinites and australites. The spectra were recorded at room temperature using excitation by 532 and 738 nm lasers.

Typical Raman spectra of studied tektites are shown on Fig.1. The spectra are largely similar despite differences in samples provenance and composition.

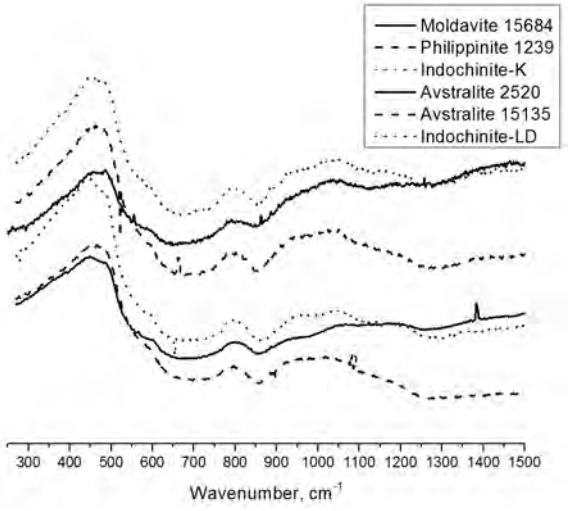

Fig.1. Raman spectra of glasses.

It is known that in Fe-containing silicate glasses the region between 800 and 1200 cm^{-1} can be associated with various tetrahedral Q^i species (i – number of bridging oxygen per tetrahedrally coordinated cation). Since Fe^{3+} ions can substitute for Si^{4+} bands in this region are sensitive to iron redox state [e.g., 1].

The broad band between 900 and 1100 cm^{-1} is present in all spectra. Spectral decomposition of this broad band permits to distinguish a band around 910 cm^{-1}, which is supposed to be sensitive to Fe^{3+} (Fig. 2).

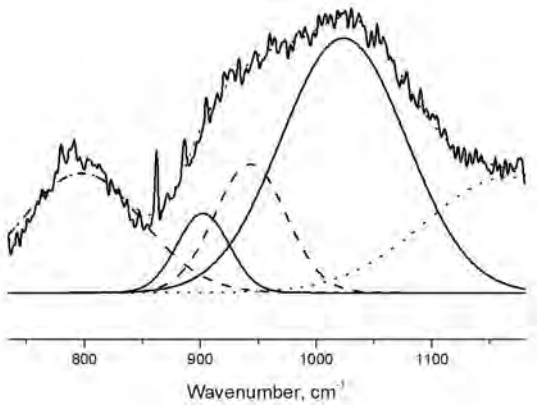

Fig.2. Deconvolution of spectra of Philippinite 1239.

In Table.1 relative intensities of the 910 band in different samples are compared with Mössbauer spectroscopy data [2].

Table.1. Relative intensity of 910 cm^{-1} band (Raman spectr.) and $Fe^{3+}/\Sigma Fe$ ratio (Mössbauer spectr. [2]).

Sample	**910 cm^{-1}**	**$Fe^{3+}/\Sigma Fe$**
Moldavite 15684	0.02	0.11
Australite 15135	0.04	0.13
Australite 2520	0.02	0.09
Philippinite1239	0.04	0.06
Indochinite-LD	0.07	0.10
Indochinite-K	0.08	0.07

Correlation is not unambigous due to the necessity of calibration of the Raman data for a given glass chemical composition. Our Mössbauer data indicate low Fe^{3+} content of tektites [2], suggesting very reducing conditions during tektite formation. The present Raman results confirm this conclusion.

References:

[1] Magnien V. et al. (2006) *Journal of Nuclear Materials, 352, 190-195.* [2] Volovetsky M.V. et al. (2008) *Hyperfine Interactions, 186, 83-88.*

RAMAN SPECTROSCOPY APPLIED TO RARE AND TINY PHASES: EXAMPLE FROM THE STUDY OF PLATINUM GROUP MINERALS (PGM). F. Zaccarini[1], R.J. Bakker[1], G. Garuti[1], O.A.R. Thalhammer, J.A. Proenza[2] and T. Aiglsperger[2], [1]Department of Applied Geosciences and Geophysics, University of Leoben, Peter Tunner Str.5, Leoben, Austria, federica.zaccarini@unileoben.ac.at, [2] Departament de Cristal.lografia, Mineralogia i Dipòsits Minerals. Facultat de Geologia. Universitat de Barcelona, C/ Martí i Franquès s/n, E–08028 Barcelona, Spain.

Raman spectroscopy is a non destructive and structurally sensitive technique that can be easily used to identify small mineral phases less than 10 microns in size. Some years ago, Raman spectroscopy was applied for the first time, to identify grains of natural platinum group minerals (PGM) [1]. However only 6 Raman spectra were published for the following natural PGM: cooperite (Pt,Pd,Ni)S, sperrylite ($PtAs_2$), platarsite (PtAsS), moncheite $(Pt,Pd)(Te,Bi)_2$, braggite (Pt,Pd,Ni)S and potarite (PdHg). Therefore, in this contribution we present the preliminary Raman results obtained on a great variety of PGM.

The PGM are the carriers of the platinum-group elements (PGE): osmium (Os), iridium (Ir), ruthenium (Ru), rhodium (Rh), platinum (Pt) and palladium (Pd). Recently, the PGE have gained tremendous importance due to their application in many modern and advanced technologies. However, with a concentration of about 10^{-6} to 10^{-7} % in the earth crust, the PGE are numbered among the ultra-trace elements. PGM occur naturally, as alloys, native elements or combinations with other elements, mainly S, As, Te, Bi, Sb, Se and O. Also the PGM are rare, representing only less than the 3% of the approved minerals by the Commission on New Minerals and Mineral Names of the International Mineralogical Association (IMA). According to the literature data updated to 1997 [2], only 96 phases containing the PGE has major components, have been approved, whereas more than 500 PGM are still waiting for a clear identification, in particular for crystallographic characterization to the degree required for acceptance as new mineral species. From 1997 to the present days, only 25 new PGM have been discovered. The main reason for the significant lack of in sufficient identification of PGM is their mode of occurrence, i.e. as minute inclusions, prevents characterization using structural data. Optical and electron microscopy, electron microprobe analysis are the most used techniques for chemical and physical identification of PGM. However, PGM are notoriously difficult to identify during petrographic investigation owing to their small sizes and the similarity of the optical properties of many minerals. Furthermore, where the PGM are only a few microns in size, the electron microprobe generally provides only semi-quantitative analyses due interferences from surrounding minerals. Therefore, there is a need of an innovative and complementary methodology able to provide mineralogical information which is difficult and sometimes impossible to obtain from other widely used techniques. As a consequence, Raman spectroscopy is suggested as the best candidate to solve this technical problem, as previously proposed by [1]. Our results of Raman spectroscopy applied on selected PGM, such as sulphides, arsenides, sulpharsenides revealed that all the analyzed grains display a very well-defined and characteristic spectrum, as typical for the compounds characterized by the presence of covalent bonding. On the contrary, the Raman spectra of a number of alloys and native elements show no discernible scattering bands suggesting that the possible bonds present in these PGM are metallic or ionic. Few PGM, classified as possible Ru bearing oxides, show a broad and weakly scattered spectrum over the range of about 100–800 cm^{-1}. The collected data also demonstrated that Raman is sensitive on the compositional variation, particularly in the PGM characterized by a solid solution substitution such as laurite (ideally RuS_2)-erlichmanite (ideally OsS_2) series. These results confirm that Raman spectroscopy can be considered an innovative and complementary technique with a huge potential to better characterized and identify rare and tiny phases such as PGM. The two main disadvantages of the Raman spectroscopy applied to the investigation of PGM are: 1) some PGM, such native elements and alloys, are not sensitive to this technique and 2) it does not provide a chemical composition of the investigated minerals. Therefore, it is intended to apply the Raman spectroscopy to a great number of different PGM, already chemically characterized by electron microprobe, with the target to create a future and accessible data base of Raman spectra of a great number of different PGM.

References:

[1] Mernagh T.P. and Hoatson D.M. (1995) *Can. Mineral., 33*, 409-417.

[2] Daltry V.D. and Wilson A.H. (1977) *Mineral. Petrol., 60*, 185-229.

NOTES

NOTES